

INAUGURAL-DISSERTATION

am Leibniz-Institut für Atmosphärenphysik in Kühlungsborn
zur Erlangung der Doktorwürde
der Mathematisch-Naturwissenschaftlichen Fakultät
der Universität Rostock

Variability-Lifetime Relation of Atmospheric Tracers

Based on Aircraft Measurements
during the INDOEX
and STREAM 98 Campaigns

von
Stefanie Yi Chuin Wong

Abstract: Within the framework of the INDOEX (Indian Ocean Experiment) campaign, which took place in February and March 1999, a number of trace gases were measured from onboard a jet aircraft. During the STREAM 98 campaign (Stratosphere Troposphere Experiment by Aircraft Measurements), which took place in July 1998, the same aircraft was based in Timmins, Canada. This thesis concentrates on the analysis of tropical marine boundary layer, or tropopause region data, respectively, of CO, CH₄, nonmethane hydrocarbons (NMHC's), carbonyls and chlorofluorocarbons. The main focus of this work is the estimation of OH concentrations along the back trajectory of sampled air masses based on a variability analysis of the trace gas concentrations. Furthermore, the state of atmospheric mixing is assessed.

Based on the variability-lifetime concept a mean OH concentration of $3.4_{-1.0}^{+1.1} \cdot 10^6$ molecules/cm³ was estimated in the marine boundary layer. During STREAM 98, OH concentrations of $(1.5 \pm 0.3) \cdot 10^6$ molecules/cm³ in the troposphere and $(1.2 \pm 0.25) \cdot 10^6$ molecules/cm³ in the lowermost stratosphere were derived. For both campaigns, the results agree well with model computations for the respective regions. The results of the variability-lifetime analysis show that during INDOEX the measurement area was remote from pollution sources and that chemical processing and photolytical degradation determined the variability of the measured trace gases rather than mixing. Moreover, it is shown that the age distribution of the measured air masses was rather uniform, consistent with the measurement location over the Indian Ocean remote from pollution sources. The STREAM 98 variability study is performed for two layers in the atmosphere, the upper free troposphere and the lowermost stratosphere. The results of the variability-lifetime analysis show that both layers were influenced by air masses with very different air mass ages.



Variability-Lifetime Relation of Atmospheric Tracers

Based on Aircraft Measurements
during the INDOEX
and STREAM 98 Campaigns

von
Stefanie Yi Chuin Wong

Dieser Forschungsbericht wurde als Dissertation von der
Mathematisch-Naturwissenschaftlichen Fakultät der Universität Rostock
angenommen.

Gutachter: Prof. Dr. F.-J. Lübken (Universität Rostock)
Prof. Dr. J. Lelieveld (Max-Planck-Institut für Chemie, Mainz)
Prof. Dr. P. J. Crutzen (Max-Planck-Institut für Chemie, Mainz)

verteidigt am: 27. Januar 2006

Summary

The main focus of this thesis is the estimation of the OH concentrations along the back trajectory of air masses. Furthermore, the state of mixing of the sampled atmosphere is assessed. These issues are investigated using the variability of the concentrations of a range of trace gases, which were measured during two airborne measurement campaigns.

Within the framework of the INDOEX (Indian Ocean Experiment) and STREAM 98 campaigns (Stratosphere Troposphere Experiment by Aircraft Measurements) a number of trace gases were measured simultaneously from onboard a jet aircraft. During INDOEX, which took place in February and March 1999, the aircraft was based on Hulhule, Maldives, to study the Indian Ocean region. This work concentrates on the analysis of the tropical marine boundary layer data. During STREAM 98, which took place in July 1998, the same aircraft was based in Timmins, Canada, to study chemical and dynamical processes, which influence the chemical composition and chemistry of the tropopause region. Among the measured trace gases were CO, N₂O, CH₄, nonmethane hydrocarbons (NMHC's), carbonyls and chlorofluorocarbons. The measurements of CO were performed by the Max-Planck Institute for Chemistry, Mainz, using a TDLAS (Tunable Diode Laser Absorption Spectroscopy) instrument.

The variability-lifetime concept proves to be an indirect method that is valuable to determine the average OH concentration along the back trajectory of the sampled air mass. This average OH concentration is calculated by optimising the OH concentration value in the lifetime calculation of the individual species. During INDOEX, the OH concentration that we derive by this method is $3.4_{-1.0}^{+1.1} \cdot 10^6$ molecules/cm³ in the marine boundary layer. During STREAM 98, OH concentrations of $(1.5 \pm 0.3) \cdot 10^6$ molecules/cm³ in the troposphere and $(1.2 \pm 0.25) \cdot 10^6$ molecules/cm³ in the lowermost stratosphere are derived. For both campaigns, the results agree very well with model computations for the respective regions.

The variability-lifetime analysis allows to draw further conclusions. The results of the INDOEX campaign show that the measurement area was remote from pollution sources and that chemical processing and photolytical degradation determined the variability of the measured trace gases rather than mixing. Moreover, it will be shown that the age distribution of the measured air masses was rather uniform. This is consistent with the measurement location over the Indian Ocean far away from pollution sources and the fact that air masses sampled from the research aircraft mainly originated from two source regions - the Arabian Sea and the Bay of Bengal.

The STREAM 98 variability study is performed for two layers in the atmosphere, the upper free troposphere (altitude > 7 km and O₃ < 75 ppbv) and the lowermost stratosphere (75 ppbv < O₃ < 335 ppbv). The results of the variability-lifetime analysis show that both layers were influenced by air masses with very different air mass ages; the free troposphere by boundary layer and free tropospheric air masses; and the lowermost stratosphere by stratospheric and free tropospheric air masses. The reported measurements were performed close to the polar jet stream, where mixing between stratospheric and tropospheric air masses occurs very frequently. The strong convective activity in the measurement region caused the mixing of boundary layer air into the free troposphere.

The estimation of OH concentrations from measurements using the variability method and the derivation of the parameters of the variability-lifetime relation offers the opportunity to compare chemistry and dynamics of in-situ measurements and helps understanding the processes controlling the chemical composition of the sampled air mass.

Contents

1	Introduction	1
1.1	The measurement campaigns INDOEX 99 and STREAM 98	2
1.2	Overview	3
2	Structure, dynamics and chemistry of the lower atmosphere	5
2.1	The structure of the atmosphere	5
2.2	Dynamics of the atmosphere	6
2.3	Tropical climatology	7
2.4	Chemistry of the atmosphere	10
2.4.1	Hydroxyl radicals	10
2.4.2	Ozone	13
2.4.3	Units of concentration	14
3	Variability	15
3.1	Estimation of OH concentrations	15
3.1.1	Global model simulations of OH	15
3.1.2	Measurement methods for the hydroxyl radical	18
3.2	Decomposition of trace gases	19
3.3	Definitions of lifetime in an atmospheric reservoir	19
3.3.1	Turnover time	20
3.3.2	Residence time	20
3.3.3	Age	20
3.3.4	Lifetime	21
3.4	What is variability?	21
3.4.1	Variability in trace gas mixing ratios	21
3.4.2	Variability in different reservoirs	23
3.4.3	Derivation of the variability-lifetime relationship	24
3.5	A historical review	29
3.6	The variability method in practice	32
3.7	Processes affecting variability	34
3.7.1	Photochemistry	36
3.7.2	Gas phase reactions	37
3.7.3	Heterogeneous reactions	37
3.8	Prerequisite for the application of the variability-lifetime method	38
4	The tuneable diode laser absorption spectrometer	39
4.1	The measuring principle	39
4.2	Optical setup	40
4.3	Electronic setup and data acquisition	40

4.4	Gas flow and calibration	42
4.5	Characteristics during the INDOEX campaign	44
4.5.1	The lasers	44
4.5.2	Data quality and handling	46
4.6	Characteristics during the STREAM 98 campaign	48
5	The INDOEX campaign	51
5.1	The measurement region and the meteorological background	51
5.1.1	The main wind flow channels	52
5.1.2	The inter tropical convergence zone	53
5.2	The aircraft and the instrumentation	54
5.2.1	The Cessna Citation II	54
5.2.2	The aircraft instrumentation	55
5.3	Atmospheric layers during INDOEX	59
5.4	Variability during INDOEX	64
5.4.1	OH concentrations	71
5.4.2	The parameters A and b	75
5.5	Summary and conclusions	77
6	The STREAM campaign 1998	79
6.1	The measurement region	79
6.2	Meteorological background	79
6.3	The aircraft instrumentation	81
6.4	Separation of different air masses during STREAM 98 – Definition of the tropopause	83
6.5	Variability during STREAM 98	84
6.5.1	OH concentrations	91
6.5.2	The parameters A and b	94
6.6	Summary and conclusions	96
7	Summary and outlook	99
7.1	Summary	99
7.2	Outlook	100
	References	103
	Acknowledgements	115

List of Figures

2.1	Radiative budget and vertical temperature profile	5
2.2	Scheme of the global atmospheric circulation	6
2.3	Dynamical aspects of stratosphere-troposphere exchange	8
2.4	OH - the major oxidising agent of the lower atmosphere	11
3.1	Zonally and monthly averaged OH concentrations	16
3.2	OH distribution at 700 hPa	16
3.3	Annual zonal mean OH distributions	17
3.4	Decomposition of trace gases	19
3.5	Reservoir scheme	19
3.6	Measurements at different locations or at different times	22
3.7	Time series of the trace gas CO measured onboard the research aircraft Citation during the INDOEX campaign	23
3.8	Variability of measured data	24
3.9	Variability versus lifetime	24
3.10	Variability in trace gas mixing ratios	25
3.11	Variability in different layers	26
3.12	Variability - lifetime relationship	28
3.13	Relative standard deviation versus tropospheric residence time τ of the respective species	30
3.14	Standard deviation σ of the natural logarithm of the mixing ratios of PEM-West B data versus photochemical lifetime τ of the respective species	31
3.15	Flow chart: estimation of OH concentrations	33
3.16	Influence of different OH concentrations on lifetime	35
3.17	Variation of OH concentrations to find the minimum in χ^2	35
4.1	Schematics of the TRISTAR optical setup	41
4.2	TRISTAR optics and the complete setup in the aircraft	42
4.3	Schematic diagram of the TRISTAR inlet system, gas flow and calibration system	43
4.4	CO raw data and final data measured during INDOEX on February 16	46
4.5	N ₂ O, and CO measured with the TDLAS during STREAM 98 on July 1	50
5.1	Geographical distribution of all measurement flights performed during the INDOEX campaign	52
5.2	Main wind flow channels (arrows) in the measurement region of the INDOEX intensive field phase	53
5.3	The configuration of the inlet probes during the INDOEX campaign	56
5.4	Payload configuration during the INDOEX campaign	58
5.5	Airborne measurements during INDOEX on March 1	60
5.6	CO mixing ratios observed during INDOEX	61

5.7	Virtual potential temperature profile taken during INDOEX	62
5.8	Concept of sea- and land breeze circulation	63
5.9	Temporal development of CO mixing ratios during INDOEX	65
5.10	Variability during INDOEX	66
5.11	χ^2 for various OH concentrations during INDOEX	71
5.12	Location of the quasi-Lagrange experiment during INDOEX	73
5.13	Vertical profiles of modelled OH concentrations in the INDOEX region	74
6.1	Geographical distribution of all measurement flights performed during the STREAM 98 campaign	80
6.2	The payload configuration of the STREAM 98 campaign	81
6.3	Ozone to acetone correlation	84
6.4	Variability during STREAM 98	85
6.5	Histograms and cumulative Gaussian distribution plots for STREAM 98	89
6.5	continued	90
6.6	Vertical profile of modelled OH concentrations for Northern Hemispheric midlatitudes	93

List of Tables

3.1	Measurement methods for the hydroxyl radical	18
5.1	All flights performed with the Cessna Citation during the INDOEX intensive field phase 1999	55
5.2	Instrumentation onboard the Cessna Citation during the INDOEX campaign	57
5.3	Number of data points in variability study during INDOEX	69
5.4	Reaction rates and photolysis rates of all species during the INDOEX campaign	70
5.5	Results and comparison of OH concentrations for INDOEX	72
5.6	Results and comparison of fit-parameters A and b INDOEX	75
6.1	All flights performed during STREAM 98	80
6.2	Instrumentation onboard the Cessna Citation during the STREAM 98 campaign	82
6.3	Number of data points in variability study during STREAM 98	86
6.4	Reaction rates and photolysis rates of all species during the STREAM 98 campaign	88
6.5	Results and comparison of OH concentrations for STREAM 98	92
6.6	Results and comparison of Fit-parameters A and b for STREAM 98	95

Acronyms

Institutes and Organisations

DLR	Deutsches Zentrum für Luft- und Raumfahrt
DUT	Faculty of Aerospace Engineering, Delft University of Technology, The Netherlands
ECMWF	European Center for Medium Range Weather Forecast
ILK	Institut für Luft- und Kryotechnik, Dresden
IMAU	Institute for Marine and Atmospheric Science, Utrecht, The Netherlands
IMG	Institute for Meteorology and Geophysics, University of Frankfurt
IPCC	Intergovernmental Panel on Climate Change
IPM	Fraunhofer-Institut für physikalische Messtechnik
ISC	Institute for Stratospheric Chemistry, Research Centre Jülich
ITM	Institute of Applied Environmental Research, Stockholm University, Sweden
KCO	Kaashidhoo Climate Observatory, Maldives
KNMI	Royal Netherlands Meteorological Institute, De Bilt , The Netherlands
MPI-A	Max-Planck-Institute for Chemistry, Atmospheric Chemistry Dept., Mainz
MPI-B	Max-Planck-Institute for Chemistry, Biogeochemistry Dept., Mainz
MPI-N	Max-Planck-Institute for Nuclear Physics, Heidelberg
NCAR	National Centre for Atmospheric Research, Boulder, USA
NCEP	National Centers for Environmental Prediction, USA
NLR	National Aerospace Laboratory of The Netherlands
NOAA	National Oceanographic and Atmospheric Administration
WMO	World Meteorological Organisation

Models

ECHAM	European Centre Hamburg Model
MATCH-MPIC	tropospheric photochemistry version of the Model of Atmospheric Transport and Chemistry
NCAR CCM	National Center for Atmospheric Research - Community Climate Model
TM3	Chemistry Transport Model of the University Utrecht

Projects and Campaigns

AASE	Airborne Arctic Stratospheric Expedition
ABLE	Arctic Boundary Layer Expedition
ASHOE	Airborne Southern Hemisphere Ozone Experiment
INDOEX	Indian Ocean Experiment
LBA-CLAIRE	Large Scale Biosphere-Atmosphere Experiment in Amazonia - Cooperative LBA Airborne Regional Experiment
MINOS	Mediterranean Intensive Oxidant Study
PEM West B	Pacific Exploratory Mission in the Western Pacific Ocean Phase B
PEM Tropics A,B	Pacific Exploratory Mission Tropics A, B
SPADE	Stratospheric Aerosols and Dynamics Expedition
STREAM	Stratosphere Troposphere Experiment by Airborne Measurements
TRACE A	Transport and Atmospheric Chemistry Near the Equator - Atlantic

Experiments and Instruments

AAMAS	Automatic Aircraft-borne Mass Spectrometer
ACIMS	Active Chemical Ionisation Mass Spectrometry
CNC	Condensation Nuclei Counter
DIRAM	Directional Radiance Distribution Measurement
DOAS	Differential Optical Absorption Spectrometry
ECD	Electron Capture Detector
FISH	Fluorescent in-situ hygrometer
FLAIR	Four Laser Airborne Infra Red
FSSP	Forward Scattering Spectrometer Probe
GC	Gas chromatograph
GHOST	Gas Chromatograph for the Observation of Stratospheric Tracers
GOME	Global Ozone Monitoring Experiment onboard the ERS-2 satellite
GPS	Global Positioning System
HALOE	Halogen Occultation Experiment
INSAT	Indian National Satellite
LIF	Laser-Induced Fluorescence
PTR-MS	Proton-transfer reaction mass spectrometer
ScaRab	Scanner for Radiation Budget
TDLAS	Tunable Diode Laser Absorption Spectroscopy
TRISTAR	Tracer in situ TDLAS for Atmospheric Research
TTFM	Two Tone Frequency Modulation
UARS	Upper Atmospheric Research Satellite

Chapter 1

Introduction

The industrial revolution has brought prosperity and social changes to Western civilisations. On the other hand, it increased requirements on energy, food and space for the growing population, causing severe environmental pollution. The source of air pollution changed from extensive use of coal in the nineteenth century to combustion of oil products and particularly vehicle fuels in the twentieth century [Holgate *et al.*, 1999]. The most important pollutants are oxides of nitrogen, ozone, carbon monoxide, polyaromatic hydrocarbons and suspended particulates, although their proportion varies according to geographical location and prevailing weather conditions.

The chemical composition of the atmosphere is crucial for the radiation and energy budget of the atmosphere. For example, ozone absorbs light in the range from 210 to 310 nm, and as a consequence it protects life by preventing harmful UV radiation from reaching the Earth's surface. Moreover, in particular in the upper troposphere ozone contributes to a radiative heating effect, termed the greenhouse effect, by absorbing light in the infrared spectral range emitted from the Earth's surface.

Water vapour, carbon dioxide, methane, and nitrous oxide, are also greenhouse gases. Their greenhouse potential depends on their atmospheric concentration and on their spectral absorption bands. Atmosphere-Ocean General Circulation Model simulations for a range of scenarios are being used to quantify the mean climate change due to the greenhouse effect [McAvaney *et al.*, 2001]. The IPCC (Intergovernmental Panel on Climate Change) scenarios describe different narrative storylines (demographic, economic and technological), that determine the emission driving forces of greenhouse gases and sulphur, as well as their evolution. For the end of the 21st century (2071 to 2100) one of their scenarios yields a mean change in global average surface air temperature relative to the period from 1961 until 1990 of 3.0°C (with a range of 1.3 to 4.5°C) [Houghton *et al.*, 2001]. Rising temperatures, in turn, caused by the greenhouse effect influence chemistry via temperature dependant reaction rates and emissions.

Atmospheric trace gases are not only important for the Earth's radiation budget, but they can also cause health problems, e.g. diseases of the respiratory and cardiovascular system [Holgate *et al.*, 1999]. This was demonstrated in a dramatic way during the London fog of 1952, when 4000 additional deaths compared to the expected mortality rates during this period occurred - over a time period of only about 1 week - and which was attributed to the air pollution [Ministry of Health, 1954]. Bell and Davis [2001] even attribute 12000 excess deaths in the following three months to the high air pollution episode (mortality rates in those months were 50-300% higher than the previous year). During this event, highly elevated concentrations of SO₂ and smoke or particles (total suspended matter) were reported.

The concentration of trace gases in the atmosphere is determined by their sources and sinks. Different chemical cycles take place in polluted or clean regions, and in different altitude regimes - close to the Earth's surface, in the troposphere and through the tropopause also in higher regions

like the stratosphere. Moreover, transport processes play an important role for the dispersion of the trace gases throughout the atmosphere, especially for gases with a long lifetime, so that chemical and physical processes, like emissions, transport and fates of anthropogenic, biogenic and geogenic atmospheric constituents in one region influence those in other regions. The fact that atmospheric regimes are connected is demonstrated by the vertical transport of long-lived chloroflourocarbons (CFC's) from the surface into the stratosphere, or ozone from the stratosphere into the troposphere [Finlayson-Pitts and Pitts, 2000].

The counterpart to air pollution as a source of atmospheric constituents are removal processes from the atmosphere (sinks). Most atmospheric trace gases, for example carbon monoxide, methane and volatile organic compounds, are transformed and ultimately removed from the atmosphere after reaction with the hydroxyl radical (OH) [Hofzumahaus *et al.*, 1998]. Often, this oxidation reaction is the first and rate limiting step in the decomposition process. Therefore, the concentration of OH affects the concentrations of atmospheric trace gases. On the other hand, these gases influence the concentration of OH in the atmosphere, so the chemistry of OH and the trace gas cycles are coupled and complex [Perner *et al.*, 1987].

Obviously, the oxidation efficiency of the atmosphere is determined by the concentration of OH (see section 2.4). Together with the sources of atmospheric trace gases and transport pathways, the OH concentration is crucial for the distributions and lifetimes of trace gases, of which several are of great importance for climate and public health [Jöckel *et al.*, 2002]. Thus, knowledge about the concentration of OH and its possible trends is of great interest. Yet, OH concentrations are difficult to measure, due to its low atmospheric concentrations (10^5 to 10^6 molecules/cm³ during daytime and 10^4 molecules/cm³ or less during nighttime [Finlayson-Pitts and Pitts, 2000]), as well as its short lifetime. A compilation of measurement methods is given in chapter 3. Prediction of OH concentrations by models is challenging, because it must be based on incomplete knowledge of present trace gases and reaction mechanisms, and might be complicated by limits of available machine time for models.

As can be seen in the previous sections the interaction between the numerous different gases in the atmosphere as well as transport processes determine the chemical composition of the atmosphere. The self cleaning capability of the atmosphere, that is the capability of the atmosphere to remove chemical species from itself, remains a major point of interest in atmospheric sciences, as well as transport pathways of air parcels in the atmosphere, and the lifetime of emitted species.

The study of the relationship between the variability of trace gas concentrations and their respective residence times is a powerful tool for the understanding of chemical and dynamical processes in the atmosphere. The concept of variability can be used to estimate OH concentrations. In this work, OH concentrations from airborne trace gas measurements in the marine boundary layer during INDOEX and in the troposphere and lowermost stratosphere during STREAM 98 are derived using the variability-lifetime relationship.

1.1 The measurement campaigns INDOEX 99 and STREAM 98

In this thesis, the observations from two airborne measurement campaigns will be analysed: the Indian Ocean Experiment (INDOEX, chapter 5), which took place over the Northern Indian Ocean, close to the interhemispheric tropical convergence zone (ITCZ), and the Stratosphere Troposphere Experiment by Aircraft Measurements 1998 (STREAM 98, chapter 6), which was conducted in Canada, north of the Great Lakes Area.

The objectives of the INDOEX 99 campaign were the assessment of the nature and the extent of the chemical pollution over the tropical Indian Ocean and how the high population on the Indian subcontinent affects the chemistry of the troposphere. In this context, the question of the impact of the

pollution on the oxidation power of the atmosphere was a main focus. Furthermore, the importance of sulfates, soot and other continental aerosols for radiative forcing was studied. Here, the main question was if the influence is only locally restricted to urban areas or if it spreads to remote regions, and could possibly influence the ocean heat budget and the planetary albedo far away from the sources.

The STREAM 98 campaign took place in close proximity to the polar jet stream, where stratosphere-troposphere-exchange does occur frequently. Moreover, this region is often influenced by regional biomass burning as well as long-range transport and deep convection during summer. Hence, for exploring the chemical and dynamical processes of the tropopause region, this geographical region offers good opportunities. The main focus during STREAM 98 was the influence of long range transport, deep convection and stratosphere-troposphere-exchange, as well as the chemistry of the lowermost stratosphere.

In order to achieve these objectives, it was necessary to simultaneously probe a variety of species over a wide geographical region in several altitude layers. Therefore, atmospheric trace gas measurements, aerosol number concentrations and radiation measurements were conducted from onboard a research aircraft. The use of a research aircraft offers the additional opportunity to react relatively fast to interesting features in the atmosphere, and to study those with special diligence.

1.2 Overview

The observed concentrations of a range of trace gases were used to investigate the state of mixing in the atmosphere, sources and sinks and to estimate the OH concentration. For this, the variability-lifetime method was applied, which will be explained in chapter 3. The tuneable diode laser absorption spectrometer (TDLAS), which was operated during the aforementioned campaigns to measure CO and N₂O, is described in chapter 4. Background information on atmospheric structure, dynamics and chemistry are given in chapter 2. The measurement campaigns and the obtained data are presented in chapters 5 and 6. In these chapters, the objectives of the measurement campaigns, the meteorological situation, the aircraft and the instruments operated by other research groups and/or institutes of which data were used for this thesis, as well as data and the results of the variability study are presented - in chapter 5 for the INDOEX 99 campaign, and in chapter 6 for the STREAM 98 campaign. A summary and outlook of this thesis will be given in the last chapter 7.

Chapter 2

Structure, dynamics and chemistry of the lower atmosphere

2.1 The structure of the atmosphere

The classification of the atmosphere into layers based on the temperature gradient of the atmosphere is well established. The vertical temperature profile of the atmosphere is mainly determined by three processes: irradiation of sunlight into the atmosphere, absorption of re-emitted thermal energy from the Earth's surface and transport processes. Figure 2.1 shows an average temperature profile for June at 50° N, and the nomenclature of the different altitude regimes. In the troposphere ($\lesssim 8-18$ km), the lowest layer, temperature decreases with height. The temperature gradient is a result of radiation of heat from the Earth's surface and convection of the air. In the above lying stratosphere ($\sim 10-50$ km), temperatures rise to values nearly as high as at the Earth's surface, which is a result of heating by UV-absorption by ozone molecules. The tropopause separates troposphere and stratosphere. Its position varies with latitude and season between about 8 km altitude in polar regions and 18 km in the tropics. An often used definition of the location of the tropopause is thermal, so that the tropopause is at the lowest altitude, at which the temperature gradient reaches -2 K km^{-1} or less and stays below this value for the next 2 km altitude. Alternative definitions of the tropopause will be discussed in detail in section 6.4.

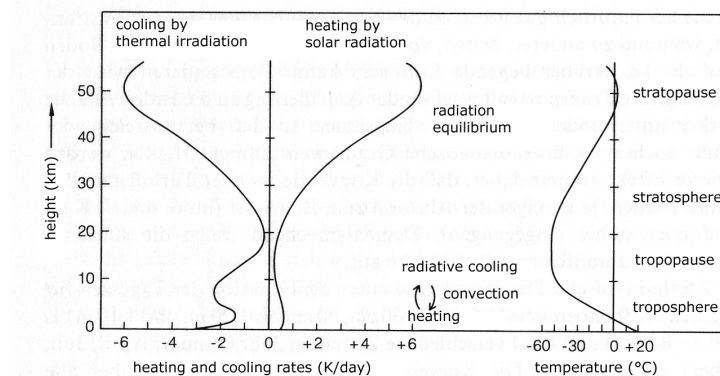


Figure 2.1: Radiative heating and cooling in the atmosphere (left) and vertical temperature profile (right) for the troposphere and stratosphere, after Roedel [1994].

2.2 Dynamics of the atmosphere

In the following section, the main features of zonal and meridional circulations will be described for the Northern Hemisphere. The main flows in the Southern Hemisphere mirror that of the Northern Hemisphere qualitatively. A scheme of the global lower circulation is given in Figure 2.2. The main meridional wind field is weak compared to the zonal, but it is important in maintaining the heat flux to balance the global energy budget.

Close to the equator, warm air raises, flows poleward and subsidises in the subtropics. From here, the surface flow of air directs from the east to the southwest close to the equator, which are the northeast trade winds. This large scale circulation is called the Hadley cell. There are two tropical Hadley cells, separated by a region of ascending warm air called interhemispheric tropical convergence zone (ITCZ), which forms a transport barrier between the tropospheric air masses of the two hemispheres: north and south. In summer and again in winter (not in spring and autumn), one large Hadley cell dominates the circulation, whereas the other cell diminishes. This causes the ITCZ to seasonally oscillate northward and southward in a wavelike pattern, with an average position near the equator (5°N in annual average). Above the oceans, the position of the ITCZ varies by about $\pm 5^\circ$ from the average position, whereas under the influence of the continents displacements of up to $\pm 25^\circ$ can be observed. The oscillation of the ITCZ opens an opportunity for the exchange of air masses between the hemispheres.

Further poleward, the weaker Ferrel circulation describes an average meridional movement of air in opposite direction (compared to the Hadley cells): subsidence of air in the subtropics, a poleward surface flow, ascending air in subpolar regions and an equatorward flow at higher altitudes. The Ferrel circulation is an indirect, dynamically generated circulation. In the northern-hemispheric mid-

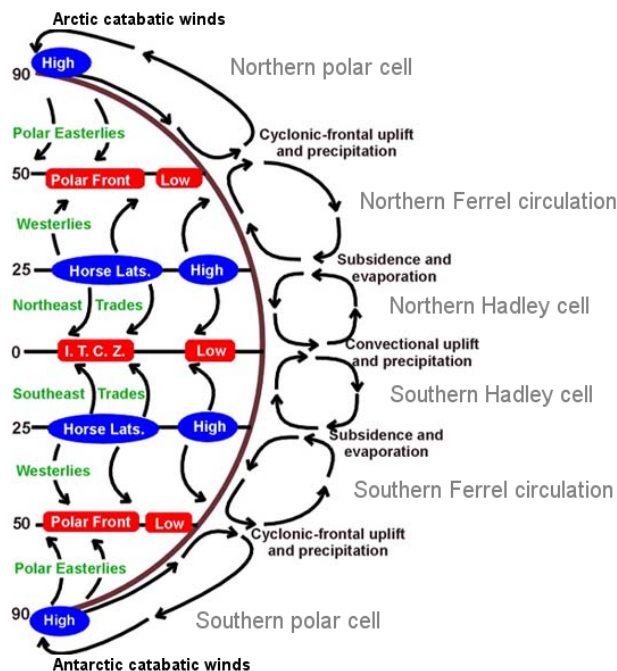


Figure 2.2: Scheme of the global lower atmospheric circulation: most important air motions near the Earth's surface (green text and arrows "in" the globe), high pressure regions (blue) and low pressure regions (red), most important meridional air motions (black and arrows "outside" the globe) and circulations (grey). For details see text. From ESPERE Website (www.atmosphere.mpg.de/enid/067a3f5137b38fa7c44350981c3e68e8,0/1pd.html) with additions.

latitudes, the mean zonal surface wind direction is from west to east (westerlies), with maximum wind speeds at about 30° latitude near the subtropical jet stream (current of fast moving air found in the upper levels of the troposphere, resulting from the effect of meridional air movement at the boundaries of adjacent air masses with significant differences in temperature, and the Coriolis force). Typically, fronts (areas where air masses with different temperature concur), cyclones (low pressure areas) and anticyclones (high pressure areas) superimpose the westerlies.

The polar jet stream, which is associated with the polar front, is much weaker. At the polar front, warm air masses of the mid-latitudes and subtropics concur with cold air masses from higher latitudes. The front is unsteady and strongly structured. Above the poles, circumpolar easterlies prevail, which are restricted to the lowest 3 km of the atmosphere in contrast to the other global wind-systems. This system is driven by katabatic winds, which are generated by cooling of air above the ice, and diverted by the Coriolis force. A detailed description of atmospheric dynamics can be found in *Roedel* [1994] and *Brasseur and Solomon* [1986].

In the lower stratosphere, the mean meridional motion is less well defined than that in the troposphere. In the stratosphere, the mean circulation is cancelled to a large degree by eddy transport¹ [*Brasseur and Solomon*, 1986]. However, a net ascent of air can be observed over the tropics, and a net subsidence prevails above the poles (Brewer-Dobson circulation [*Brewer*, 1949; *Dobson*, 1956]). An exchange of air masses between the stratosphere and the troposphere occurs via this vertical air movement (Figure 2.3). Additionally, quasi-horizontal exchange takes place along the isentropes that cross the tropopause. This is caused by baroclinic disturbances in the extratropical upper troposphere or by exchange across the sub-tropical jet, which is associated with the summer monsoon circulation. The time scales for this transport (wavy arrows) are much shorter than those of the Brewer-Dobson circulation [*Holton et al.*, 1995].

2.3 Tropical climatology

Additionally to the mean annual circulation described in the section above, a number of seasonally and non-seasonally variations are superimposed. This section describes the most important features in the tropical region.

Non-seasonal variations

Non-seasonal variations include

- **the quasi-biennial oscillation (QBO):** an oscillation between strong easterly stratospheric winds dominating in one year, and strong westerlies dominating in the next year (with a period of about 27 months). The influence of this oscillations on other tropical circulations such as the southern oscillation [*Gray et al.*, 1992], the monsoons [*Knaff and Gray*, 1994] and the tropical cyclone activity [*Gray and Schaeffer*, 1991] is not yet fully understood. However, at some low latitudes, the temporal variations in rainfall and temperature resemble the temporal variations of the QBO [*Ogallo*, 1979; *Shapiro*, 1982; *Hastenrath and Rosen*, 1983; *Chu*, 1984].
- **40-50 day tropical oscillation:** also called Madden-Julian/Intraseasonal Oscillation (MJO) [*Madden and Julian*, 1971, 1972]. The MJO describes a variation of strength in upper atmospheric winds, of temperature (at a variety of levels), and of surface pressure with a periodicity of about 45 days. These variations explain some aspects of the low frequency variability in the tropical circulation and climatic variability. As will be discussed in chapter 5.3, it also influenced the measurements during the intensive field phase of the INDOEX campaign. The

¹Eddies are fluctuations about the zonal mean air motion

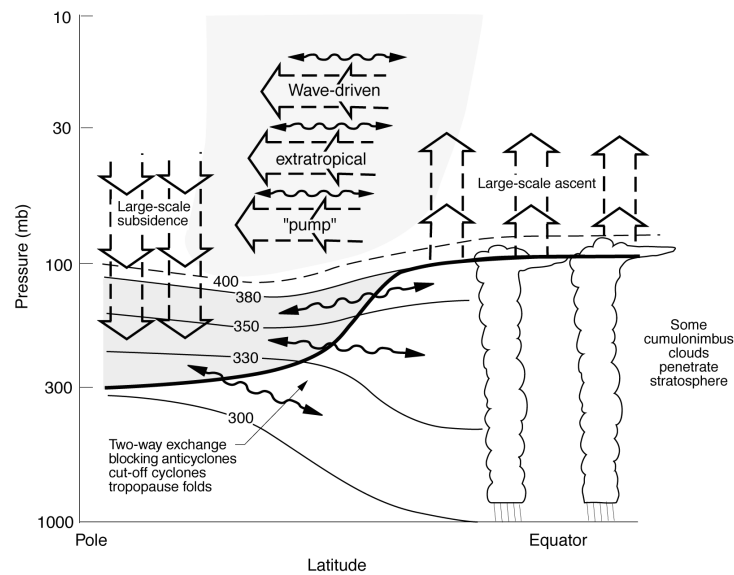


Figure 2.3: Dynamical aspects of stratosphere-troposphere exchange (from *Holton et al.* [1995]). The tropopause is indicated by the thick solid line. Thin lines show isentropic or constant potential temperature surfaces, labelled in Kelvin. The region between the tropopause and the 380 K line is the lowermost stratosphere. The region above 380 K is termed the “overworld”, in which isentropes are located entirely in the stratosphere. The horizontal arrows in the overworld mark poleward air motion due to eddy motion, a global-scale circulation, called “wave driven circulation”. The broad arrows show the vertical transport belonging to this global scale circulation. The wavy double ended arrows denote meridional transport by eddy motions of air along isentrops, including tropical upper tropospheric troughs and their cutoff cyclones, as well as respective midlatitude phenomena. Not all eddy transports are shown, and the two-headed arrows are not meant to imply two way symmetry.

oscillation is described to consist of eastward propagating zonal circulating cells among the equator, associated with variations in tropical convective activity.

- **El Niño southern oscillation (ENSO):** The southern oscillation is characterised by east to west variations in the pressure across the equatorial Pacific. In it, variations in scale and intensity of the so called Walker-circulation² do manifest. The southern oscillation is associated with fluctuations in sea level pressure in the tropics, monsoonal rainfall, and wintertime circulation over the Pacific, as well as fluctuations in the circulation patterns over North America and other parts of the extratropics.

El Niño is the name given to the phenomenon of anomalously warm surface water off the American coast. *Bjerknes* [1969] showed the association between the fluctuations in sea surface temperature and rainfall, and large-scale variations in the equatorial trade wind system. These variations, in turn, affect the major variations of the SO pressure pattern as well as the ocean currents and hence ocean temperatures [*Smith*, 2003].

The coupled ocean-atmosphere phenomenon of the SO and the El Niño are referred to as ENSO.

- **diurnal variations**, including sea and land breezes, mountain and valley winds, and pressure variations. Thermal changes between day and night are the major driving force for the sea and land breeze or mountain and valley wind systems. The cause is the difference of the change

²zonal east to west circulation along the equator, characterised by ascending air in the western Pacific region in the Indonesia region, and descending air in the eastern Pacific, offshore South America.

intensity over the respective surfaces, or high- and lowlands. Proof of the influence of sea and land breezes was found during INDOEX measurements, where it will be discussed in more detail (see section 5.3).

Furthermore, diurnal pressure cycles have been observed, and several theories have been suggested to explain them. The discussion of these theories is beyond the scope of this work, but details can be found in *Frost* [1960] and *Chapman and Lindzen* [1970].

Seasonal variations: the monsoons

The monsoons (from Arabic “Mausim” meaning season) are seasonal variations in regional circulation systems. Their main characteristic is the “seasonal reversal of the prevailing wind system and seasonal contrasts in regimes of cloudiness, precipitation and temperature” [*McGregor and Nieuwolt*, 1998].

The monsoons are generated by

- **differential seasonal heating of the oceans and continents:** different land surface temperatures result in pressure changes and hence seasonal changes in the pressure gradients - the wind driving force. This results in major changes of the winds.
- **moisture processes in the atmosphere:** energy transport in the form of latent heat³ raises the land-ocean pressure difference especially during summer, adding to the strength of the monsoon.
- **the Earth’s rotation:** the Coriolis force, caused by the Earth’s rotation, causes the monsoons to move on curved paths. When crossing the equator, the conversion in the direction of the Coriolis force even brings on a change in wind direction.

The first two generation processes already imply the seasonality of the monsoons, because of the warming up of air above of the huge landmasses during the respective hemispheric summer. This is also the cause of the seasonality of the Hadley cells, which was discussed in the section above. The summer monsoons describe westerly air streams crossing the equator: southwesterly in the Northern Hemisphere, northwesterly in the southern Hemisphere.

Tropical disturbances

Tropical disturbances are initiated by short-term perturbations of pressure, and hence in winds and moisture field, leading to atmospheric instabilities. The condition for this is the presence of warm and humid air in which no inversion exists, hence it can easily become unstable. Upward movement of air leads to the release of latent heat, which in turn reinforces the upward movement. Thus the uplift can reach high atmospheric levels. This process is the main source of energy for tropical disturbances.

Uplift of air can be caused by

- **convection** due to heating from the Earth’s surface
- **convergence** due to the deceleration of air, for example as the trade winds approaching equatorial latitudes or due to surface friction
- **confluence** of air masses, which is often matched by divergence of air at higher altitudes, leading to an uplift of air

³evaporation of water that condensates in the atmosphere subsequently and passing on the evaporation heat to the atmosphere

- **orographic forcing** by mountains and hills or coastlines

The consequence of this vertical transport is the uplift of warm, moist air to higher altitude, where the air is drier. This can cause convective or potential instability, because the air cools at a greater lapse rate than the saturated adiabatic lapse rate. Consequently, the lapse rate is steepened, and the air becomes unstable, which can even result in an overturning of the layer of air, leading to further vertical air movement.

These temporal aberrations lead to a variety of disturbances in the tropics:

- **convective cells**, which can be individual (thunderstorms) or with quasi-circular or linear form (numerous thunderstorms, moving as more or less organised system)
- **cyclonic vortices**: tropical cyclones, which are low pressure systems with no fronts. They occur over tropical or subtropical waters with organised thunderstorm activity.
- **wave disturbances or easterly waves**: troughs of low pressure, extending from southwest to northeast, moving easterly in the Northern Hemisphere.
- **cold air surges**: outbreaks of cold air, which are initiated by baroclinic processes relating to the north-south temperature gradient and the pooling of cold air.
- **subtropical cyclones**, e.g. cyclones from the polar front, which may regenerate into tropical disturbances without fronts.

The result of the tropical disturbances are enhancement of the rainfall intensities and winds. This is of climatological significance because the separate effects sum up to an considerable contribution to the annual rainfall in the tropics. Details on tropical climatology can be found in *McGregor and Nieuwolt* [1998] and *Smith* [2003].

2.4 Chemistry of the atmosphere

The transport phenomena described above play an important role in the chemical composition of the atmosphere. Anthropogenic and biogenic trace gas species can be transported into the stratosphere and play a dominant role in catalytic ozone depletion, there. Conversely, transport from the stratosphere to the troposphere is the main sink for certain trace species, e.g. nitric acid (HNO₃) and NO_x (NO + NO₂), but also brings ozone and other reactive trace species to the upper troposphere. There, ozone is a precursor for the production of OH molecules, the most important detergent of the atmosphere (Figure 2.4): the main decomposition process of naturally and anthropogenically emitted gases is reaction with OH radicals due to their high electron affinity. Therefore, the concentration of OH radicals in the atmosphere is decisive for its self cleaning capacity.

2.4.1 Hydroxyl radicals

The hydroxy radical is a fragment of the water molecule, which is thermodynamically stable. The radical aims to convert to this stable state, (H₂O), by capturing a hydrogen atom from another molecule. Because many of the trace gases in the atmosphere include one or more hydrogen atoms, reactions of the hydroxyl radical with those gases are quite frequent. This causes the generated radical to be much more reactive, more soluble, and hence to be much faster removed from the atmosphere.

OH is formed in the troposphere via photolysis of ozone [*Levy*, 1971]:



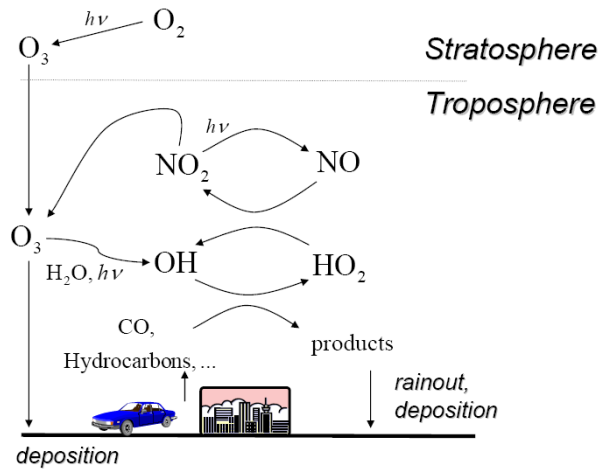
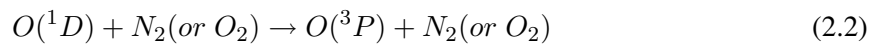


Figure 2.4: Production and destruction cycles of OH - the major oxidising agent of the lower atmosphere. Adapted from *Potter and Colman* [2003].

after which the $O(^1D)$ radical deactivates to the ground state $O(^3P)$ by collision with N_2 (or O_2):



or it reacts with water vapour to form OH radicals:



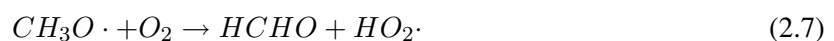
While OH does not react with the main atmospheric constituents N_2 , O_2 , H_2O and CO_2 , its reaction with methane and carbon monoxide is the predominant sink in the global atmosphere. However, in the planetary boundary layer reactions with nitrogen dioxide and formaldehyde also play important roles. The lifetime of OH due to reaction with these gases is in the range of 0.3 to 2.5 s. Thus, continuous production of OH would be necessary to keep the OH concentration in the atmosphere constant. Reactions of OH with methane, carbon monoxide and non-methane hydrocarbons (NMHC) are the fuel for new ozone formation in the free troposphere (with NO and NO₂ acting as catalysts) [Graedel and Crutzen, 1994; Warneck, 2000]. As stated at the beginning of this section, photolysis of ozone is a precursor to OH formation, so that a cycle is formed. During nighttime, when no radiation is available, the OH is diminished very fast.

The methane oxidation cycle

The importance of OH is due to its ability to oxidise hydrocarbons in a chain reaction in the presence of nitric oxide [Weinstock, 1971; Heicklen *et al.*, 1971], in which OH itself is regenerated. In the following, the methane oxidation cycle will be described. The sequence of reactions is initiated by:



where M is an abundant third-body molecule.



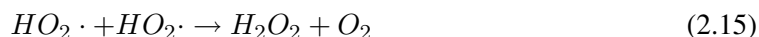
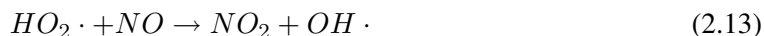
Formaldehyde, HCHO, is an immediate stable product in this reaction sequence. Also, for each consumed OH radical, a new radical, HO₂, is formed.

Formaldehyde can undergo photodissociation or react with OH to form more HO₂ radicals:

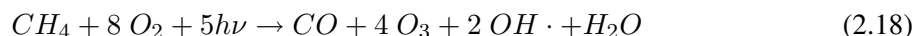


In this sequence, photodissociation of HCHO to HCO is the most important loss process, so that the oxidation of methane produces more than one HO₂ for each OH lost in reaction with methane.

The main reactions of HO₂ are:



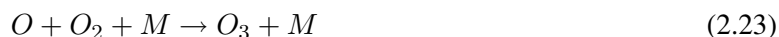
from which only the first two regenerate OH, whereas the other reactions lead to a termination of the chain. The net from this reaction chain is



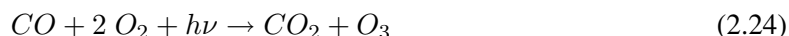
The methane oxidation cycle proceeds with reaction of **carbon monoxide**. CO that was generated either by the above reaction mechanism or was emitted directly into the atmosphere, can react with OH:



This last step is very fast and induces the next chain. In presence of high⁴ NO_x concentrations, NO and NO₂ act as catalyst and ozone is produced:



Which is net:



In the unpolluted atmosphere, where NO_x concentrations are low, the first two steps of the above reaction sequence 2.19 leads to ozone destruction via:



Which is net:



⁴NO to O₃ ratio more than about 1: 4000, which is about 5 to 10 pptv NO in the lower troposphere

Hydrocarbon oxidation cycles

Similar, but more complex reaction cycles take place during the atmospheric oxidation of hydrocarbons, which are emitted anthropogenically, from vegetation and soils, and from the ocean. In general, the oxidation may be initiated via reactions with OH radicals, with NO₃ radicals or with ozone. The oxidation then proceeds via alkylperoxy radicals (ROO·) and alkoxy radicals (RHO·) to generate aldehydes and ketones.

For **alkanes**, e.g. C₂H₅ or C₃H₇, the oxidation via OH can be generalised by:



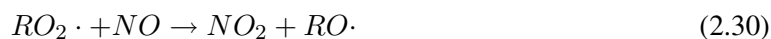
where R is an organic fragment. In air, the alkyl radical only reacts with O₂:



The alkylperoxy radical (RO₂·) reacts primarily with NO, HO₂ and other RO₂·, and during nighttime also reactions with NO₃ play an important role. For larger alkylperoxy radicals, a reaction path exists, in which the stable alkyl nitrate is formed:



But the main reaction is:



By this path, NO is oxidised to NO₂ without loss of ozone. A large amount of ozone can be formed in the atmosphere where of high amounts of NO_x and NMHC are present.

The alkoxy radical, RO·, may then react with O₂, undergo decomposition and isomerisation, depending on their particular structure.

The formation of alkyl radicals (R) from the oxidation of organics is a general characteristic of the latter. Therefore, the principles are transferable to other organics, as well, even if the primary reaction pathway of the initial reaction is addition of OH to the hydrocarbon, like in the case of **alkenes** (in contrast to abstraction of an H atom like in the case of alkanes). Reactions of **alkynes** with OH form as major products corresponding dicarbonyls, e.g. acetylene (C₂H₂) gives glyoxal ((CHO)₂). To describe all those reactions in detail is beyond the scope of this work, but can be found in *Finlayson-Pitts and Pitts [2000]* and *Warneck [2000]*.

2.4.2 Ozone

Ozone plays a central role in the chemistry of the atmosphere. It is highly reactive and absorbs light in the infrared and the ultraviolet range⁵; thereby it contributes to the greenhouse effect and protects the Earth's surface from harmful UV radiation. Moreover, O₃ is a source of OH in the troposphere (see section 2.4.1).

Ozone is mainly produced in the stratosphere by photodissociation of O₂, after which the resulting oxygen atoms can react with other O₂ molecules to form O₃. This mechanism, as well as destruction processes of O₃ via reaction with oxygen atoms, is described by the Chapman cycle [*Chapman, 1930*]. Important destruction pathways in the stratosphere are catalytic destruction by NO_x, as well as ClO_x (= Cl + ClO), HO_x (= HO + HO₂) and BrO_x (= Br + BrO) cycles.

In the troposphere, the main sources of O₃ are injection from the stratosphere, or reaction of HO₂ or CH₃O₂ with NO. O₃ is effectively destroyed at the Earth's surface (deposition velocities ranging between ~0.02 cm/s over water or snow and ~1 cm/s over grass covered soil [*Warneck,*

⁵absorption in the Chappuis band (440 to 850 nm) is weak

2000]), and O_3 is lost by photodissociation with subsequent formation of OH molecules when water vapour concentrations are high, as e.g. in the surface boundary layer, and NO_x concentrations are low. Another sink of O_3 is its reaction with HO_2 or OH [Crutzen *et al.*, 1995]. These complex mechanisms result in a steep gradient of O_3 concentrations with high values in the stratosphere and low values in the troposphere. The reason for the gradient in O_3 concentrations is the slow time scale of mixing in the atmosphere in comparison to the lifetime of ozone. The time scale of transport in the planetary boundary layer is estimated to be about 1 hour, and about 1 month in the troposphere. However, local deep convection events transport air in hours from the boundary layer into the upper troposphere. The time scale for transport from stratosphere to troposphere is about 2 years, or 50 years for vice-versa, respectively [Rodhe, 2000]. The residence time of ozone in the troposphere, which involves only final loss of ozone at the ground and not the frequent photochemical loss and production processes, is about 2 to 3 months. The photochemical lifetime is about 3 weeks, globally. Residence- and lifetimes vary seasonally, with latitude and altitude. For example, the lifetime of O_3 in the tropical forested boundary layer is shorter than 5 days, while it is more than a year in the free troposphere in polar regions [Warneck, 2000; Hauglustaine *et al.*, 1998]. Obviously, mixing between the stratosphere and the troposphere is slower than mixing within the troposphere. In the troposphere, ozone has a strong sink at the ground, but transport time scales are so short, that ozone is rather well mixed.

High concentrations of ozone can exist during hot summer days in strongly polluted areas. Under conditions of high pressure areas with stationary temperature inversions, polluted air may be “trapped” and severe photochemical smog may result. During summer smog, reaction 2.30 is a major by-pass of the following ozone destruction reaction 2.31



Reactions 2.22 and 2.23 follow the formation of NO_2 and so O_3 is produced.

2.4.3 Units of concentration

Concentration is a measure of the amount of one specified element or component in a mixture. In this work, the following *units* are used to express the concentrations of species in the atmosphere:

- The **number density** is the number of particles (e.g. atoms, molecules or aerosols) of a substance per unit volume of air expressed in particles per m^3 or particles per cm^3 .
- The **mole fraction** is the number density of a substance divided by the number density of air (dimensionless variable). The ratio of moles, molecules or volumes of the substance to the number of moles, molecules or volumes in dry air is commonly known as mixing ratio. Atmospheric abundances are expressed in parts per million (ppm), parts per billion (ppb), and parts per trillion (ppt), for example. An index “v” may be added to indicate volume mixing ratios. Another common unit to describe mole fractions is $\mu\text{mol/mol}$, nmol/mol , and pmol/mol . These units correspond to mixing ratios of one molecule of substance in 10^6 , 10^9 , and 10^{12} molecules of air, respectively.

Because the total air pressure, and hence the total number density of air decreases with altitude, a constant mixing ratio does not imply a constant concentration. Concentrations of trace gases in the atmosphere are in general in a range that can be conveniently expressed by mole fractions, or volume mixing ratios in this work. E.g. mixing ratios may be 200 ppbv of CO, or 1.7 ppmv of CH_4 . In contrast, the number density is generally used, when abundances are very low, such as for free radicals like OH (10^4 - 10^6 molecules/ cm^3). The units can be converted into each other using the ideal gas law: $2.46 \cdot 10^6$ molecules/ cm^3 = 0.1 ppt = $0.1 \cdot 10^{-12}$ at 1 atm total pressure and 25°C .

Chapter 3

Variability

The study of the relationship between the variability of trace gas concentrations and their respective residence times is a powerful tool for the assessment of data quality and the understanding of chemical and dynamical processes in the atmosphere, and has gained considerable attention recently.

In the following chapter the variability concept and its application for estimating OH mixing ratios is introduced. First the methods of measuring atmospheric OH concentrations are summarised. After that, the decomposition of trace gases is discussed, and the term “lifetime” is defined for further use in this work. Subsequently, the variability of trace gas mixing ratios as consequence of the aging processes of air masses is pointed out and the relation between variability and lifetime is introduced. In addition, a theoretical introduction of the variability lifetime formula is given and the formal use of the variability method to estimate OH concentrations will be explained in detail. Finally, processes affecting variability are discussed.

3.1 Estimation of OH concentrations

The hydroxyl radical (OH) plays an important role in atmospheric chemistry. Since it is the main oxidising agent in the lower atmosphere, it influences the trace gas composition [Graedel and Crutzen, 1994]. As it initiates the oxidation of most anthropogenic trace gases, a change in the OH concentration could have a considerable effect on the chemistry of the atmosphere.

3.1.1 Global model simulations of OH

The Global simulations of OH concentrations are generally carried out using 3-D models. In this section, three types of models will be briefly introduced, which are distinguished by the category of constraints: a) emission sources and atmospheric transport, b) observed distributions of OH precursors, c) observed distributions of OH proxies. The following overview is adopted from Wang [2000].

The *chemistry and transport model* is the most general type of these three models, and not specially designed to calculate OH distributions. It simulates the primary components of the natural system, emissions, atmospheric transport, chemistry, and deposition. The transport is implemented by the use of meteorological fields from weather forecast models or general circulation models. Emissions for NO_x, CO, and nonmethane hydrocarbons (NMHCs) are implemented, and often CH₄ concentrations are specified in the models. Figures 3.3 (b) to (d) from Lawrence *et al.* [2001] shows annual zonal mean OH fields from the tropospheric photochemistry version (MATCH-MPIC [Lawrence *et al.*, 1999, 2003a]) of the Model of Atmospheric Transport and Chemistry (MATCH [von Kuhlmann *et al.*, 2003a]). Differences in the OH distributions result from changes in the model. Figures 3.3 (a) shows results from Spivakovsky *et al.* [2000], derived by *precursor-constrained modelling*. By con-

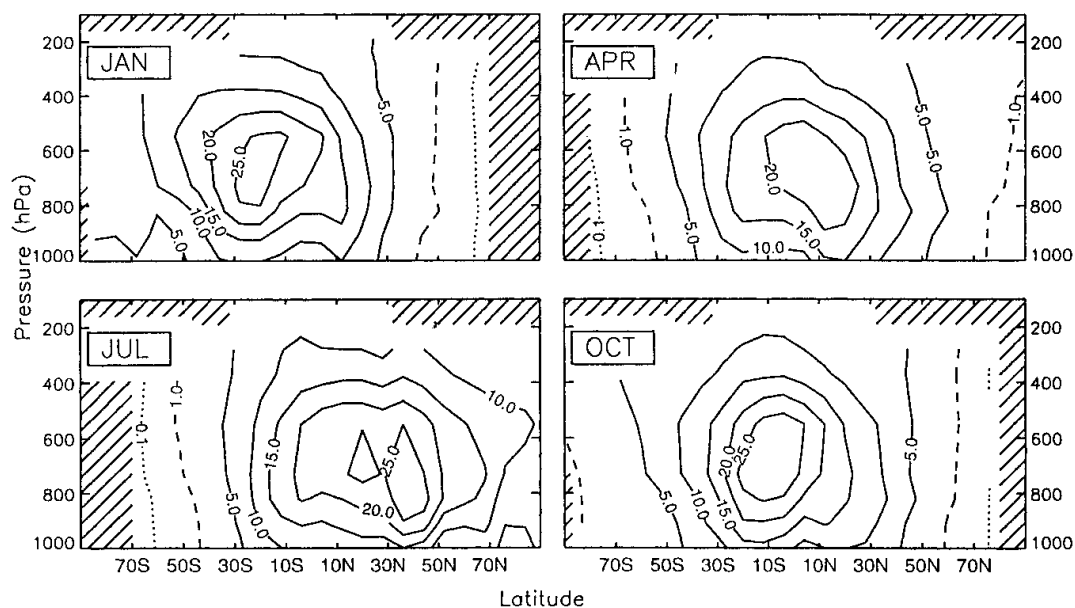


Figure 3.1: Zonally and monthly 24h averaged OH concentrations [10⁵ molecules/cm³] for January, April, July, October. The contours are given for 0.1 (dotted lines), 1 (dashed) and from 5 to 30, with increments of 5 (solid). From *Spivakovsky et al.* [2000].

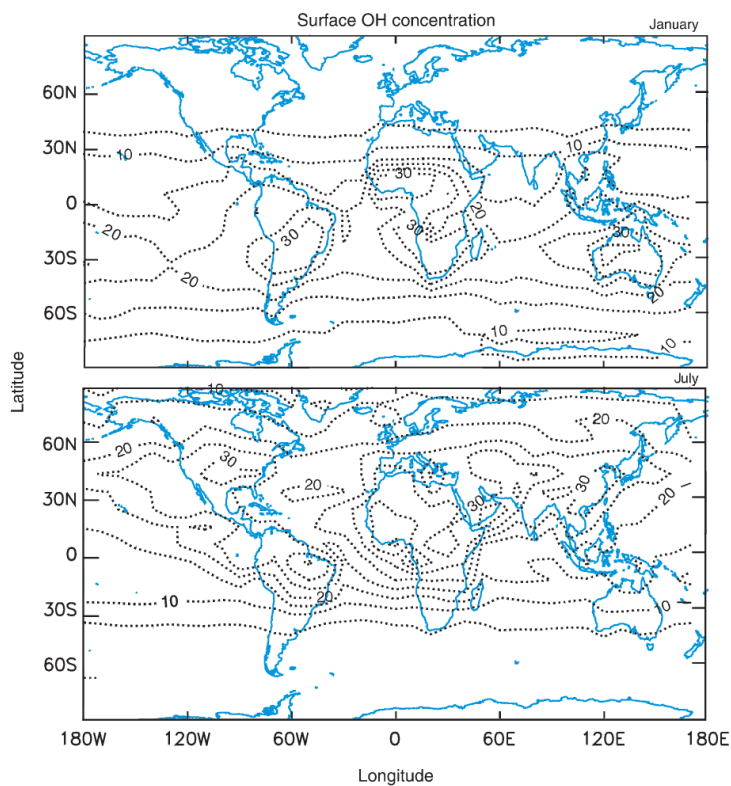


Figure 3.2: Monthly 24h averaged OH distribution [10⁵ molecules/cm³] at 700 hPa for January (top) and July (bottom). Contours are given for values from 5 to 50 with increments of 5. From *Spivakovsky et al.* [2000].

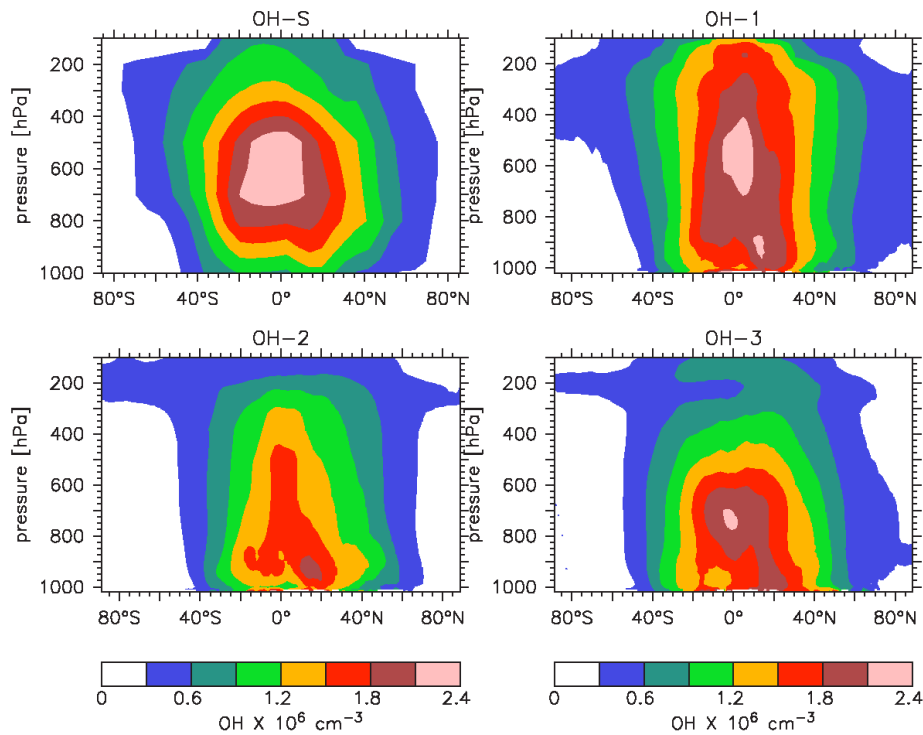


Figure 3.3: Annual zonal mean OH fields based on four different distributions: (a) from *Spivakovsky et al.* [2000], (b) from *Lawrence* [1996], (c) from *Lawrence et al.* [1999] and (d) from *von Kuhlmann* [2001]. Figure from *Lawrence et al.* [2001].

straining the model to atmospheric observations, uncertainties in emissions and atmospheric transport can be reduced to some extent. Figure 3.1 and 3.2 show OH concentration distributions derived by compilation of climatologies for meteorological variables and OH precursors including O_3 , CO, NO_x , and hydrocarbons from available atmospheric observations and subsequent application of these data to global OH simulations [*Spivakovsky et al.*, 2000]. Figure 3.1 gives an overview of the zonally and monthly averaged OH concentrations for 4 different months computed by *Spivakovsky et al.* [2000]. Figure 3.2 shows the OH distribution at 700 hPa around the globe from the same model. The OH concentrations vary with altitude and geographical location and seasonally. However, the formation mechanisms, as presented in section 2.4.1, explains the main features of global OH distributions (see Figures 3.1 to 3.3): the formation of OH is controlled by O_3 , UV radiation and water vapour. The UV-radiation flux depends on the solar zenith angle and the overhead ozone column. Therefore, OH concentrations are highest in the tropics, where the amount of stratospheric ozone is smallest, and the humidity, especially at the Earth's surface, is highest [*Graedel and Crutzen*, 1994; *Lelieveld et al.*, 2002].

The *proxy-gas constrained model* type inversely deduces global OH concentrations from long-term observations of OH proxy gases, e.g. CH_3CCl_3 . CH_3CCl_3 is emitted by industry and is decomposed by OH. Losses to the oceans and in the stratosphere are minor compared to reaction with OH. Initialised with a priori global OH concentrations, taken for example from global chemistry and transport models, the objective of the proxy-gas constrained modelling is to find the global mean OH concentration and temporal trend that best reproduces the observed CH_3CCl_3 [*Prinn et al.*, 1995; *Krol et al.*, 1998].

3.1.2 Measurement methods for the hydroxyl radical

Hydroxyl radicals are difficult to measure directly, because of low atmospheric concentrations (10^5 to 10^6 molecules/cm³ during daytime and 10^4 molecules/cm³ or less during nighttime [Finlayson-Pitts and Pitts, 2000]) and their short lifetime (~ 1 s). Nevertheless, in-situ OH measurements have been performed by laser-induced fluorescence (LIF) [Wang and Davis, 1974; Brauers et al., 1996; Chan et al., 1990], long-path differential optical absorption spectrometry (DOAS) [Perner et al., 1976] and mass spectrometry [Eisele and Tanner, 1991].

Laser-induced fluorescence is a spectroscopic method, in which the laser frequency is kept at a specific transition of the target molecule or atom. The fluorescence wavelength may be longer than the absorption wavelength, but in any case, absorption and fluorescence are characteristic for a given molecule. The fluorescence intensity is a measure for the target molecule concentration. Compared to absorption spectroscopy, LIF has the advantage of higher sensitivity.

Another optical method for determining in-situ OH concentrations is long-path differential optical absorption [Perner et al., 1976], which uses light in the ultraviolet (UV) and visible range. Since the absorption bands of the target molecules superimpose with Rayleigh and Mie scattering, the “true” background intensity in absence of the molecule can not be measured. Nevertheless, broad scanning of the spectral region allows to interpolate the superimposed absorption background. The difference of the absorbed intensity relative to this background is used to calculate concentrations. Advantages of DOAS are its high sensitivity for species with narrow absorption bands in the UV and visible range, and that it can be used in open-path configuration, allowing measurements of chemically active species, species with very low concentrations, background measurements over wide areas and fence-line monitoring.

Measurement of OH with mass spectrometry is also possible [Eisele and Tanner, 1991]. The technique is based on the reaction of OH with isotopically labelled $^{34}\text{SO}_2$ to produce $\text{H}_2^{34}\text{SO}_4$. $\text{H}_2^{34}\text{SO}_4$ is not present in the natural atmosphere in measurable quantities, but can be quantified by mass spectrometry. The concentrations of this labelled H_2SO_4 is equal to the initial OH (conversion efficiency > 99 %). Further addition of HNO_3 , which reacts to NO_3^- (HNO_3), and proton transfer to $\text{H}^{34}\text{SO}_2(\text{HNO}_3)$ leads to HSO_4^- ions, which are then detected. Quadrupole mass spectrometers are used for mass separation. With this method, very low concentrations of OH can be measured when integration times are sufficiently long.

All above described measurements require lots of effort, large instrumentation and expertise. Moreover, those measurements give a momentary, local view of atmospheric OH concentrations.

An indirect method to assess OH concentrations is by budget analysis of CH_3CCl_3 [Singh, 1977] or ^{14}CO [Brenninkmeijer et al., 1992]. These methods provide averaged OH concentrations on a global or hemispheric scale. For particular air masses, indirect estimation of OH concentrations is also possible by analysing the relative decay rates of several hydrocarbons [Blake et al., 1993]. This method assumes that there are no sinks other than reaction with OH, and no mixing with air masses of different composition. However, the use of ratios of trace gases should account for mixing with zero background air [McKenna et al., 1995]. Both assumptions are often not met in the real atmosphere.

spacial scale	mode	method
local	in-situ	LIF, CIMS, DOAS
global	indirect	CH_3CCl_3 , ^{14}CO
regional	indirect	hydrocarbon ratios, variability

Table 3.1: Measurement methods for the hydroxyl radical. For a description of the methods see text.

The estimation of the OH concentration from the variability-lifetime relation (which will be ex-

plained in the rest of the chapter), is not biased by mixing processes, but one has to be aware that if mixing between different air masses has occurred, the derived OH concentration is valid for the resulting mixed air mass. The OH concentrations derived from the variability-lifetime relation are valid along the trajectory of the sampled air masses. In contrast to the hydrocarbon method, additional sinks (other than reaction with OH) are no problem, as long as they can be quantified. The implementation of this method will be demonstrated in detail in section 3.6 and the chapters 5 and 6.

In this work, OH concentrations from airborne trace gas measurements in the marine boundary layer during INDOEX and in the troposphere and lowermost stratosphere during STREAM 98 are derived using the variability-lifetime relationship.

3.2 Decomposition of trace gases

When a trace gas is decomposed, for example by reaction with OH, its concentration diminishes with time. Obviously, the faster the decomposition process, the faster the concentration diminishes (see Figure 3.4). This connection leads to the definition of lifetime, which will be discussed in the next section.

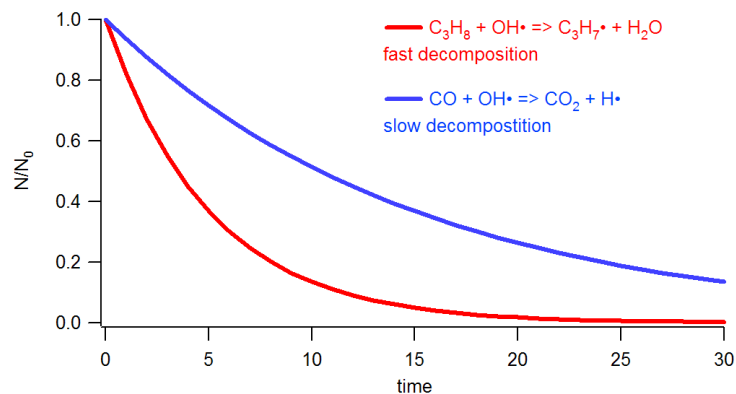


Figure 3.4: The effect of decomposition on the mixing ratio of trace gases over time.

3.3 Definitions of lifetime in an atmospheric reservoir

Before we turn to the details of the variability method, it is important to survey the definitions of time constants of a trace gas in an atmospheric reservoir, such as turnover time, residence time and lifetime. In a reservoir, the total mass of a trace gas is determined by its internal production, internal destruction (e.g. due to chemical reactions) and fluxes in mass entering and leaving the reservoir through the boundaries. The following definitions of turnover time and residence time have been adopted from Rodhe [2000]. The term lifetime, as it is being used in the context of this work, will be defined at the end of this section.



Figure 3.5: Reservoir scheme

3.3.1 Turnover time

The *turnover time* is the time needed to empty a reservoir of a substance, after turning off all sources but keeping the sinks constant (see Figure 3.5). Therefore, it is often called *renewal time* or *flushing time*. In mathematical form, the turnover time τ_0 is described as the rate of the amount M of a substance in a certain reservoir divided by the total flux S of this substance leaving the reservoir:

$$\tau_0 = \frac{M}{S}, \quad (3.1)$$

or, when several removal processes S_i are involved:

$$\tau_0^{-1} = \sum \frac{1}{\tau_{0i}}. \quad (3.2)$$

In the latter case, obviously, the fastest processes dominate the total turnover time of the species. If the sink of the species in the reservoir is proportional to the species' concentration, then a proportionality constant k ($S = kM$) can be defined analogous to first order chemical kinetics law, and for the turnover time follows

$$\tau = \frac{1}{k}. \quad (3.3)$$

3.3.2 Residence time

The *residence time* is the time, that a single atom or molecule stays in the reservoir. When a physical transport from source to sink is given, one can also use the term *transit time*. Individual atoms or molecules of the substance have different residence times in the reservoir, due to macro- or micro-physical effects, or chemical processes. The *average residence time* of individual species in the reservoir is given by

$$\tau_r = \int_0^{\infty} \tau \phi(\tau) d\tau \quad (3.4)$$

where the probability density function of residence times is given by $\phi(\tau)$ and $\phi(\tau)d\tau$ describes the fraction of atoms or molecules with residence times in the interval between τ and $\tau + d\tau$. In the literature, it is common to shorten the term *average residence time* to *residence time*. We will follow this convention in the subsequent text.

3.3.3 Age

In addition, the term age can often be found. The age of a molecule in a reservoir is the time since it entered the reservoir. Analogous to the section above, the average age of the substance is given by

$$\tau_a = \int_0^{\infty} \tau \Psi(\tau) d\tau \quad (3.5)$$

where the probability density function $\Psi(\tau)$ describes the ages of the individuals, and $\Psi(\tau)d\tau$ describes the fraction of atoms or molecules with residence times in the interval between τ and $\tau + d\tau$. An "everyday life"-example illustrates the difference between residence time and age: the average life expectancy of men is the average residence time of men on Earth. In contrast to that, the average age is the average of age of men living "now".

3.3.4 Lifetime

Depending on the publication, the term *lifetime* is used instead of the terms above. Some authors even mix the terms residence time and turnover time, which complicates reading even more. *Junge* [1974] uses the (*tropospheric*) *residence time*, stating that *Bolin and Rodhe* [1973] called this *turnover time*. In his paper, the loss processes include chemical processes in the reservoir and its boundaries (e.g. the Earth's surface) as well as loss by transport through the boundaries, for example transport across the tropopause. *Jobson et al.* [1998] used “(*global atmospheric*) *lifetime* or *residence time*”, to describe

$$\tau = \frac{\text{atmospheric burden}}{\text{atmospheric loss}} \quad (3.6)$$

Similar to this, *Johnston et al.* [2002] wrote: “The *global mean atmospheric lifetime* (τ) is an integrative measure of the sinks, relating atmospheric loss to atmospheric burden in steady state conditions.” In the end, all authors who work on variability refer to the terms lifetime and residence time in a way that is formally known as the turnover time. However, in steady state turnover time and residence time, as defined above, are equal [*Eriksson*, 1971; *Bolin and Rodhe*, 1973]. In the following text we will use the term lifetime in the meaning of turnover time, adopting the definition of *Johnston et al.* [2002], given above.

3.4 What is variability?

Intuitively, one expects the concentration of atmospheric trace gases with short lifetimes to vary strongly, both temporally and spatially, depending on the distance from their sources. Close to the sources, or after short transit time, relatively high concentrations prevail. Concentrations will fall off strongly further from the source, or after longer transit time. Figure 3.6 schematically illustrates the outflow of a trace gas from a constant point source (here an isolated island), and its measurement at some distance. Figure 3.6 (a) shows the result of the decomposition of the trace gas at different measurement locations, Figure 3.6 (b) shows the result for measuring after different travelling times of the air mass. For Figure 3.6 (b), the different transit time could as well be due to a change of the travelling path, or due to a change in the wind speed along the same travelling path. A reduction of the trace gas mixing ratio will be found in all these cases, since it is an effect of the aging of the air mass.

3.4.1 Variability in trace gas mixing ratios

When performing airborne measurements, the sampling averages over both, space and time. An example for the aging effect of air masses can be seen in Figure 3.7, showing carbon monoxide measurements performed during the INDOEX aircraft campaign, which will be discussed in detail in chapter 5. Due to the transport pattern over the northern Indian Ocean, air masses in the marine boundary layer contain relatively fresh pollution, whereas air masses at higher altitudes are more aged. In the young air masses at low altitudes the CO concentrations are higher than in the aged air masses at higher altitudes. The same effect can also be seen with other species, as shown in Figure 3.8, for CO, benzene and isoprene. The left column Figure 3.8 gives the time series of their mixing ratio, clearly showing their variation. A clearer view of the variation of a measured trace gas is obtained from a histogram of the measured values. The right column of Figure 3.8 shows the corresponding histograms for the three species. A wider range of trace gas mixing ratios gives broader histograms. The standard deviation is a measure for the variability of the trace gas. The relative standard deviation¹, which is also given in the figure, increases from CO to benzene to isoprene.

¹ standard deviation divided by the average

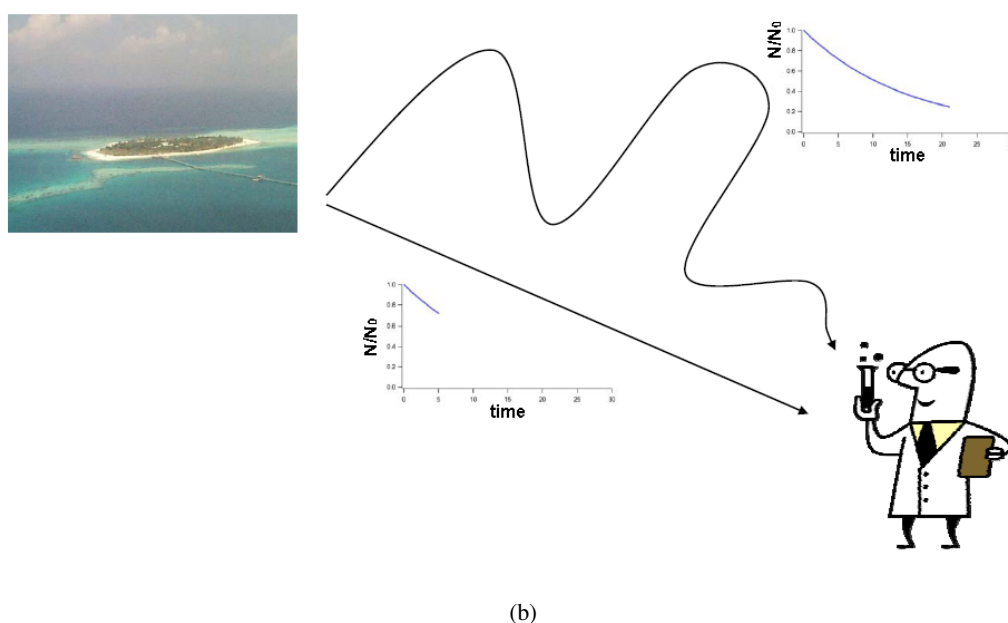
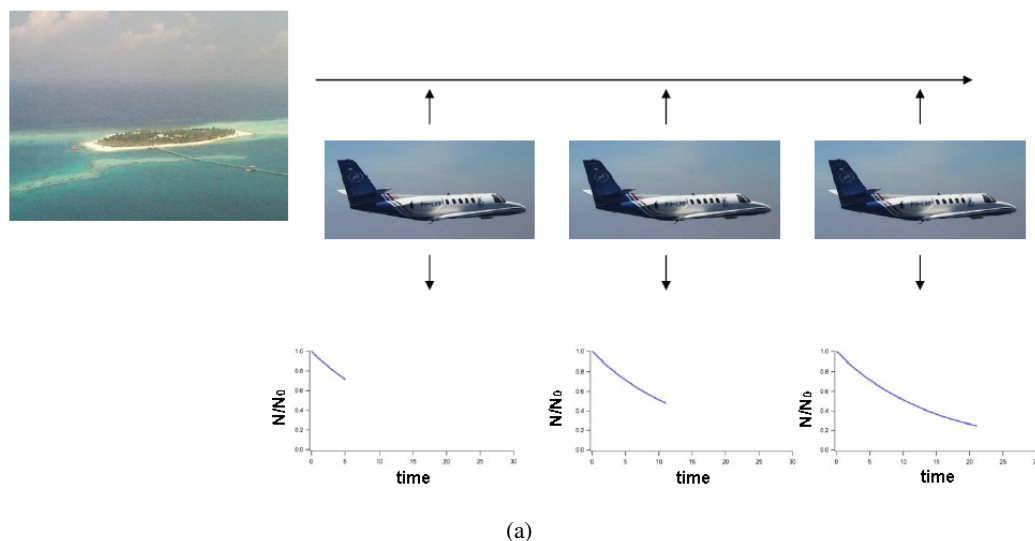


Figure 3.6: Measurements of an atmospheric trace gas at different locations (a) or at different times (b)

A comparison shows that in contrast to the relative standard deviation, the lifetime of the species decreases from CO to benzene to isoprene. For INDOEX, the lifetimes were 14 days (CO), 2.6 days (Benzene) and 0.034 days or ~ 2 hours (Isoprene). Atmospheric components with long lifetimes are more evenly distributed in the atmosphere, hence their mixing ratios show a lower variation. So, the smaller the lifetime, the bigger the variability. This relation between lifetime and variability can more easily be seen, when graphed, as in Figure 3.9.

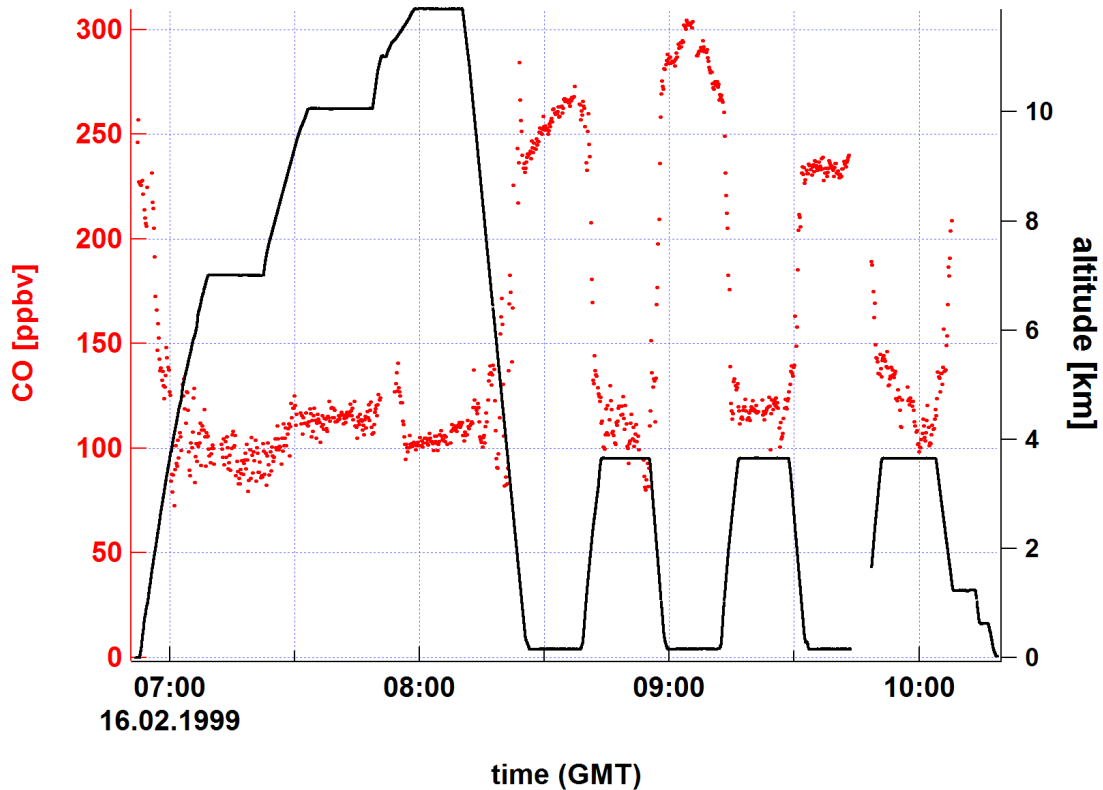


Figure 3.7: Time series of the trace gas CO (red dots) measured onboard the research aircraft Citation during the INDOEX campaign on February 16, 1999. The measured CO concentration shows a distinctive dependence on the flight altitude (black solid line) of the aircraft: high concentrations prevail in young air masses at low altitudes and lower concentrations in older air masses at higher altitudes.

3.4.2 Variability in different reservoirs

In section 3.4.1 the variability of trace gas concentrations in the atmosphere was demonstrated with the help of INDOEX measurements. When scrutinising the data, however, different trace gas mixing ratios are found not only at different altitude levels, but also within individual atmospheric levels. This is demonstrated in Figure 3.10(a), where the gray shaded areas highlight the measurements taken below 1 km altitude (marine boundary layer). The histogram 3.10(b, left) shows the entire record, whereas histogram 3.10(b, right) only shows data below 1 km altitude. Of course, the range of data values is narrowed in the lowest atmospheric level, but still atmospheric variability is observed. The distribution of the data values is broader than the instrumental noise (grey shaded area) of the measuring device. This means that the distribution is a result of atmospheric processes and not an instrumental artifact.

Figure 3.11 displays the variability versus lifetime of the entire record and the one restricted to the lowest 1 km altitude. Obviously, a correlation is present in both cases, but slope and especially axis intercept are different. This shows, that for the interpretation of the results it is very important to carefully consider the reservoir that is analysed.

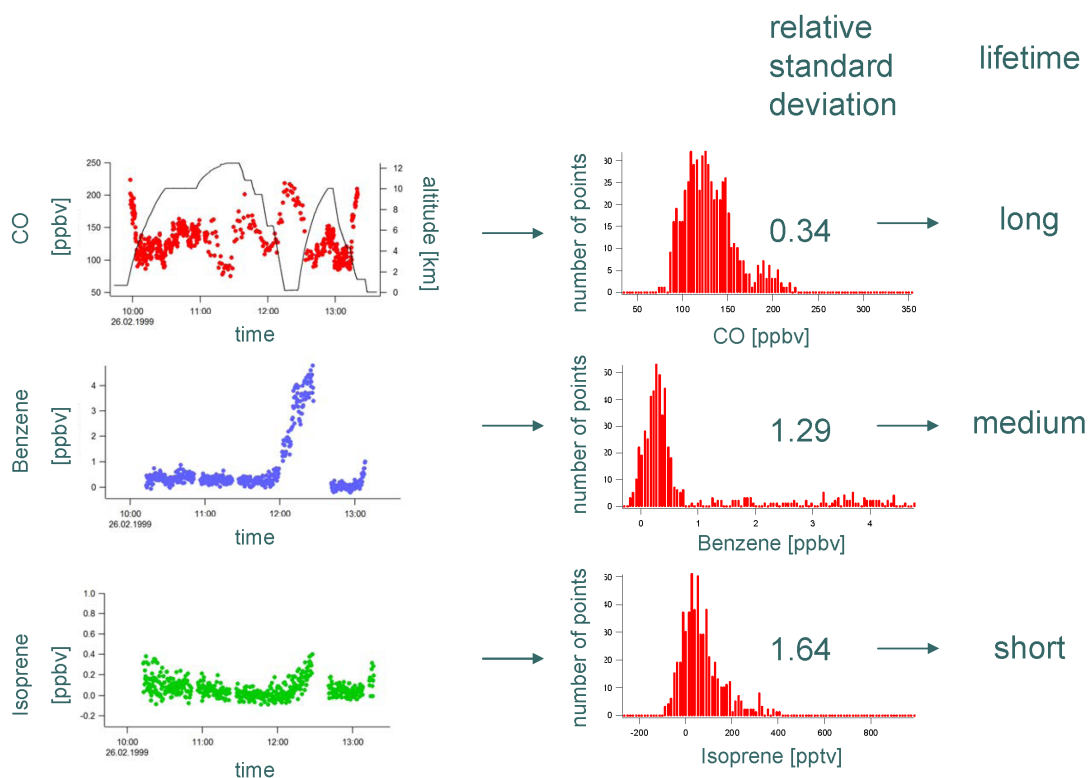


Figure 3.8: Variability of measured data. Time series of CO (red dots), benzene (blue dots) and isoprene (green dots) and flight altitude data (black line) measured onboard the Citation during INDOEX on February 26, 1999. The right part of the graphics shows histograms of the measured mixing ratios for each trace gas, including its relative standard deviation. For INDOEX, the lifetimes were 14 days (CO), 2.6 days (Benzene) and 0.034 days or ~ 2 hours (Isoprene).

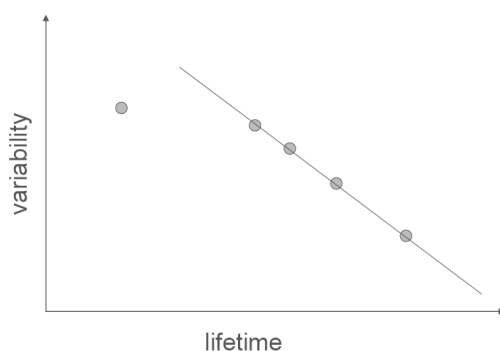


Figure 3.9: Relation between variability and lifetime: the smaller the lifetime, the bigger the variability.

3.4.3 Derivation of the variability-lifetime relationship

Junge's approach

Whereas the concept of the variability-lifetime relationship is an intuitive one, a derivation of the general mathematical relationship between the trace gas variability and lifetime is more challenging. *Junge* [1974] made a first attempt in deriving a mathematical formulation by evaluating the relative

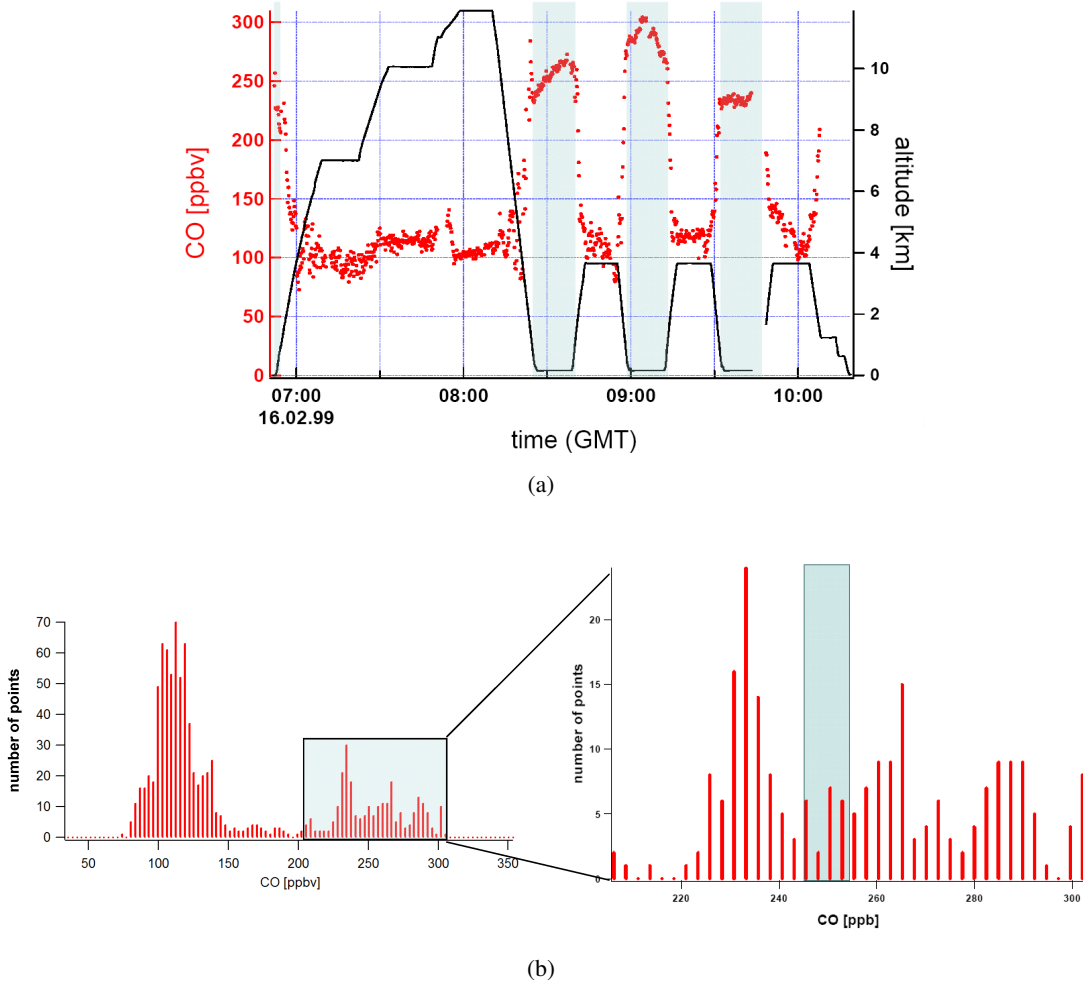


Figure 3.10: Variability in trace gas mixing ratios. CO measurements taken onboard the Citation aircraft on February 16 during the INDOEX campaign. (a) Even within one atmospheric layer, variability of trace gases can be seen. The grey shaded areas show altitudes below 1 km. (b, left) Histogram of the measured mixing ratios for the whole flight. (b, right) Histogram of the measured mixing ratios below 1 km altitude. The axis range of (b, right) corresponds to the grey shaded area in (b, left). The gray shaded area in graph (b, right) indicates the error of the instrument, which is significantly smaller than the atmospheric variability.

standard deviation σ' , or RSD, of a trace gas as a measure for tropospheric variability:

$$\sigma'(X') \equiv \frac{\sigma(X')}{\bar{X}} \quad (3.7)$$

where the mixing ratio X of a gas was splitted into its average \bar{X} and the deviation from that average, X' :

$$X = \bar{X} + X' \quad (3.8)$$

and the standard deviation σ is defined as:

$$\sigma = \sqrt{\frac{1}{n-1} \sum (X_i - \bar{X})^2}. \quad (3.9)$$

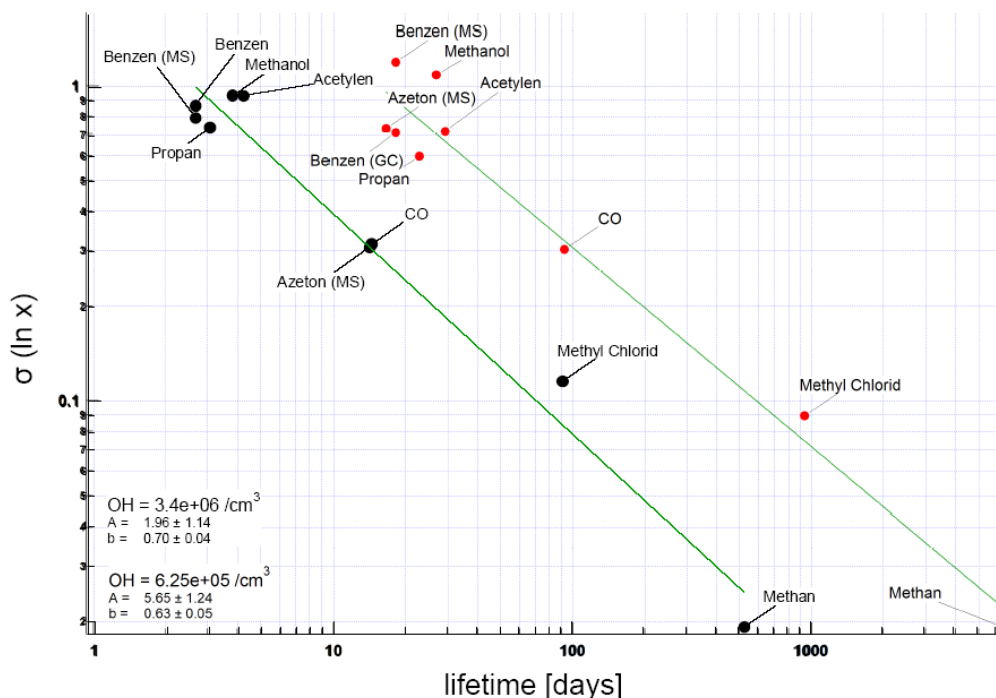


Figure 3.11: Variability in different layers - the right data set (red circles) is for the whole troposphere, the left (black circles) incorporated only data of the lowest 1 km altitude.

in which n is the number of points, X_i the data value for the point i , and \bar{X} is the average value of all data points X_i . In his considerations, *Junge* [1974] regarded the whole troposphere as reservoir for trace gas species. This corresponds to the concept introduced in section 3.3.1. He assumed that the reservoir is in equilibrium state, and that the averaging time was long enough so that all averages were constant. Then the turnover time (equation 3.1), as defined in section 3.3.1, is given by

$$\tau = \frac{M_{tot}}{Q_{tot}} \quad (3.10)$$

Here, M_{tot} is the total mass of the compound in the reservoir and Q_{tot} are global sources. For the idealised case of an isobaric atmosphere M_{tot} is

$$M_{tot} = C \cdot \bar{X} \quad (3.11)$$

where C is a constant related to the molecular weight of the trace gas, the average molecular weight of the air and the total mass of air in the atmosphere. Using equation 3.11 in equation 3.10 gives

$$\bar{X} = \frac{Q_{tot}}{C} \cdot \tau \quad (3.12)$$

and together with equation 3.7

$$\sigma'(X') = \sigma(X') \cdot \frac{C}{Q_{tot}} \cdot \frac{1}{\tau} \quad (3.13)$$

Obviously, $\sigma(X')$ is influenced by sources and sinks. For species which are removed by photochemical processes or by reaction with e.g. OH, the sinks are distributed quite uniformly throughout the atmosphere. Therefore their variability is caused only by their sources. When the source strength is

independent of the atmospheric mixing ratio of the species, then $\frac{\sigma(X')}{Q_{tot}}$ is equal for all species with the same source locations. Then equation 3.13 can be written as

$$\sigma'(X') = A \cdot \tau^{-1} \quad (3.14)$$

Jobson's approach

As demonstrated by *Junge* [1974] an expression for the variability–lifetime relationship can be found, using a steady state treatment. In addition, other authors attempted to theoretically derive the variability–lifetime relationship. *Gibbs and Slinn* [1973] used a stochastic analysis approach to describe the temporal concentration variation of exponentially decaying trace gases at one point in space over time. *Jaenicke* [1982] and *Slinn* [1988] made an approach in considering the statistics of an exponentially decaying function sampled over a finite period. However, *Jobson et al.* [1998] noted that the previous authors had “yielded results that are difficult to reconcile and to apply in the real atmosphere”. *Jobson et al.* [1998] found the exponential approach could be improved, by using the logarithm of the mixing ratios, instead of the relative standard deviation.

Jobson's approach assumed the absence of atmospheric mixing. He further assumed that the trace gas mixing ratio in an air parcel decreases linearly with time due to a first order removal process (see section 3.7), e.g. oxidation by OH. If so, the time dependant mixing ratio of the species is described by an exponential decay law and the ln–transformed mixing ratio can be written as

$$\ln \frac{X}{X_0} = -\frac{t}{\tau} \quad (3.15)$$

where t is the time between emission and sampling, X_0 is the initial mixing ratio and τ is the $1/e$ –lifetime. When a data set consists of air parcels with the same initial mixing ratio but with varying t , the variance of equation 3.15 is given by

$$\sigma_y^2 = \left(\frac{\partial}{\partial t} \ln \left(\frac{X}{X_0} \right) \right)^2 \sigma_t^2 = \left(\frac{-1}{\tau} \right)^2 \sigma_t^2 \quad (3.16)$$

when τ is constant. Hence,

$$\sigma_y = \frac{1}{\tau} \sigma_t \quad (3.17)$$

Or, since X_0 is constant and does not contribute to the standard deviation,

$$\sigma_y = \sigma \left(\ln \frac{X}{X_0} \right) = \sigma(\ln X) = \frac{1}{\tau} \sigma_t \quad (3.18)$$

Hence for chemical kinetic conditions the standard deviation of the ln-transformed data is inversely proportional to the lifetime.

Figure 3.12 shows a double-logarithmic plot of the general relationship

$$\sigma_{\ln x} = A \cdot \tau^{-b}, \quad (3.19)$$

Obviously, the parameters A and b in the last equation can be derived from the axis intercept and slope of the straight line. As shown above, with purely chemical kinetic conditions, the parameter b equals 1 and A is the standard deviation of sampled transit times.

For species with long lifetime and thus low variability, the ln-transformed standard deviation used by *Jobson et al.* [1998] and the relative standard deviation used by *Junge* [1974] converge. This can be demonstrated by substituting equation 3.8 in equation 3.18:

$$\sigma(\ln X) = \sigma(\ln(\bar{X} + X') - \ln \bar{X}) = \sigma \left(\ln \frac{\bar{X} + X'}{\bar{X}} \right) = \sigma \left(\ln \left(1 + \frac{X'}{\bar{X}} \right) \right) \quad (3.20)$$

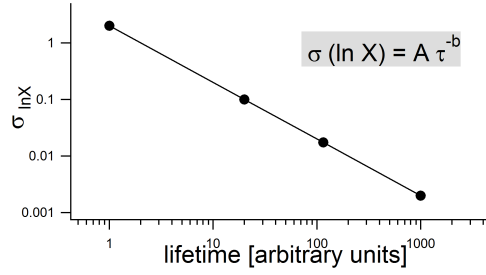


Figure 3.12: Variability - lifetime relationship

For $X' \ll \bar{X}$ (low variability) the approximation $\ln(1 + y) \approx y$ can be used, so that

$$\sigma(\ln X) = \sigma\left(\frac{X'}{\bar{X}}\right) = \frac{\sigma(X')}{\bar{X}} \quad (3.21)$$

Combining Ehhalt's and Jobson's approach

Ehhalt et al. [1998] introduced an exponential decay formula for the description of the decrease of trace gas concentrations downwind of their sources, including terms for transport and mixing with background air. It is easier to recognise the origin of the respective terms in the mixing ratio formula, when only transport (mixing) and chemical loss are considered. Thus, for the sake of clarity, at first the background mixing ratio will be assumed to be zero. On that condition, *Ehhalt et al.* [1998] followed *McKeen et al.* [1990] in assuming that the function describing the decrease of the trace gas mixing ratio could be separated into two terms, one “solely depending on transport $T(t, x)$, and the other solely depending on chemical loss $L(t, x)$ ”. They used a Lagrangian approach and further assumed that the chemical operator is given by an exponential decay in time. Thus the mixing ratio of a species can be written as

$$M(t, x) = M(0, x) \cdot T(t, x) \cdot e^{-\left(\frac{t}{\tau}\right)} \quad (3.22)$$

where t is the time since the observation at time zero, x represents the geographical coordinates and τ is the chemical lifetime. $T(t, x)$ is the transport function with τ_{trans} as time constant for mixing or dilution with background air of vanishing trace gas concentration:

$$T(t, x) = e^{-\left(\frac{t}{\tau_{trans}}\right)} \quad (3.23)$$

The time constant T_{trans} is assumed to be the same for all species.

In a second step, they assumed that the air parcel could mix with background air that had the finite mixing ratio MB instead of zero. The differential equation for the mixing ratio of each species is

$$\frac{dM}{dt} = -\frac{M}{\tau} - \frac{M - MB}{\tau_{trans}} \quad (3.24)$$

The solution of this equation is

$$M(t) = \frac{MB}{1 + \frac{\tau}{\tau_{trans}}} + \left[M(0) - \frac{MB}{1 + \frac{\tau}{\tau_{trans}}} \right] \cdot e^{-t \cdot \left(\frac{1}{\tau_{trans}} + \frac{1}{\tau} \right)} \quad (3.25)$$

When we use 3.25 in Jobson's approach, we derive

$$\sigma(\ln M) = \sigma_t \cdot \left[1 + \left(\frac{M(0)}{MB} \cdot \left\{ 1 + \frac{\tau_{trans}}{\tau} \right\} - 1 \right)^{-1} \cdot e^{t \cdot \left(\frac{1}{\tau_{trans}} + \frac{1}{\tau} \right)} \right]^{-1} \cdot \left(\frac{1}{\tau_{trans}} + \frac{1}{\tau} \right) \quad (3.26)$$

When the background term MB in this equation is set to zero, the solution for the first approach (equation 3.22) is derived. Considering solely chemical loss by setting MB to zero and the time constant τ_{trans} to infinity, the simpler formula from Jobson's approach is obtained. The solution 3.26 looks rather complicated, however, expressions for A and b like in equation 3.19 can be derived.

3.5 A historical review

Junge [1963] and *Junge et al.* [1971] were the first to formulate the dependency between variability and the tropospheric residence time τ . They investigated the spatial variability of trace gases over the global troposphere, supposing that the gases had similar sources (same source functions) and fairly uniformly distributed sinks, that they were well mixed in the troposphere and in steady state condition, and that the period of data averaging was at least one year². *Junge* [1974] applied 2-D numerical calculations for species with lifetimes from 5 days to 1.5 years. The upper limit in lifetime was chosen due to limited computer time. He found that the relative standard deviation³ (RSD) of mixing ratios is inversely proportional to the residence time τ of the species:

$$RSD = \frac{\sigma}{\bar{x}} = A \cdot \tau^{-b} \quad (3.27)$$

where A and b are proportionality parameters. Obviously, the unit of A depends on the value of b . In fact, the unit is $(1s)^b$. As b changes with every data set, and even for a single data set ranges or uncertainties of b are calculated, this would lead to rather unreadable expressions for results in A (for which also ranges and uncertainties are calculated, which then relate to different b values). Therefore, the unit of A is omitted in this text, which is also in accordance with the literature. However, it should be kept in mind, that A has the unit of $(1s)^b$.

For the model data *Junge* [1974] found the values $A = 0.0216$ and $b = 0.95$. From measured data, he determined: $RSD = \frac{0.14}{\tau}$, known as the Junge relationship. However, *Junge* [1974] found this formula was only valid for species with tropospheric residence times greater than about one week, using lifetimes between 5 days (radon) and 10^7 years (helium).

In his theoretical approach, *Junge* [1974] used the assumption that the variation of the sinks is much smaller than the variation of the sources ("fairly uniform sinks"). After reviewing his results, he noted that the deviation of b from 1.0 might reflect that this assumption was not fulfilled in the numerical model/experiment. With regard to the parameter A , he stated that he had kept the distribution of sources and sinks constant in his numerical calculations, but with constant lifetimes and variations of sources and sinks the value of A would cover a certain range.

Hamrud [1983] used a numerical 2-D model to describe variability and showed that the spatial relation between sources and sinks and the type of sinks influences spatial trace gas variability. He used 3 different source and sink functions and found values of A from 0.048 to 0.49, and b from 0.63 to 0.91. The inverse proportionality with lifetime ($b = 1$) was only found for very long-lived species. *Gibbs and Slinn* [1973] used a stochastic analysis approach to describe the temporal concentration variation of exponentially decaying trace gases at one point in space over time. They found a value of $b = 0.5$ for residence times greater than the temporal variation of sources and sinks. *Ehhalt et al.* [1998] used 3-D model results to investigate spatial variability of trace gases with lifetimes from one to 100 days. They distinguished among three regimes of parameter b : $b = 0$ if the "tracer gradient is caused by local mixing", $b = 0.5$: if "local transport and chemical loss are about equally responsible for a change in tracer concentration", and $b > 0.5$ when "local chemistry is causing most of tracer

²Because he wanted to derive global residence times, and by averaging over at least one year wanted to account for annual variations in the data.

³standard deviation divided by the average

removal". Figure 3.13 illustrates the global spatial variability-lifetime relationship, showing Junge's original data along with updates by *Jaenicke* [1982] and *Hamrud* [1983].

Lenschow and Gurarie [2002] applied an analytical 1-D model, which divides the atmosphere into three layers (the planetary boundary layer, the free troposphere and the stratosphere) to species with lifetimes in the region of days to years. This approach relates the concentration fluctuation to transport across the boundaries of each layer and diffusion across the free troposphere. They found that the *RSD* is approximately inversely proportional to τ with b between 0.5 and 1. Furthermore, this study predicts a relationship between the surface emission, mean concentration and lifetime, so that two of them can be used to estimate the third. The authors deduced from the general transport equation, that the factor A in equation 3.27 relates to the sampling time⁴ T like $A = \frac{T}{2\sqrt{3}}$ for $T \ll \tau$, and $A = \sqrt{\frac{T}{2}}$ for $T \gg \tau$.

Jaenicke [1982], *Slinn* [1988] and *Ehhalt et al.* [1998] introduced an exponential decay formula for the description of the decrease of trace gas concentrations downwind of their sources (temporal variability). *Jobson et al.* [1998] used this exponential decay approach to deduce that the use of the standard deviation σ of the natural logarithm of the mixing ratios is better suited for describing the variability lifetime dependency:

$$\sigma_{\ln x} = A \cdot \tau^{-b}, \quad (3.28)$$

with $0 < b < 1$. Figure 3.14 shows an example of PEM-West B data⁵ fitted to this formula. In his study the authors used species with lifetimes of the order of days to several hundred years. For long-lived species, $\sigma_{\ln x}$ and the formerly used RSD converge. The parameter b must be greater than 0 for species that undergo a net decomposition processes. On the other hand, the authors found that b was smaller than one, most likely because atmospheric mixing processes influence the trace gas concentration. In addition, differences of the source/sink distribution of sampled species may weaken

⁴(maximum time between production and measurement)

⁵Pacific Exploratory Mission in the Western Pacific Ocean Phase B

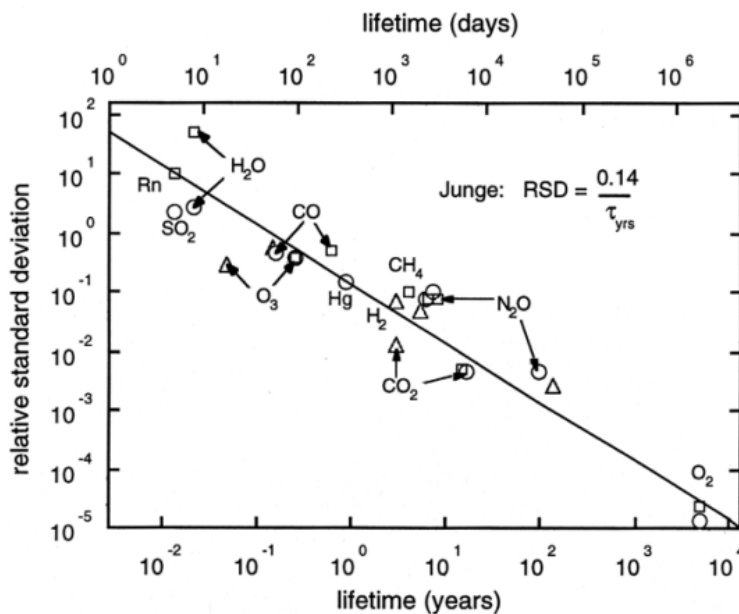


Figure 3.13: Relative standard deviation versus tropospheric residence time τ of the respective species. The line is $RSD = \frac{0.14}{\tau}$. The Figure is taken from *Jobson et al.* [1999] and shows the original *Junge* [1974] data (squares), with updates by *Jaenicke* [1982](circles) and *Hamrud* [1983] (triangles).

the variability-lifetime dependency.

Jobson et al. [1998, 1999] applied the variability-lifetime relationship to nonmethane hydrocarbon data, estimating the lifetime of the species from their removal by reaction with OH. Following *Ehhalt et al.* [1998], they interpret b as an index relating to source-receptor distances. Near source sites they derived $b \sim 0$, indicating that the variability $\sigma_{\ln x} = A$ was driven by differences in the strength of local sources and independent of the lifetime of the species. For Arctic data, they obtained $b \sim 1$, concluding that chemistry was the major source of variability. For remote tropospheric sites they derived $b \sim 0.5$. The influence of the source-receptor-distance on the trace gas concentration has already been discussed in section 3.4 and illustrated in Figure 3.6. However, when the measurement instrument is located too close to the sources, the variability of the trace gases no longer depends on the lifetime, but on other factors, like natural or anthropogenic production cycles. Hence the parameter b , which is identical to the slope of the variability lifetime-plot, depends on the source-receptor distance.

The parameter A is the axis intercept in the variability-lifetime plot. *Jobson et al.* [1999] made a first attempt for interpreting A by substituting it with a parameter Ψ , so that

$$\sigma_{\ln x} = A \cdot \tau^{-b} = \left(\frac{\psi}{\tau}\right)^b. \quad (3.29)$$

This has the advantage, that the unit of ψ is [time], independent of the value of b . As *Jobson et al.* [1999] stated, in this definition ψ is related “to some measure of transit time distributions from sources”. For the case $b = 1$, A is a measure for the standard deviation of the sampled transit times. The interpretation of parameter A has not been widely studied. High A values in the variability-lifetime relationship, result from high σ values of short-lived species. Naturally, high standard deviations can result either from one broad concentration distribution, or from several (smaller) concentration distributions. Sampling of two discrete air masses with sufficiently different chemical composition would result in the two discrete peaks in a concentration histogram, which result in a higher standard deviation. Hence, A can be interpreted as a measure of the homogeneity of the sampled air masses.

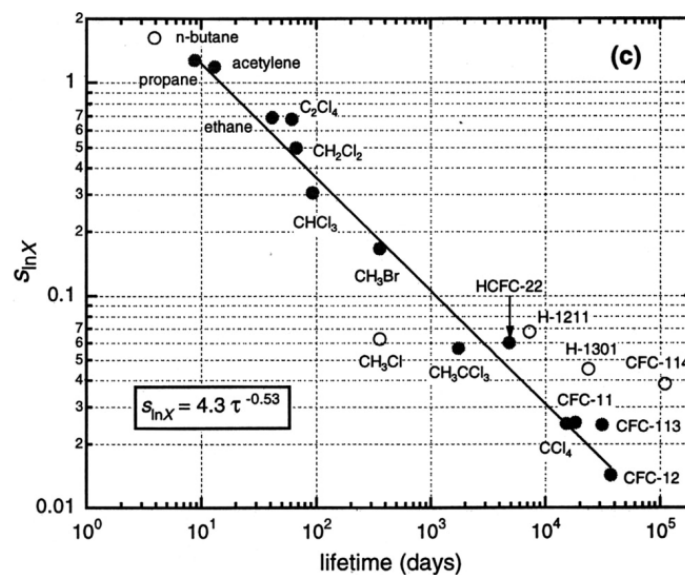


Figure 3.14: Standard deviation σ of the natural logarithm of the mixing ratios of PEM-West B data versus photochemical lifetime τ of the respective species. The line is the fit to $\sigma_{\ln x} = A \cdot \tau^{-b}$, with $A = 4.3$ and $b = 0.53$. [*Jobson et al.*, 1999].

Besides investigating the variability of trace gases itself, the concept of variability can be used to estimate OH concentrations. *Ehhalt et al.* [1998] used the Junge relationship to deduce tropospheric OH concentrations with ozone as independent species. *Williams et al.* [2000, 2001] applied Jobson's formula on data collected in Suriname (northern South America) and Amsterdam Island (Indian Ocean) for deducing average OH concentrations along back trajectories of sampled air masses. In the first case, they used acetone as independent species, in the latter case CO and radon were used. Furthermore *Colman et al.* [1998] applied the variability method to the PEM-Tropics A campaign data in order to estimate the lifetime of CH₃Br to 0.8 ± 0.1 years. *Johnston et al.* [2002] used a 3-D chemical transport model with several source and sink types to investigate the variability–lifetime relationship of trace gases with lifetimes of 0.04 to 7 years. They conclude, that the results of the variability–lifetime study strongly depend on the source/sink patterns and spatial/temporal sampling patterns, and that therefore the method should only be applied to data sets of gases with similar source and sink patterns. The model results gave *A* values in the range of 0.04 to 0.51 and *b* values from 0.57 to 0.98. The variability of CH₃Br-like gas was analysed in particular with regard to the *Colman et al.* [1998] study. Different scaling of the sinks while maintaining a lifetime of about a year resulted in a $\pm 17\%$ variation in σ , and finally in a $\pm 20\%$ variation of τ .

In addition to the estimation of OH concentrations and calculation of the parameters *A* and *b*, the variability study can be used as a tool in the assessment of data quality and compound identification. For example, for proton transfer reaction mass spectrometer measurements, a wrong assignment of the molecule to the measured mass could occur. In this case, the calculated lifetime would not match the assumed species. This leads to an offset of the species data point to the straight line of the variability lifetime relationship, as discussed in more detail by *Williams et al.* [2000].

3.6 The variability method in practice

When applying formula 3.28 ($\sigma_{\ln x} = A \cdot \tau^{-b}$) to derive OH concentrations, one faces an analytical insolvable equation with three unknowns, namely *A*, *b* and OH. Therefore, we use an iterative approach, which is illustrated in Figure 3.15. Each side of equation 3.28 is evaluated separately.

- $\sigma_{\ln x}$
The logarithm of each single measured concentration value is calculated. Then the standard deviation of a whole data set for one species is calculated. When *n* is the number of points, *y_i* the data value for the point *i*, and \bar{y} is the average value of all data points *y_i*, the standard deviation is defined as:

$$\sigma = \sqrt{\frac{1}{n-1} \sum (y_i - \bar{y})^2}. \quad (3.30)$$

The standard deviation is calculated for every species, so that one $\sigma_{\ln x}$ value is obtained for each species.

- $A \cdot \tau^{-b}$
The lifetime of each species is calculated according to

$$\tau = \frac{1}{k_{phot} + k_{OH} \cdot [OH] + \dots}, \quad (3.31)$$

where *k_x* is the rate coefficient for the respective reaction or decomposition process and [X] is the mixing ratio of the reaction partner X for a second order reaction. For the derivation of OH concentrations from the variability-lifetime method, two types of species must be included:

- species that react only with OH and

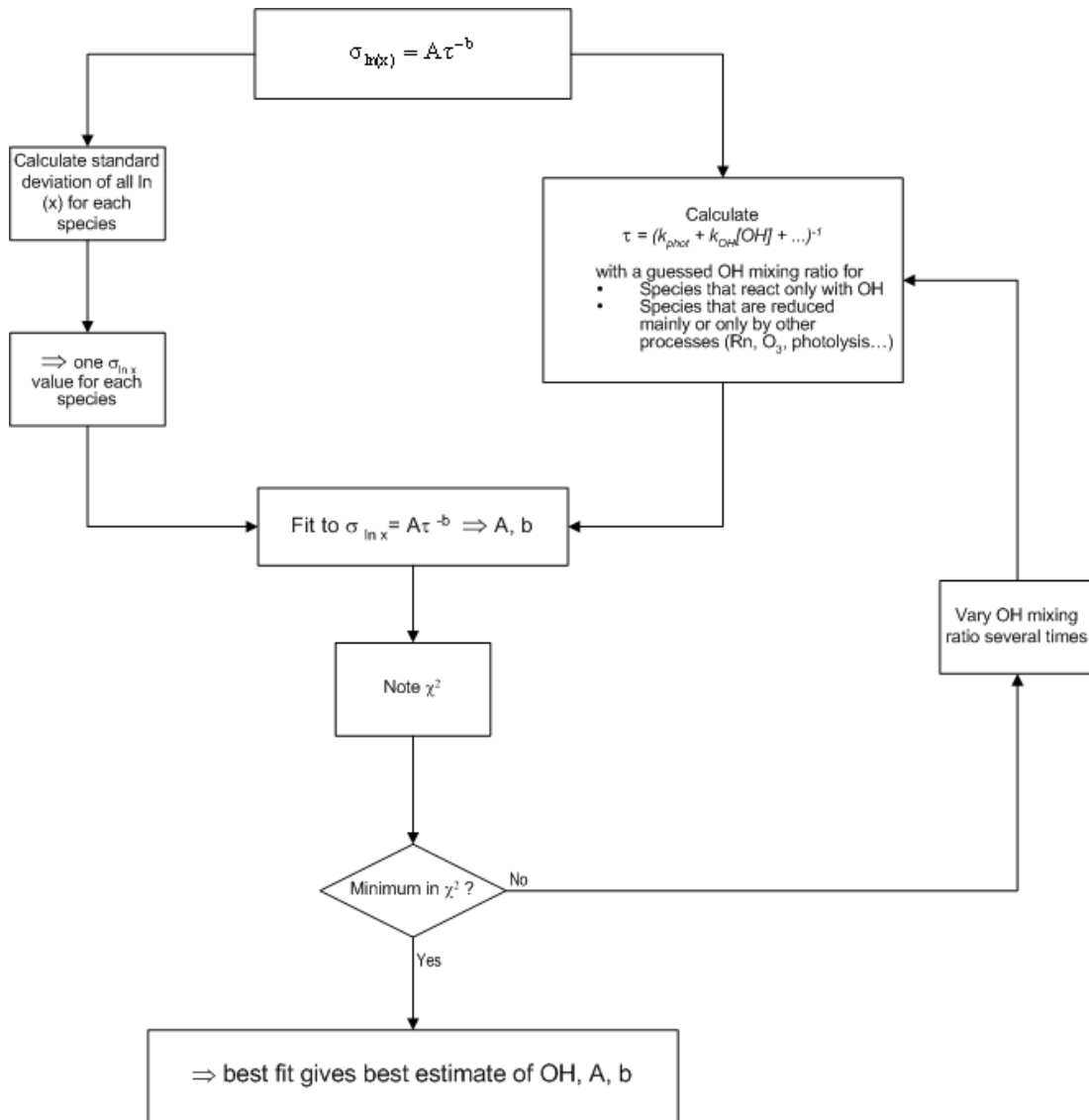


Figure 3.15: Estimation of OH concentrations: both sides of the variability-lifetime relation are calculated separately, then the results are fitted to the formula. OH concentrations in the formula are varied several times until the best fit is found by a minimum in χ^2 .

- species that are reduced mainly or exclusively by other processes (photolysis, radioactive decay, reaction with O_3 , ...).

The initial OH concentration for the calculation of the lifetimes has to be guessed. Note, that only those species are taken into account for the variability lifetime study, of which the lifetime determining reactions or processes are known, rates are available with sufficient accuracy, and all parameters (e.g. pressure and temperature) that are needed for the calculation of the lifetime are accessible.

- **Fit to equation 3.28**

Before σ and τ are fitted to equation 3.28, a transformation is made to:

$$\ln(\sigma_{\ln(x)}) = \ln(A) - b \cdot \ln(\tau), \quad (3.32)$$

where, A is obtained from the axis intercept $\ln(A)$ and b results from the slope. Implicitly this is done in all variability-lifetime plots published, because both axes are graphed logarithmic. *Jobson et al.* [1999] noted, that compared to an exponential fit “the linear regression to the transformed data yielded more reliable estimates of the uncertainties for A and b ”.

- **Calculate χ^2**

The value χ^2 as a measure of the goodness of the fit is calculated. χ^2 is defined by

$$\chi^2 = \left(\frac{y - y_i}{w_i} \right)^2, \quad (3.33)$$

where y is a fitted value for a given point, y_i is the original data value for the point i and w_i is the weighting.

- **Iteration of OH concentrations**

The OH concentration in the calculation of the lifetimes is varied several times, leading to different values of A , b and χ^2 . An example for this can be seen in Figure 3.16 and 3.17, using data for STREAM 98. The minimum in χ^2 is per definition the best fit, because the deviation of the measured data points from the calculated line is minimal. Thus the minimum χ^2 gives the best estimate of the OH concentration, A and b .

3.7 Processes affecting variability

Until now, only the “technical” side of variability was examined. In the following paragraph, the different processes affecting variability are discussed (relating to atmospheric chemistry). Processes that, considered individually, increase the variability of a measured species are decomposition by photochemistry, gas phase reactions and/or heterogeneous processes, emissions (natural and/or anthropogenic), variations in source/sink strength and heterogeneity of the sampled data set. On the other hand, production of the measured species by either of those processes can enhance or diminish variability, depending on the spatial distribution. The effect of a combination of several processes is difficult to predict, because processes can be opposing or reinforcing. Moreover, the dependence of the source strength on atmospheric trace gas concentrations in the background air (stronger emission when background is low, less emission when background is high - saturation) decreases variability. A high noise level of the detector might cause either of the effects, dependant on the signal to noise ratio.

- **Photochemistry:** Photochemical reactions as sink processes enhance variability because they diminish trace gas concentrations and thus “broaden the range” of measured trace gas concentrations. As source processes, they can produce new species and thus cause enhanced variability, or variability can be suppressed by reaction products filling up an otherwise diminishing reservoir. These considerations have also to be taken into account for the following processes described.
- **Gas phase reactions**
- **Heterogeneous processes**
- **Additional Emissions (natural and/or anthropogenic)** Additional emissions alter variability, because they add fresh material to an otherwise potentially aged air mass. Depending on the source, natural or anthropogenic, only single species or groups of species are affected. The direction of the alteration depends on the amount of the added material.

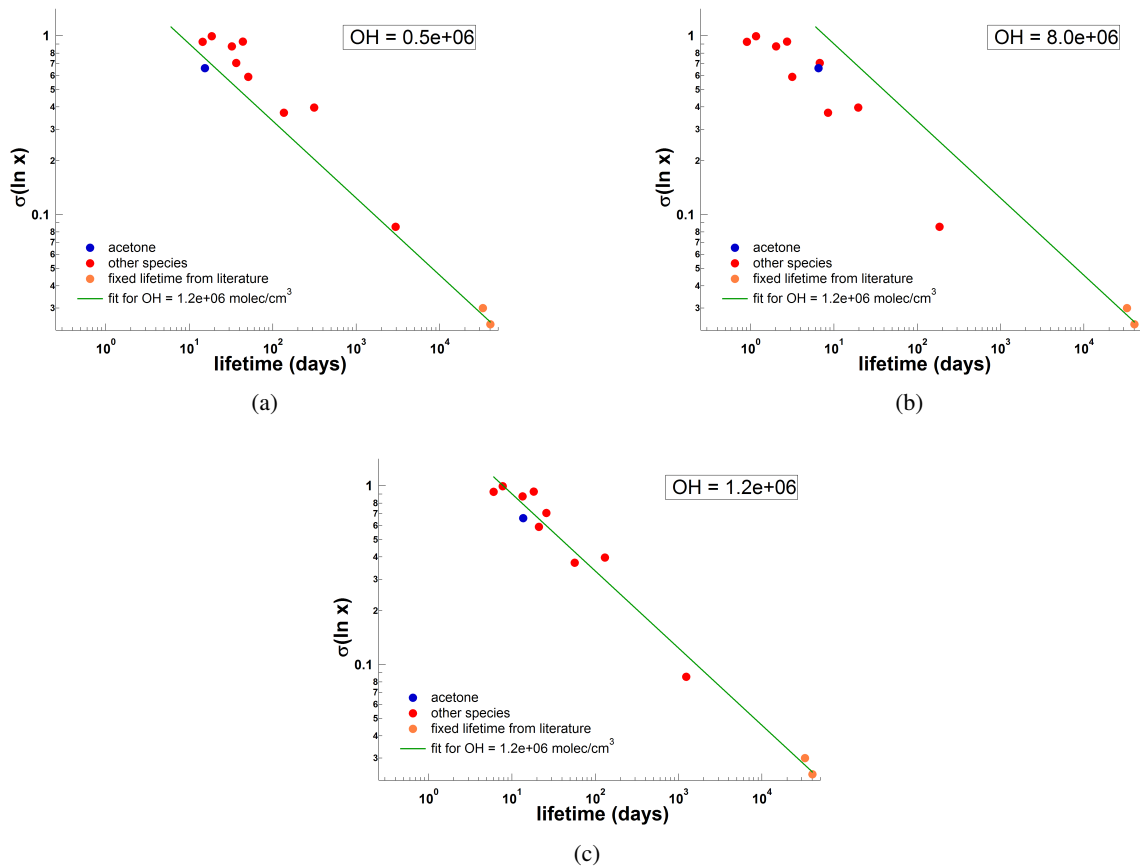


Figure 3.16: Influence of different OH concentrations on the lifetime of the species. The lifetime of Acetone (blue), which is decomposed by photolysis and reaction with OH, and the lifetime of other species, decomposed by reaction with OH (red), is varied by using different OH concentrations in the calculation of the lifetime. OH concentrations [10^6 molec/cm^3] used are: (a) 0.5, (b) 8.0, (c) 1.2. The lifetime of very long-lived species (orange) in this example is taken from literature. The lifetime of the “red” species varies stronger than the lifetime of acetone. In each graph the optimum fit, which results from $1.2 \cdot 10^6 \text{ molec/cm}^3$ OH is shown as green straight line.

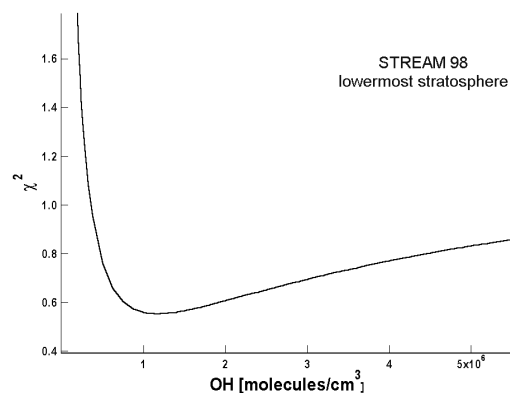


Figure 3.17: By varying the OH concentration in the calculation of the lifetime and subsequently fitting to equation 3.28 ($\sigma_{\ln x} = A \cdot \tau^{-b}$), the best fit is found at the lowest χ^2 . This gives the OH concentration and also the parameters A and b . This graph shows data from the lowermost stratosphere during STREAM 98.

- **Variations in source/sink strength** Similar to additional emissions, also variations in the source strength or sink strength alter the variability of trace gases. These variations are for example caused by daily and/or annual production cycles for plants, or daily or weekly production cycles for industry, or annual emission cycles caused by air conditioning and heating.
- **Heterogenous air masses and their mixing** When two or more air masses with different trace gas concentrations mix, the resulting new trace gas concentration is different, and thus generally the spectrum of sampled mixing ratio values is broader. This results in a greater standard deviation of the trace gas, hence a greater variability. In principle, the same is applicable when sampling two chemically distinct air masses.
- **High noise level of the detector** As well as natural causes, instrumental properties or handling by the analyst can also lead to influences on the measured variability of trace gases. When examining a histogram of measured mixing ratios, in a data region close to the detection limit of the instrument, the peak at lower mixing ratios could be real or just instrumental noise when measuring close to or below the detection limit. If it is instrumental noise, the variability calculated from the measured concentrations is higher than the natural variability of the data. This is easily comprehended, when recalling the definition of variability, equation 3.28, where the standard deviation of the data is calculated.
- **Data Handling** Finally, also data handling by the analyst can also lead to artificial influences on the measured variability of trace gases. In the example above, measurement close to the detection limit of the instrument, one is tempted to discard the problematic data (cut them off) and go on analysing the rest of the measurements. However, this would artificially decrease the standard deviation of the measurement and thus lower variability.

In the next section, photochemistry, gas phase reactions and heterogeneous processes are discussed in more detail, because they determine the lifetime of atmospheric trace gases. For the first two processes, the formulas for the calculation of the lifetimes are given - which this will be needed in the application of the variability-lifetime method.

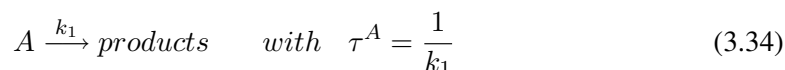
3.7.1 Photochemistry

In general, atoms in molecules can undergo various motions relative to each other: vibration, where the chemical bonds of the molecule are involved, rotation of the molecule as a whole, and translation, where the whole molecule moves in one or more coordinates of space. As the latter does occur as a direct consequence to the absorption of light, it will not be further discussed in this work (although transfer of energy from vibrational-rotational modes into translational modes is possible, leading to an increase of temperature). Energy capable of being absorbed to cause vibrational or rotational transitions is typically in the infrared. Vibrational transitions require a change in the dipole moment, rotational transitions require a permanent dipole moment. Furthermore, the absorption of light can lead to electronic transitions in the molecule. This transition requires energy in the ultraviolet and visible range, which can lead to splitting of chemical bonds. These electronic transition processes are in general the most important in atmospheric chemistry. Of course, also combinations of the described transitions can take place.

After the molecule has absorbed a photon and is in an electronically excited state, photophysical and/or photochemical processes will follow.

- Photophysical processes include *radiative* transitions by e.g. fluorescence or phosphorescence from the excited state to the ground state, and *non-radiative* transitions, in which a part or all of the energy of the absorbed photon is transferred into heat, e.g. internal conversion and inter-system-crossing.

- Photochemical processes are those in which the species dissociate, isomerise, rearrange, or react with other species. Of those, photodissociation is by far the most important in atmospheric chemistry. Photochemical processes yield new chemical species. The photodissociation process can be described as a first order reaction process:



In this equation, the lifetime τ is defined as the time, after which $[A] = [A]_0/e$, that means the concentration of species A is reduced to one over e of its initial value $[A]_0$.

3.7.2 Gas phase reactions

Gas phase reactions are reactions of or between gaseous components. Elementary reactions consist of one reactant species (called unimolecular, for example thermal decomposition, analogue to photochemical reaction, see equation 3.34) or two reactant species (bimolecular, equation 3.35).



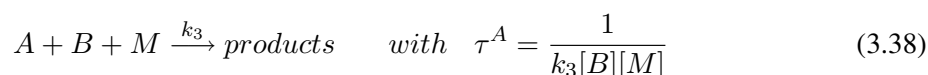
When the concentration of B is constant or can be assumed to be constant, e.g. because its concentration is much higher than that of A , or because it is recycled, then one derives a (pseudo-) exponential law for the concentration of A , and the lifetime is given by:

$$\tau^A = \frac{1}{k_2[B]} \quad (3.36)$$

The reaction rates of bimolecular reactions are often temperature dependant, which can be described by the Arrhenius law (3.37), generally.

$$k_{bim} = \mathcal{A} \cdot e^{(-E_a/R_gT)}, \quad (3.37)$$

with absolute temperature T , R_g the gas constant, the activation energy E_a and the parameter \mathcal{A} relating to the collision frequency. If a third molecule, an inert molecule, acting only as a collision partner to absorb excess energy, is involved, the reaction is called termolecular. Analogue to the bimolecular case, one obtains:



The rates of termolecular reactions depend on total pressure of the atmosphere. The reason is that the third molecule M must absorb excess energy in order to prevent, for example, a falling apart of one of the products, which might then re-form the reactants.

3.7.3 Heterogeneous reactions

For atmospheric chemistry heterogeneous reactions are defined as reactions between gases and either liquids or solids. In the troposphere liquid particles often contain sulfate, nitrate, organics, trace metals, carbon, whereas in marine areas sea salt particles are most common. Also, dust or soot as solid particles are found in the troposphere. In the stratosphere, ice crystals containing nitric acid, liquid sulfuric acid-water mixtures, and ternary solutions of nitric and sulfuric acids and water are most common. Direct emissions of particles containing carbon soot, alumina and metal oxides by rocket exhaust constitute a large but spatially limited source of surfaces [Finlayson-Pitts and Pitts, 2000]. Examples for heterogenous processes are uptake of components in clouds or destruction of

38.8. PREREQUISITE FOR THE APPLICATION OF THE VARIABILITY-LIFETIME METHOD

components at the Earth's surface. Examples of species that were measured during STREAM98 and INDOEX were SO₂, which can be taken up in clouds and fog, where it is subsequently oxidised, and HNO₃ and acetonitrile, which can also be removed by wet deposition. If heterogenous processes influenced the variability of the mixing ratio of the species can easily be tested by means of the variability-lifetime method: if the species follow the variability - lifetime relation, the lifetime was calculated correctly. If this calculation did not include heterogenous processes, they were obviously negligible for these air masses.

Reactions involving the gas- and liquid phase can be described by the following steps:

- Diffusion of the gas to the surface
- Uptake at the interface (region where one phase ends and the other begins)
- Diffusion into the bulk
- For reactions that are slow compared to the diffusion of the molecules into the liquid an equilibrium between gas and liquid builds up
- Reactions in the bulk, or
- Reactions at the interface without crossing it previously

Reactions involving the gas- and solid phase follow similar steps. The gas molecules can undergo physisorption or chemisorption at the surface, or the surface can act as a catalyst.

3.8 Prerequisite for the application of the variability-lifetime method

Several prerequisites must be met for the application of the variability-lifetime method:

- The species must, relative to the receptor, originate from the same source region.
- The source strength must be independent from the atmospheric concentrations.
- The lifetime of the species must be long enough compared to the variation of sources and sinks.
- The lifetime of the species must be long in comparison to the transit time to the receptor.
- The precision of the measurement instrument must be smaller than the atmospheric variability of the species, and hence limits the radius of the transit times, in which this species can be analysed.
- The number of data points must be sufficient for significant statistics.

Of the range of species that were measured during the campaigns, only those species were accounted for in the variability study, that fulfil the above stated prerequisites. Species that did not meet these requirements were excluded - this and the respective causes are discussed in detail in section 5.4 for INDOEX and section 6.5 for STREAM 98.

Chapter 4

The tuneable diode laser absorption spectrometer

A tuneable diode laser absorption spectrometer (TDLAS) called TRISTAR (*TR*acer *I*n *S*itu *T*DLAS for Atmospheric Research) [Wienhold *et al.*, 1998], developed by the Max Planck Institute for Chemistry, Mainz, Germany, was successfully used to measure the trace gases CO, N₂O and CH₄ during several aircraft campaigns. In the following paragraphs, the principle of measurement will be described, followed by a description of the instrument. The settings used during the INDOEX and STREAM 98 campaigns are given in the following paragraphs.

4.1 The measuring principle

Most atmospheric trace gases absorb light in the infrared region by rotational-vibrational transitions. Absorption spectroscopy makes use of this for example by employing tuneable diode lasers that emit in this range. Lead-salt lasers are selected for the specific absorption line regions of the target molecule. The absorption follows the *Lambert-Beer* law:

$$I(l, \tilde{\nu}) = I_0 e^{-n_x l \sigma(\tilde{\nu})} \quad (4.1)$$

where I_0 is the light intensity at the path length $l = 0$, n_x the concentration of the target trace gas x in the absorption cell, and $\sigma(\tilde{\nu})$ is the absorption cross section of the molecule, which depends on the wave number $\tilde{\nu}$. Obviously, the longer the absorption cell the stronger the absorption. Therefore a multi-reflection cell of White's design is used [White, 1976]. For small absorptions, the linear approximation of the *Lambert-Beer* law is valid, so that a linear relationship between the absorbed intensity and the concentration of the target trace gas concentration is given. In order to avoid overlap with absorption lines of other gases, it is desirable to have a narrow absorption line.

The line width is dominated by *Doppler* broadening at sufficiently small pressures, and dominated by pressure broadening at high pressures. Therefore the absorption cell pressure is reduced to below 30 hPa.

To measure the absorption line, the frequency of the laser must be tuned over the range of the line width. In the *single tone frequency modulation* technique, the frequency used is in the order of the targeted molecules line width. The tuning of the laser frequency over the absorption line can be realised by frequency modulation technique. First, the working point of the laser is fixed by the bias laser current and the temperature of the laser, both depending on the target molecule and the individual laser. For the lead salt lasers used in the TRISTAR instrument, temperatures were adjusted slightly above liquid nitrogen temperatures, at 85–90 K. A ramp current is added to the bias to tune

the wavelength of the light over the absorption line. Then the laser frequency is modulated by wobbling the ramp current with the modulation frequency ω_m . By applying the frequency modulation the signal is shifted into regions where the noise characteristics is dominated by white noise (frequency independent noise). The signal to noise ratio of the measurements is improved by this shift, because lasers, detectors and other active electronic components in the instrument follow $1/f$ noise characteristics. *Wienhold* [1992] even took further advantage of this by introducing a *two tone frequency modulation* technique, mixing two frequencies ω_m (102 MHz) and $\Omega/2$ (122 MHz), so that the laser is modulated at the frequencies $\omega_{1,2} = \omega_m \pm \Omega/2$. The frequency Ω is limited by the bandwidth of the detector, which can, in contrast to the single tone frequency modulation, be smaller than the line width now - another advantage of this technique. During the campaigns described in this work, the detectors had bandwidths of about 10 MHz.

4.2 Optical setup

The optical layout of the TRISTAR spectrometer was developed at the Fraunhofer Institut für Physikalische Meßtechnik (IPM) in Freiburg in close co-operation with the Max-Planck-Institute for Chemistry in Mainz [*Wienhold et al.*, 1998]. The cryostat was build by the Institut für Luft- und Kryotechnik (ILK), Dresden. Figure 4.1 shows the schematic of the optical setup of the TRISTAR TDLAS. The most important units of the spectrometer are:

- The cryostat, housing up to three lasers, the two detectors and a supply of liquid nitrogen for cooling. By placing all three laser diodes and the detectors into one dewar, instead of putting each into an own dewar, the TRISTAR instrument became considerably smaller than previous models. The lasers and detectors are mounted on cold fingers, which are connected to the liquid nitrogen supply by small tubes. The cooling is based on evaporation of the liquid nitrogen at the cold fingers. The cooling rate for the lasers is regulated by limiting the outflow of gaseous nitrogen through small orifices and hence limiting the liquid nitrogen flow to the stations. Temperatures are measured by PT-1000 sensors and fine tuned by ohmic heating to 80-120 K, typically. This design allows a temperature stabilisation of ± 0.003 K. The mercury cadmium telluride (MCT) photovoltaic detectors are operated at liquid nitrogen temperature (77 K), in order to reduce shot noise. TRISTAR can be operated up to 12 h without refilling the liquid nitrogen, enabling measurement flights with several aircraft-refuelling stops on short notice. This means that flight planning is independent of the availability of liquid nitrogen at the refuelling stops but can concentrate on atmospheric features.
- The multi-pass absorption cell has a base length of 0.5 m, providing a maximum optical path length of 64 m at 128 passes, and a volume of about 2.7 l.

Laser beams are adjusted by telescope optics and parallelised and collimated to widths of 14 mm by off-axis ellipsoids. By the use of CaF_2 beam splitters, the light paths are unified before the laser beams are redirected into the White cell. After leaving the White cell, the laser beam is split up into the signal part, which goes directly into the signal detector, and the reference beam, which must pass a reference cell before being focussed onto the reference detector. The reference cell is filled with a mixture of the target gases prior to the measurements, so that the absorption line can be identified and locked during all times, even when atmospheric concentrations are extremely low. The used mirrors are gold coated, their reflectivity is greater than 99 % in the used spectral range.

4.3 Electronic setup and data acquisition

The important electronic units are:

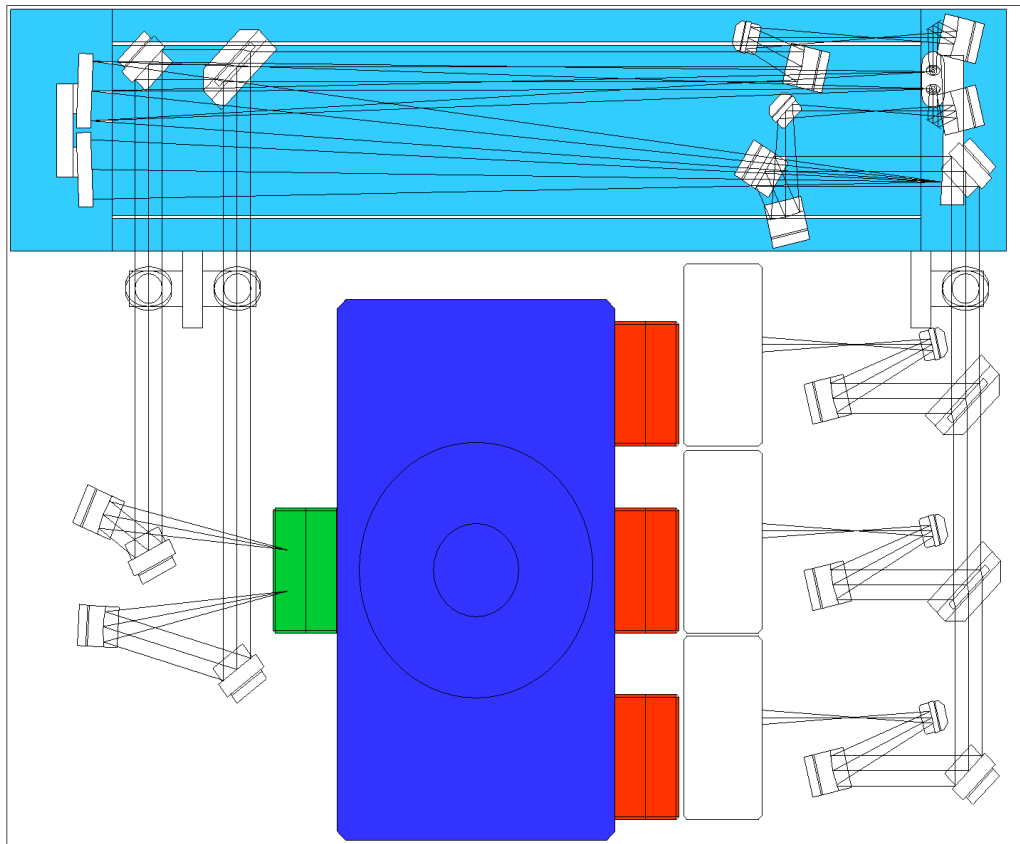


Figure 4.1: Schematics of the TRISTAR optical setup in top view. The dark blue part represents the cryostat. The three red boxes on the right are the three laser stations. The laser beams are redirected and enter/leave the White cell (light blue) from the top side. From here the beams are split up and passed to the detector stations (green) visible left of the cryostat. After *Wienhold et al.* [1998]

- The laser controllers and modulation units. The laser controllers (modified *Profile* controllers) regulate laser current and temperature, each for a single laser. The modulation modules provide high frequency current components that are added to the dc currents of the controllers, and demodulation modules for phase-sensitive detection of signal and reference channels.
- A computer (PC) with digital signal processors (AT&T, DSP32 C) is used for controlling the instrument and performing realtime-data analysis. The direct-mode signal is used for laser power measurement in both signal and reference channel, the high frequency part is used for the actual concentration measurement.

As stated in the description of the optical setup, the three laser beams are coupled into the optics with stationary mirrors and dichroic beam splitters. Therefore, another way of time multiplexing was introduced for the TRISTAR instrument. It is realised by pulse-current operation of the three lasers, meaning that each laser is operated for a short time, here 2 ms, and then pauses for 4 ms whilst the other lasers are being operated. During this operating period, the laser current is set higher than the desired operation point for the first 0.5 ms, in order to “warm up” the lasers and stabilise them for the following ramp. An ascending ramp current is used afterwards to correct line drifts during tuning, resulting from warming up of the laser by the additional heating of the operating current, and thus correcting the absorption line to an optimal line shape. Now the spectrum is analysed, while the next

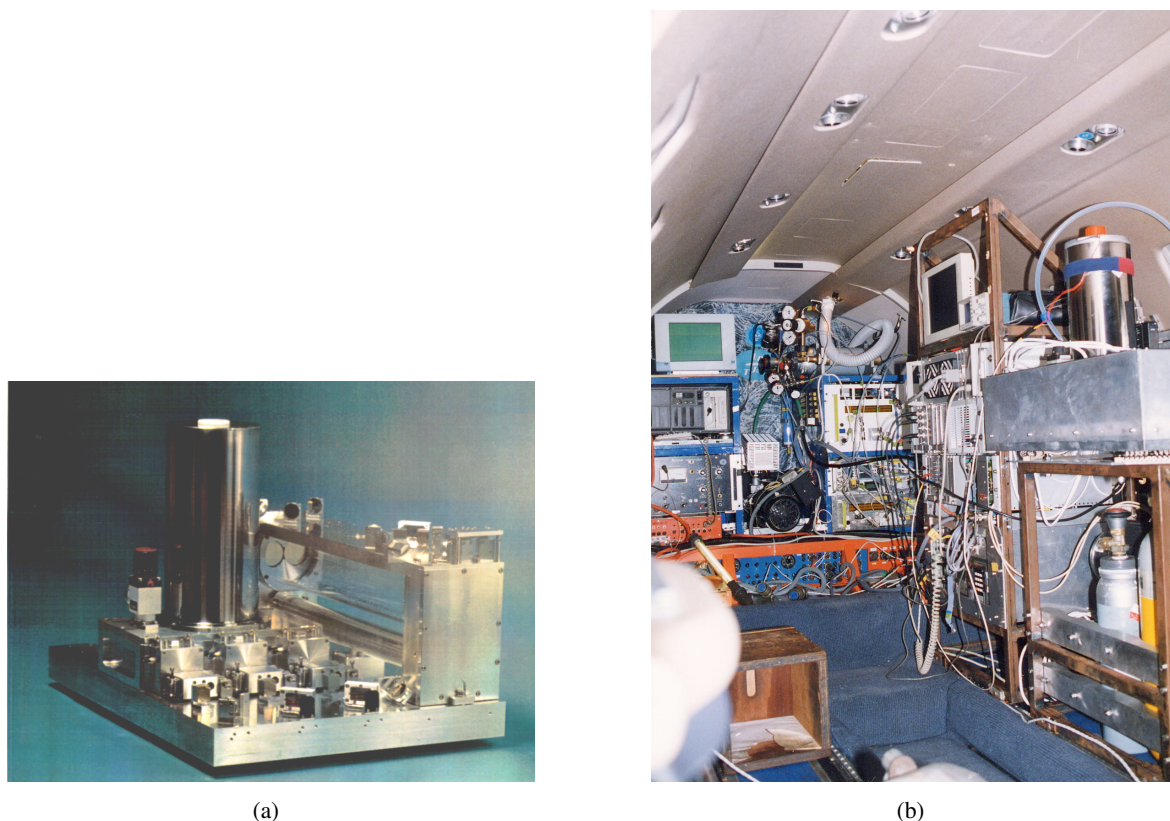


Figure 4.2: TRISTAR optics (a) and the complete setup in the aircraft as flown during STREAM 98. The front right rack carries the TRISTAR optics, the calibration gas and the pump. In the front left rack, the electronics is housed: monitor and oscillograph, the PC, laser controllers and modulation units.

channel is operated. 100 single spectra for one laser are averaged to calculate the concentration. This results in a time resolution of 1 second regarding the electronics. The absolute concentration of the sampled air is calculated by scaling the measured spectra to those of a calibration gas. Calibration gas is let into the White cell every 10 to 15 minutes. One electronic calibration cycle is 5 seconds, during which the spectra are averaged. Several cycles can be run in succession, in practice about 9 cycles per calibration, corresponding to 45 seconds on average. The operator ends the calibration manually, when the difference between two following calibrations cycles is small. The calibration gas in the White cell is then replaced by the continuous sample air flow. The concentration values, as well as laser power, and the error of the concentration as well as “housekeeping data”, used to control the lasers and the White cell are stored on hard disk for further analysis after the campaign.

4.4 Gas flow and calibration

The gas inlet tubes are implemented into the emergency exit doors of the aircraft. The inlet tube starts about 15 cm away from the fuselage outside of the aircraft. During INDOEX, the inlet was pointing in backward direction, as is shown in the photograph 5.3 on page 56. Figure 4.3 shows a schematic of the inlet system, gas flow and calibration system as operated during the INDOEX campaign. Perfluoroalkoxy (PFA) tubing led the gas to the White cell. The pressure was measured inside the White cell and regulated by a solenoid valve in front of the cell. The flow was maintained

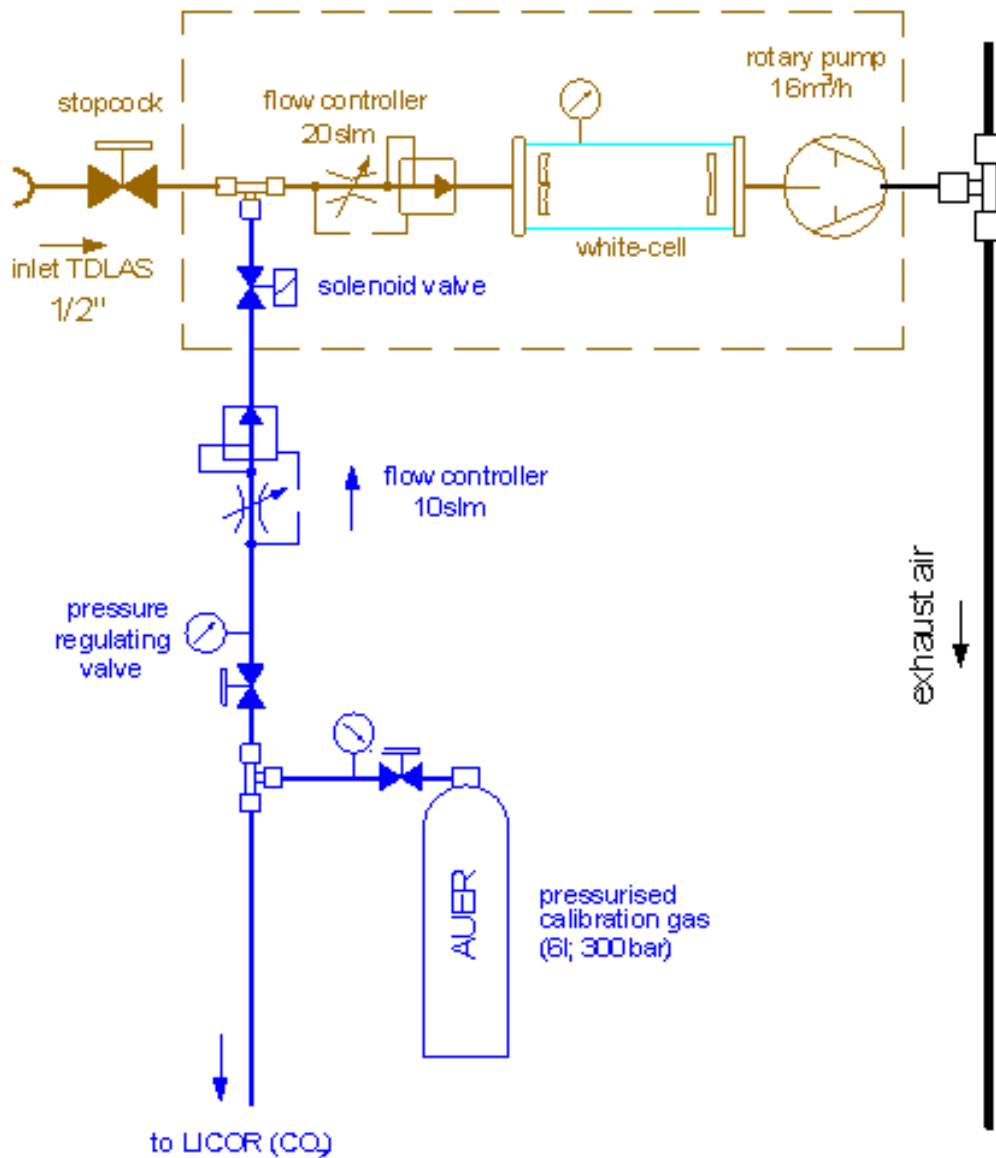


Figure 4.3: Schematics of the TRISTAR inlet system, gas flow and calibration system, as operated during the INDOEX campaign.

by a rotary pump after the White cell. At high flight levels, above ~ 10 km altitude, the pressure difference before and after the flow controller in front of the White cell was too small, so that the flow controller was not able to regulate the White cell pressure to 26 hPa at a flow of 3.2 litres/minute. Therefore the cell pressure was reduced to 16 hPa at flows of 1.8 litres/minute when the cell pressure started dropping. The gas exchange time in the White cell limits the time resolution of the TRISTAR instrument to 2-3 seconds. At aircraft speeds of 50 to 200 m/s, this results in high spatial resolution of 100 to 600 m.

The instrument was calibrated against pressurised gas standards in-flight, which were cross-calibrated with a gas chromatograph against NOAA (National Oceanographic and Atmospheric Administration) standards prior to the campaign. Each "in-flight" gas standard was checked with the TDL itself against a secondary standard (BOC gas mixture, cross-calibrated with a gas chromato-

graph against NOAA) prior to and after its use in the aircraft. During the flights, a solenoid valve is set to open the line to the calibration gas cylinders every 10-15 minutes. The calibration is activated by the operator. The calibration gas was supplied in over pressure, so that it prevents ambient air from mixing with the calibration gas in the White cell. This valve is in close proximity to the aircraft inlet, so that the whole sample line is calibrated. Calibration spectra are generally averaged over 5 seconds to reduce instrumental noise.

For the second half of the INDOEX campaign, after flight 10 on the 2nd of March, a cartridge containing Drierite, CaSO₄, was inserted into the inlet line, prior to the White cell. It was used for drying the sampled air, because water changes the partial pressure of the other gases in the sample, compared with dry air. Since the air taken from the calibration gas bottles is dried, there would be an error of up to 6 ppbv CO (real values are overestimated) in the atmospheric measurements. The cartridge was built in with a bypass, so that it could be chosen to use it or not during the flight. It was only used at lower flight levels, in order not to worsen the gas flow problem at higher altitudes. At higher altitudes H₂O mixing ratios are several orders of magnitude smaller than at sea level, thus the absence of the cartridge does not influence the concentration measurements any more. For measurements that were performed prior to the use of Drierite, the CO concentration values were corrected with respect to dilution due to the water vapour in the sampled air. With the relative humidity RH defined as

$$RH = \frac{P_{H_2O}}{P_{Sat}(T)} \cdot 100\% \quad (4.2)$$

where P_{H_2O} is the partial pressure of water at temperature T and the Magnus formula, which defines the saturation pressure P_{Sat} as a function of temperature

$$P_{Sat}(T) = 6.107 \cdot 10^{\frac{a \cdot T}{b+T}} \text{ hPa} \quad (4.3)$$

with $a = 7.5$ and $b = 237$ for temperatures greater than 0°C, P_{H_2O} was calculated according to

$$P_{H_2O} = \frac{RH \cdot 6.107 \cdot 10^{\frac{7.5 \cdot T}{237+T}}}{100} \text{ hPa} \quad (4.4)$$

$$(4.5)$$

The CO concentrations were pressure corrected according to

$$n_{CO\text{final}} = \frac{n_{CO} \cdot P}{P - P_{H_2O}} \quad (4.6)$$

where P is the White cell pressure and RH is the relative humidity of the sampled air, measured by the Vaisala instrument.

During the STREAM 98 campaign, no Drierite was used, since the chosen flight levels were at higher altitude, where the relative humidity is relatively low.

4.5 Characteristics during the INDOEX campaign

4.5.1 The lasers

During the INDOEX campaign, the TRISTAR spectrometer was used to measure carbon monoxide (CO), nitrous oxide (N₂O) and methane (CH₄). CO is an excellent tracer for polluted continental air, and due to its very steep decrease at the tropopause it can be used to locate this region. N₂O is produced at the Earth's surface, has a very long lifetime and is lost only in the stratosphere. Therefore,

it is a tracer for stratosphere - troposphere exchange. Moreover it is also the main source of nitrogen oxides in the stratosphere. CH_4 is the most abundant hydrocarbon in the atmosphere. CH_4 measurements can be used to estimate the fraction of stratospheric air present in an upper tropospheric air parcel. The gases were analysed at 2176.7 cm^{-1} (CO), 2208.5 cm^{-1} (N_2O) and 3014.8 cm^{-1} (CH_4). In order to assure that the lines found in the spectrometer really belonged to the respective analysed gases, they were successfully checked with the help of cuvettes. Furthermore, the HITRAN database was used to verify that no spectral lines of other gases were close by. Otherwise, measurements could have been influenced by interferences with other gases like H_2O , CO_2 and O_3 .

A general tendency of all TRISTAR channels to loose laser power from campaign to campaign [Hoor, 2001] was continued during the INDOEX campaign. Adjusting the optics prior to and during the campaign did not significantly improve the laser power measured at the detector. Hoor [2001] discussed this phenomenon regarding the STREAM 97 and STREAM 98 campaigns. Regarding the N_2O channel, the conclusion was reached that multimode operation of the lasers could have worsened the signal to noise ratio of the measurements. Although single mode operation is desirable, it can not always be realised. In multimode operation, the laser power can be redistributed between several modes. This leads to artificial noise and drifts of the measured concentration.

During the preparation of the INDOEX campaign a leak in one of the liquid nitrogen tubes leading to the cold finger of the methane laser station was found. The leak was repaired and the sealing of the cryostat was tested by a helium leak detector. For the STREAM measurements, this leak was considered as a possible explanation for the change of the characteristic detector diode line, resulting in broad noise [Hoor, 2001]. Water may have diffused into the cryostat and frozen out. After the INDOEX campaign, another leakage in one of those metal tubes was found. During the campaign, the signal to noise ratio of the instrument decreased significantly ($\sim 50\%$). The optical path with exception of the White cell was thoroughly readjusted in the course of the campaign, but could not avert this general trend.

Unfortunately the refuelling stops on the last day of the transfer to Male took more time than estimated, including a six hour time delay in Mumbai, India, on which we had no influence. This resulted in an overall time from the liquid nitrogen supply in Bahrain to the supply on Male of about 15 hours, exceeding the duration of the liquid nitrogen supply onboard, so that a heating up of the lasers could not be prevented. By this cold-warm-cold cycling of the lasers, the methane laser changed its characteristics so drastically, that no methane absorption line could be found with this laser. The alternative was either to dispense with the methane measurements or to change the methane laser. Lasers can be changed applying one of the following options: First, by cycling the whole dewar once more, thus risking the same problem with the other lasers and the detectors. For the detectors, the characteristic diode line could change, necessitating changes in the electronics of the pre-amplifiers. The other option is to heat the laser station in question to room temperature, whilst the other stations all remain cooled. Should a power failure occur during this "operation", the laser would start to freeze down to 80 K again, which would have had the effect of water condensation onto the laser, and even the intercalation of water molecules into the laser crystal. In both cases, the station would have to be evacuated afterwards. Since evacuation of the sealed, isolated station is not very effective (small vent), the station had to be connected to the main vacuum after some time, and this would have to be evacuated overnight in order to achieve sufficient vacuum for long operation times, regarding the liquid nitrogen consumption. During the night, with the dewar cooled, the danger of a power failure, again, would have been present, this time regarding all five devices (lasers and detectors). Since we had just arrived at the Male airport facility we could not assess the probability of a power failure. For the main goals of the INDOEX campaign, measurement of methane concentrations was not crucial, in contrast to CO. On the basis of these arguments, we decided to dispense with continuous methane measurements for this campaign. Methane data were derived from canister samples instead, alas with worse time and geographical resolution.

During the campaign, impairments occurred on all channels. Details on its nature and investigations as to their origins are given in the next section. N_2O variations in the troposphere are very small, due to the long lifetime of the species. Since the impairments on the N_2O were large compared to atmospheric variations, we were forced to refrain from further N_2O data analysis and interpretation.

4.5.2 Data quality and handling

During INDOEX, more than 60 hours of CO measurements were recorded. Figure 4.4, shows a typical CO time series obtained during the INDOEX campaign. The data shown in the graph was recorded on February 16th, 1999. CO raw data is displayed in black dots, the final (processed) data in red dots. Obviously, the CO data are strongly correlated with the altitude profile (blue line). The green vertical lines indicate start and stop of the in-flight calibrations.

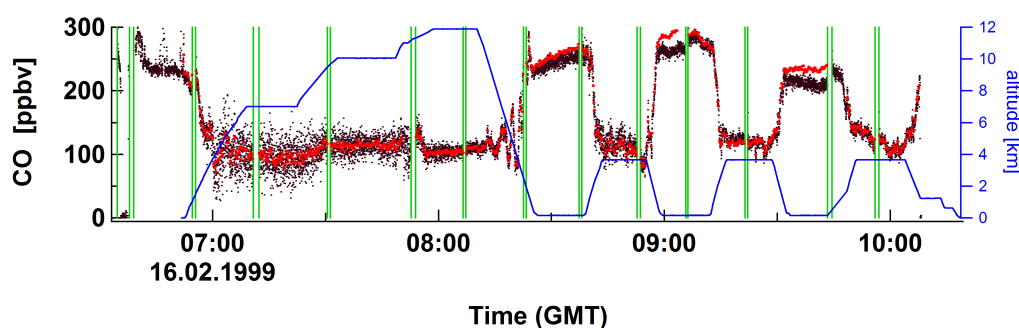


Figure 4.4: CO raw data (black dots) and final data (red dots) measured during INDOEX on February 16. The green vertical lines indicate start and stop of the calibrations. The blue line shows the altitude profile during the flight.

CO data were smoothed with a minimum of eleven second averaging to reduce instrumental noise. Instrumental noise is generated by the lasers, the detectors and the subsequent preamplifiers. However, *Kormann et al.* [2002] stated that in general the precision of concentration measurements limited by ‘optical noise’ due to interference fringes, which are mainly produced within the multipass cell. These effects generate noise which form a background to the atmospheric measurements. During some flights or parts of flights, the signal-to noise ratio worsened dramatically and abruptly. Sporadically, this correlated with the air traffic control (ATC) communications or cockpit-to-cabin intercom. Those impairments manifested itself in the high frequency signal, and on some really bad occasions, each single word transmitted on ATC could be detected as noise on the oscilloscope showing the measured spectrum. As communications with the ATC is necessary, this source could not be eliminated. In other cases, the source of the interference could not be distinguished. During the test flight, possible interferences with the communications-systems and other instruments were widely tested, but none showed up. The only exception was the switching-on of the pump for pressurising the canisters. Since this was only a momentary spike, these switches can not have caused the interferences that occurred during the INDOEX measurement flights. During the campaign, further tests were conducted, including tests inside the grounded aircraft in absence or presence of this phenomenon. On the ground, the instrument was run on external power, so electrical grounding was different than during the flight, but still, sporadically, the impairments showed up. The influence of the other instruments (each one individually switched on one after another like during normal operations) and of the aircraft electronics and communication systems was tested carefully. Also, electromagnetic “smog” was measured with a spectrum analyser in and outside the aircraft in both cases. During one flight, when such a worsening of the signal-to-noise ratio occurred, further tests concerning the aircraft systems

were conducted, during which all systems were switched on and off for some time (except the aircraft engines, of course). All these tests showed no definitive source of the interferences, so they could not be eliminated. During the STREAM 98 campaign, this kind of impairments had also been found, but not as strong as during INDOEX. At that time, it was concluded, that the source of the impairments were interferences with aircraft electronics or grounding. This was supported by the fact that the impairments never showed up in between the STREAM 98 and INDOEX campaigns, in spite of the fact that the instrument was run and tested in the laboratory. However, the thorough analysis of the phenomenon suggests two possibilities: either this is a problem of direct interferences of our instrument with a high frequency radiation, like the ATC; or some other electronic equipment, either aircraft or another instrument, picks up these frequencies and relays them passively to disturb our measurements, maybe by way of electronic ground.

As a consequence of those experiences, the TRISTAR instrument underwent major revisions after the INDOEX campaign. The two-tone frequency modulation technique (see section 4.3) was changed to a wavelength modulation scheme¹, which is easier to handle and less prone to disturbances. In addition, the time multiplexing technique based on pulse-current operation of the lasers and dichroic beam splitters was replaced by pneumatically driven pop-up mirrors, allowing continuous operation of the lasers and increasing the laser power coupled into the White-cell. Details on the revisions can be found in *Kormann et al.* [2002].

During those phases with interferences, the averaging time had to be extended for up to 53 seconds, in order to keep the signal-to-noise ratio fairly constant during the campaign. In the end, about 84 % of the CO data was smoothed with 11 seconds averaging, so the median of the smoothing time is 11 seconds. The average smoothing time was 17.1 seconds. It must be pointed out that due to the decreasing signal to noise ratio in the course of the campaign, it was a general tendency to lengthen the smoothing interval towards the end of the campaign. However, as can clearly be seen in Figure 4.4, smaller atmospheric features are conserved in the data set, in spite of the smoothing. For example, the wavelike structure at about 8:10 GMT to 8:24 GMT is found in the CO₂ data as well, so it is assumed to be real. In general, a good correlation in small scale features between CO and CO₂ was observed.

For data handling, the calibration spectra, which were recorded during flight, and the housekeeping data of the lasers were consulted. The calibrations are generated by the measurement of pressurised, canned air. In ideal case, the measured spectra and the resultant concentration should always be the same. However, after some time, parameters of the instrument or in the surrounding may change and cause a drift in the measurements. This applies also to the atmospheric measurements (spectra). In general, no correlation between the drift of two consecutive calibration spectra and the housekeeping data of the lasers, e.g. laser power or diode temperature, can be found [*Hoor*, 2001]. Therefore, none of the housekeeping data can be used to calculate the differences in the calibrations and atmospheric data. Thus, the calibration spectra are used as reference for potential drifts. Calibrations are performed frequently during flights, every 10-15 minutes. The gradient of the drift between two consecutive calibration spectra is calculated and applied to the measured data sampled these spectra. Figure 4.4 shows an example of raw data and final data, which was linearly corrected. The average reproducibility of all calibrations was 7.3 %.

At least a part of the drift is likely due to temperature changes in the instrument and optics environment, since the cabin temperature of the aircraft changed during operation: daytime temperatures onboard were about 30° to 35°C. During flights at low altitudes cabin temperatures up to 55°C were reached. Late in the night (absence of solar heating) and at high altitudes, cabin temperatures were down to about 25 °C. Naturally, the shades of the aircraft windows were used to block direct solar irradiation, but the instrument is not temperature stabilised, which might cause some drifts. On some

¹The wavelength of the beam is modulated sinusoidal with a frequency f in the kHz range. The detection takes place at one of the harmonics. The new TRISTAR setup uses 10-kHz $2f$ -wavelength modulation.

incidents, drifts were observed during very fast climb flights, dives or steep turns. The acceleration during those phases affects the optical setup of the instrument, which may then be misaligned. In addition, accelerations can alter the refrigerating capacity at the detectors, as *Hoor* [2001] already pointed out. Liquid nitrogen is led to the stations, and the evaporated N_2 flows back into the liquid nitrogen tank. Thus, the flow-through depends on the hydrostatic pressure in the cryostat, which might change, depending on amount of acceleration and its direction. A change in detector temperature results in altered sensitivity, thus in an altered signal and an altered signal to noise ratio. In contrast to the lasers, the detectors are not temperature stabilised, so that temperature changes are not corrected.

Measures for the quality of the data are accuracy and precision of the data. The precision describes the range of values around the expectation value (random error). The standard deviation of the calibration gas measurements serves as a measure for this. During INDOEX, the average reproducibility of in-flight calibrations was 7.3 %. During phases with negligible changes in concentrations the scatter of the data was analysed and a standard deviation of 8.7 ppbv was found. The accuracy describes the general tendency to hit the “target”. A deviation from the “target” is a systematic error. The calibration gas accuracy was ± 2.8 %. The overall uncertainty was estimated as 7.8 %.

In summary, CO measurements were successful and in consistency with other species measured onboard the aircraft. Moreover, agreement with the CO measurement onboard the research vessel Ronald H. Brown is good. The latter measurements were performed using the tunable diode laser absorption spectrometer FLAIR (Four Laser Airborne Infra Red) [*Roths*, 1992], which was also operated by the Max-Planck-Institute for Chemistry in Mainz [*Wagner*, 2000]. The comparison is shown in Figure 5.9b on page 65, and will be discussed in more detail in chapter 5.3.

4.6 Characteristics during the STREAM 98 campaign

During the STREAM 98 campaign, about 11 hours of CO measurements and 8 hours of N_2O measurements were gathered. The gases were analysed at 2176.7 cm^{-1} (CO) and 2208.5 cm^{-1} (N_2O). The data was averaged over 5 s. Figure 4.5 shows an example of CO and N_2O time series sampled during the STREAM 98 campaign, together with some other species for comparison. The data shown in the graph was recorded on July 1st, 1998. The top graph shows the TDLAS N_2O data in red, and for comparison the N_2O data collected by the in-situ gas chromatograph (blue) that was operated by the Johann Wolfgang Goethe-University, Frankfurt am Main, Germany (see chapter 6.3). The flight altitude is given in black. The middle panel displays the CO data and CO_2 recorded by a modified non dispersive infrared instrument (LICOR 6262). The correlation in the small scale features is very good. The bottom graph shows O_3 and H_2O measurements for comparison of the data. Between 17:40 GMT and 19:30 GMT the aircraft was in the stratosphere - note the high O_3 in contrast to low N_2O , CO and H_2O values. Variations of the trace gases in this part of the flight indicate different air mass origins [*Hoor*, 2001].

Remarks concerning the STREAM 98 the data quality and handling have already been made in the INDOEX section. Here, some additional notes concerning the STREAM 98 measurements will be pointed out. In general, it is desirable to operate the laser in one single mode. However, the sometimes single mode operation can not be realised, because no suitable absorption lines can be found at the frequency range emitted by the laser. Multimode operation leads to higher noise. When the operation point of the laser drifts, multimode operation may even cause variations in laser power at the observed mode, and hence in the signal strength. Therefore, performance of the lasers was checked between the flights and the operation point was optimised. However, due to drifts of the operation point after the start, there is always the chance of the mode performance affecting the measurements. *Hoor* [2001] noted that for the CO laser, the absorption was in the range of broad mode, so a drift in the operation point did not result in a change of the mode. For the N_2O measurements, the strongest absorptions

lines were found at relatively small modes, so that on some occasions a change of the absorption line was necessary.

During the measurement flights, the CH₄ signal (1258.5 cm⁻¹) was superimposed with strong optical interferences (etalon effect). These caused a drift in the instrumental background with an amplitude of several hundred ppbv and resulted in a degradation of the precision of CH₄ measurements of more than 10 % [Fischer *et al.*, 2002]. As this could not be eliminated by data handling, all CH₄ data had to be abandoned.

A comparison of the N₂O measurements by the TDLAS instrument and the in-situ gas chromatograph (GC) shows that the relative difference of overlapping data points is less than 1.5 %. The standard deviation of those differences is 2.5 %. A linear regression between both data sets verifies that 83 % of the variations in the TDLAS data correspond to those found by the GC. The missing 17 % can be explained by the precision of the data [Hoor, 2001]. Figure 4.5(top) shows measurements of both instruments, sampled during STREAM 98 on July 1.

The precision of the measurements was ± 3.5 % for CO and N₂O (1 σ), which is in good agreement with a ± 8 ppbv noise for CO and ± 10 ppbv for N₂O (3 σ). The calibration gas accuracy was ± 2.8 % for both gases. A detailed discussion of the characteristics of the TDLAS during the STREAM 98 campaign can be found in Hoor [2001].

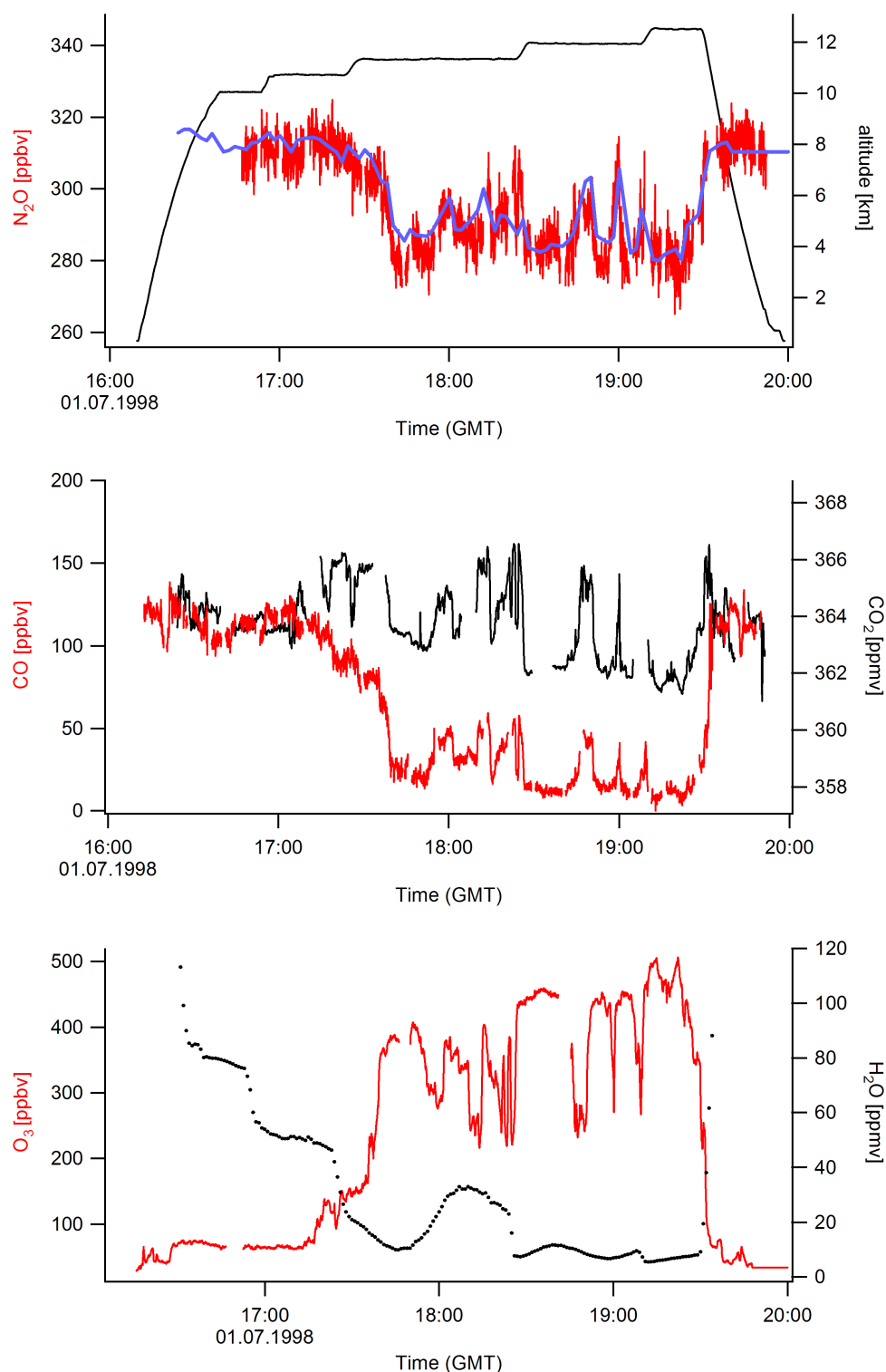


Figure 4.5: N_2O (top), and CO (middle) measured with the TDLAS during STREAM 98 on July 1. For comparison, also flight altitude (top), CO_2 (middle), O_3 (bottom) and H_2O (bottom) are shown. Between 17:40 GMT and 19:30 GMT the aircraft operated in the stratosphere. Variations of the trace gases in this part of the flight indicate different air mass origins.

Chapter 5

The INDOEX campaign

The tropical Indian Ocean is a region where strong sources of anthropogenic trace gases (SO_2 , volatile organic compounds, NO_x), their reaction products (e.g. sulphate and ozone) and continental aerosol are located in close neighbourhood to clean southern hemispheric air. During the winter monsoon, from December to March, a northeasterly flow transports polluted, continental air from South- and Southeast Asia across the Bay of Bengal and the Arabian Sea over the Indian Ocean towards the Inter Tropical Convergence Zone (ITCZ). Here, Northern and Southern Hemispheric air flow together and offer an unique opportunity to study the strong gradient of aerosols and gases and the exchange of air masses between the northern hemisphere and the southern hemisphere. The *Indian Ocean Experiment* (INDOEX) was designed to study the impact of anthropogenic trace gases and aerosols on the chemistry and radiative forcing in this region. A description of the measurement region and the meteorological background is given in paragraph 5.1. Figure 5.2 gives an overview over the measurement region and the main wind flow channels.

The objectives and main questions to be answered by the INDOEX campaign were

- to assess the nature and extend of the chemical pollution above the tropical Indian Ocean and how the high degree of population on the Indian subcontinent affects the chemistry of the free troposphere. Does this influence the oxidation power of the atmosphere on a global scale?
- to assess the importance of sulfates, soot and other continental aerosols for radiative forcing. Is this influence only locally restricted to urban areas or does it spread to remote regions, thus possibly influencing the ocean heat budget and the planetary albedo far away from the sources?

To fulfil these objectives, INDOEX was set up as a major international measurement campaign, merging various observing platforms: five aircrafts (the Cessna Citation, Hercules C-130, Mystère, M-55 Geophysica and DLR Falcon), geostationary satellites (METEOSAT-5 and INSAT) and polar orbiters (NOAA 14, 15 and ScaRaB), two research vessels (Ronald H. Brown and Sagar Kanya), several surface stations in India (including Mount Abu, Pune, Trivandrum), the Maldives (Kaashidoo Climate Observatory), Mauritius, and La Réunion. In addition, constant level balloons were launched from Goa. In this work, we focus on the first objective, and for that data from the research aircraft Cessna Citation is presented.

5.1 The measurement region and the meteorological background

The INDOEX campaign was carried out in two phases. The first-field phase (FFP) was carried out from January to April 1998 to study the major pollution sources and meteorology and to find the best places to measure during the intensive field phase. The main results obtained during the first

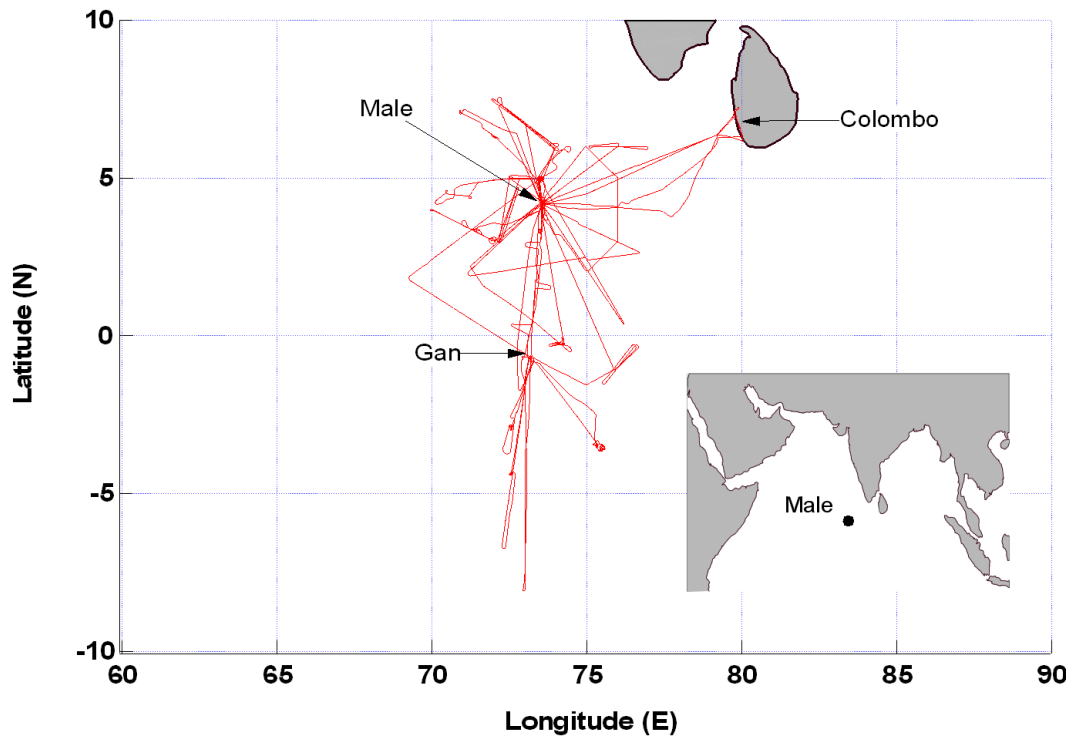


Figure 5.1: Geographical distribution of all Cessna Citation measurement flights performed during the INDOEX campaign. Figure after *de Reus et al.* [2001]

field phase can be found in *Mitra* [1999]. During the intensive field phase (IFP), which took place from January to March 1999, intensive measurements were performed in the INDOEX region, which extended from 30°N to 30°S , and 50° to 100°E . Summaries of the major findings during the intensive field phase can be found in *Lelieveld et al.* [2001] and *Ramanathan et al.* [2001]. The measurements onboard the Cessna Citation that are described in this study were part of the IFP.

5.1.1 The main wind flow channels

The two main flows in the INDOEX region for this time of the year are southeasterly trade winds transporting clean southern hemispheric air to the ITCZ, and low level outflow from India, transported to the ITCZ by northeasterly trades (see also Figure 5.2). In more detail, one observes four channels for the transport of polluted Northern Hemispheric air towards the ITCZ:

1. Northeasterly trade winds transporting air from the Arabian desert region over the western Arabian Sea.
2. Northwesterly and Northeasterly flow transporting air from the Indo-Pakistan desert region and the Indian west coast along the latter to the INDOEX region.
3. Northeasterly trade winds transporting air from central India and the Ganges valley across the western Bay of Bengal.
4. Northeasterly flow transporting air from Southeast Asia across the Bay of Bengal.

Figure 5.2 illustrates these four channels. Of course, the intensity of these channels changes on a day-to-day basis, depending on the prevailing weather system.

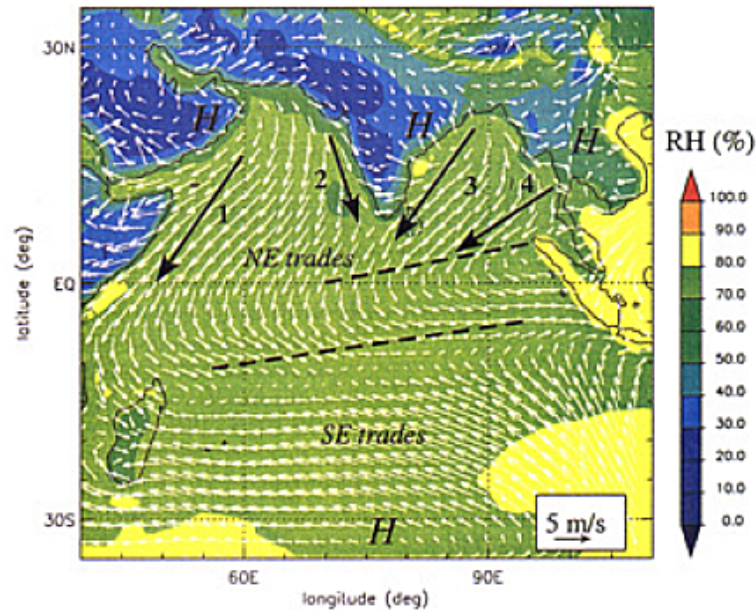


Figure 5.2: Main wind flow channels (arrows) at 1000 hPa (low level flow) in the measurement region of the INDOEX IFP. The data were calculated by the European Centre for Medium-Range Weather Forecasts (ECMWF), averaged for February 1990–1999. The colour scale gives the relative humidity (RH), the two near-equatorial convergence zones are indicated by the two dashed lines. Figure from *Verver et al.* [2001].

During the INDOEX IFP, channel 1 was the most persistent, transporting air masses into the southern hemisphere - but it did not influence the measurement region directly. Channel 2 was infrequent in February, but persistent in March. The strength of the Northeast trades are linked to baroclinic disturbances moving north of the Persian Gulf, Iran, Pakistan and the northern part of India. Channel 3, in contrast to channel 2, was persistent in February, but diminished after the 6th of March, due to a shift of the anticyclone over the central and east India region to the north and central Bay of Bengal region. This, in turn, may be caused by the heating up of the southern and central parts of India in early March. Channel 4 was quite persistent in February, but the weakest and least persistent in March. Channels 3 and 4 merged east of Sri Lanka, before passing over southern India into the Male region (Male, the capital of the Maldives, is located at 4.2°N and 73.5°E). A detailed description of the meteorological situation can be found in *Verver et al.* [2001].

For the Cessna Citation measurements, which are presented in this study, this means that in February sampled air masses mainly originated from the Arabian Sea and in March from the Bay of Bengal [*de Gouw et al.*, 2001]. This resulted in higher trace gas and aerosol concentrations in February compared to March [*de Gouw et al.*, 2001; *de Reus et al.*, 2001].

5.1.2 The inter tropical convergence zone

In 1999, the ITCZ actually dissolved into a northern and a southern convergence zone. In the second half of February, the northern convergence zone, positioned at about 0°–3°N, was more active and enabled slight cross-equatorial flow of air masses in southward direction. After the 10th of March, it was shifted to about 5°N. The southern convergence zone was positioned at about 9°S until the 7th of March. In March the southern convergence zone was more active. It moved southward to about 10°–15°S where it resided from 10th of March until the end of the Citation measurements. In the period

between 3rd-23th of March, tropical depressions formed in the southern convergence zone.

In general, organised convection observed from Meteosat-5 images was found in close proximity to, or north of the northern convergence zone. A detailed description of the meteorological conditions and atmospheric transport processes during the INDOEX IFP 1999 is given in *Verver et al.* [2001].

During INDOEX, the Southern Hemisphere was difficult to reach with the Cessna Citation, based on Male, due to its flight range (about 1000 km one way). The Citation reached the meteorological (in contrast to geographical) Southern Hemisphere only once - on the 4th of March, during flight 11b. Here, very low mixing ratios of CO (about 50 ppbv) and O₃ (about 10 ppbv) were observed near the surface. A detailed ITCZ analysis for the Citation measurements with special regard to vertical profiles of CO and O₃ cross-ITCZ gradients can be found in *Williams et al.* [2002]. For the variability study, this part of the data is not considered, since the composition of those clean air masses is determined by a totally different source and sink distribution than the data in the Northern Hemisphere. The accomplishment of a variability study of the Southern Hemisphere was not possible, because the number of data, especially hydrocarbon canisters, collected in this atmospheric region was too small for significant statistical analysis. The variability-lifetime analysis presented in this work refers to Northern Hemispheric air masses only.

5.2 The aircraft and the instrumentation

A variety of observation platforms was used during the INDOEX campaign. Satellites and polar orbiters give a good overview of the global distribution of trace gases, aerosols and the cloud coverage, but the spatial resolution in all three dimensions as well as in time is often not sufficient for detailed analysis. Balloons give only a momentary view of a height profile, which changes its geographical position, including altitude, without the possibility of being dirigible. Ground based measurements, for example by lidar, can measure rather continuously, but are stationary, unless mounted on a ship. The speed of research vessels is in general low and thus atmospheric variability due to chemistry and convection superimpose the changes in trace gas mixing ratios due to displacement of the ship. Airborne measurements are an excellent alternative to the previous platforms when studying atmospheric processes that occur on spatial scales of 1 km to 1000 km.

Aircraft campaigns place high demands on the scientific equipment. In general, space onboard is limited, so that instrumentation should be as compact and light weighted as possible, the high air-speed of the aircraft requires high time resolution of the instruments, in order to achieve high spatial resolution of the measured data, constructions of the instruments have to be robust to withstand vibrations common during flights, accelerations during take offs and changes of directions, and especially the jerks during the landing of the aircraft or in air-pockets. Moreover, it is desirable to keep power consumption as low as possible, as well as to keep the heating up of the cabin to a minimum.

Paragraph 5.2.1 gives a short description of the characteristics of the Cessna Citation aircraft, and 5.2.2 gives an overview of the instrumentation onboard, describing the measurement of the species analysed in this work.

5.2.1 The Cessna Citation II

Measurements were performed using a Cessna Citation II, a twin-engined jet aircraft, operated by the Delft University of Technology and by the National Aerospace Laboratory, NLR, in the Netherlands. The aircraft was based on Male International Airport on the island Hulhule (4.2°N, 73.5°E), Republic of Maldives. The Cessna Citation has a maximum cruising altitude of ~13 km (43000 ft) and a flight endurance of about 3.5 hours at cruising speeds of about 150 m/s or 540 km/h. This results in a flight radius of about 1100 km. In order to extend the range of the aircraft, refuelling stops at Gan (0.7°S, 73.2°E), the southernmost island of the Maldives, or at Colombo (6.9°N, 79.9°E), Sri Lanka, were

conducted. Accordingly, air masses between 70° and 80° E and 8° N to 8° S have been sampled. From the 14th of February until the 21st of March 23 individual flights, arranged in groups of 16 campaign flights (meaning with refuelling stops), were performed. Table 5.2.1 and Figure 5.1 give an overview over the measurement flights performed during the INDOEX campaign.

Flight data recordings include the geographical position, altitude, speed, direction and angle of attack of the aircraft, partly using the global positioning system (GPS), as well as meteorological data like static air pressure and temperature, wind speed and wind angle. Apart from the two pilots, two operators were onboard during each measurement flight, in order to control and maintain the scientific instrumentation.

The inlets for the air samples were build into the emergency exit: the window of the door was replaced by a metal plate, which had transfixions for the sample probes of the different instruments. Figure 5.3 shows a photograph of the inlet probes.

5.2.2 The aircraft instrumentation

Table 5.2 gives an overview of the instrumentation onboard the Citation during the INDOEX campaign. Figure 5.4 shows the payload configuration onboard the aircraft. The Cessna INDOEX pay-

Flight Label	Date	Takeoff	Landing	Departure from	Remark
1	14.2.	12:05	15:20	Male	clean stacked profile, SE
2	16.2.	11:52	14:22	Male	polluted profile, NE
3	18.2.	16:15	19:45	Male	quasi Lagrangian flights, NW part II, downwind
4	19.2.	14:20	17:40	Male	
5a	22.2.	10:10	13:35	Male	Southward, spiral descent at $2,35^{\circ}$ S to $6,35^{\circ}$ S (Diego Gracia) Spiral descent above Male
5b	22.2.	14:55	18:25	Gan	
5c	22.2.	19:10	21:25	Gan	
6	24.2.	15:30	18:10	Male	test flight PTRMS, rain
7	26.2.	14:53	18:28	Male	circling of dying cloud
8	27.2.	15:25	19:25	Male	Inter-comparison with C-130
9	01.3.	13:15	17:00	Male	quasi Lagrangian flights of Indian outflow
10	02.3.	13:40	17:05	Male	
11a	04.3.	10:40	11:52	Male	transfer to Gan southern Hemispheric air at 8° S spiral descend over Kashidoo
11b	04.3.	12:55	16:30	Gan	
11c	04.3.	17:25	20:55	Gan	
12	13.3.	09:55	13:30	Male	inter-comparison with C-130, clouds physics payload
13a	15.3.	10:20	12:25	Male	latitude gradients convective outflow of Cb possible outflow of Indonesia
13b	15.3.	13:25	16:10	Gan	
13c	15.3.	17:05	20:50	Gan	
14	18.3.	05:30	08:55	Male	dawn flight: starting photochemistry and new particle formation
15	19.3.	11:55	15:35	Male	Colombo fly by: urban pollution
16a	21.3.	08:05	10:35	Male	microphysics and radiative properties of clouds, Colombo plume convective outflow of Cb's
16b	21.3.	13:20	15:55	Colombo, Sri Lanka	

Table 5.1: All flights performed from the Cessna Citation Team during the INDOEX intensive field phase 1999. Male and Gan are both part of the Maldives. The time given is local time. Local time on the Maldives and Sri Lanka is universal time counts (UTC) + 5 hrs.

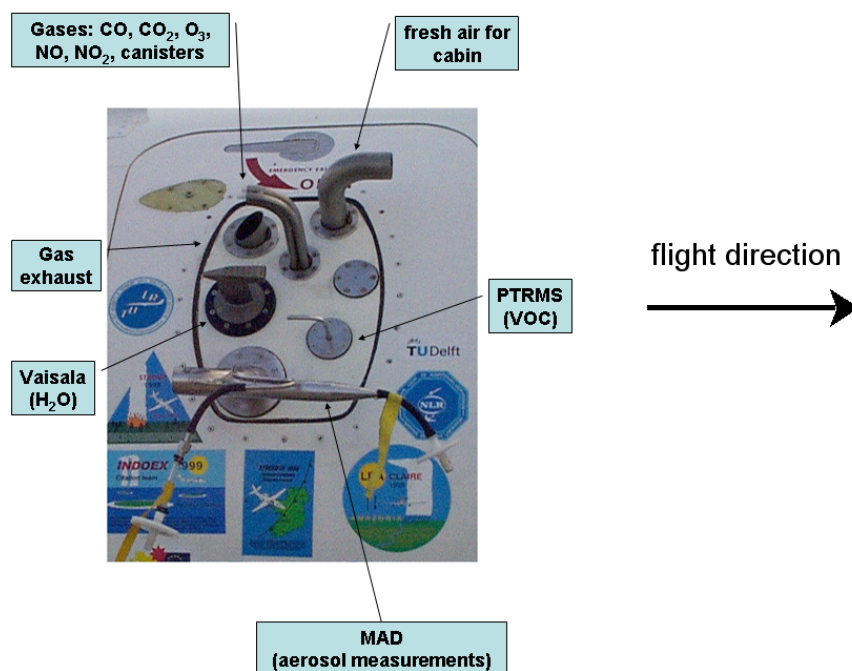


Figure 5.3: The configuration of the inlet probes during the INDOEX campaign. For the gas measurements, teflon sample lines are used. The inlet of the aerosol instrumentation (MAD) was barred by particle filters when the aircraft was grounded, to avoid contamination. The big metal hose pointing into flight direction was used for cooling the cabin with outside air as long as the outside pressure (plus impact pressure) was higher than the pressure inside the cabin.

load started with a atmospheric chemistry package, which was expanded by the build-in of a Gerber (Particle Volume Monitor - a laser diffraction instrument) and FSSP-100 (Forward Scattering Spectrometer Probe) instrument to a cloud droplet package after the 6th of March 1999. Exemplary, Figure 5.5 on page 60 displays a selection of measurements (CO, acetone, ozone, and several canister samples) performed onboard the Citation on March 1.

The instruments, whose data were analysed and interpreted in the context of this work are further described in the following paragraphs.

CO

was measured using a tuneable diode laser absorption spectrometer (TDLAS) called TRISTAR (tracer in situ TDLAS for atmospheric research) [Wienhold *et al.*, 1998], developed by the Max Planck Institute for Chemistry, Mainz, Germany. During the INDOEX campaign, CO was analysed at a wavenumber of $k = 2176,7 \text{ cm}^{-1}$. CO data were smoothed with a minimum of eleven second averaging to reduce instrumental noise, details are given in chapter 4.5. The average precision (for definition see chapter 4.5.2) during the INDOEX measurement flights was 7.3 % (1σ) and the calibration accuracy was $\pm 2.8 \%$.

Measured Species	Technique	Instrument by
CO (N ₂ O, CH ₄)	Tunable diode laser absorption spectroscopy	MPI-A, Mainz
CH ₄	Gas chromatography	MPI-A, Mainz
DMS, NMHC, carbonyls, organic acids	Proton transfer mass spectrometer	IMAU, Utrecht
Relative humidity	Vaisala humidity capacitor	IMAU, Utrecht
NMHC	Gas chromatography (from canisters)	IMAU, Utrecht
3-D wind vector	Pressure transducers, inertial reference system, global positioning system	DUT, Delft
NO, NO ₂	Chemiluminescence detector, photolytic converter (NO ₂)	MPI-A and MPI-B, Mainz
J _{NO₂} , DIRAM (actinic flux)	Photo-optical detectors (directional radiance and 360° UV-VIS)	IMAU, Utrecht
CO ₂	Infrared analyser	MPI-A, Mainz
O ₃	Chemiluminescence detector	IMAU, Utrecht
Aerosols (6 - 1000 nm) number concentration and size distribution	Optical particle counter, condensation particle counter, differential mobility analyser,	ITM, Stockholm
Aerosol chemical composition	filter samples	ITM, Stockholm
Aerosol radiative properties	Nephelometer, particle soot absorption photometer	MPI-B, Mainz, ITM, Stockholm
Liquid water content and droplet surface area	Particle volume monitor (laser diffraction instrument)	IMAU, Utrecht
Droplet spectrum	Forward scattering spectrometer probe	NCAR, Boulder

Table 5.2: Instrumentation onboard the Cessna Citation during the INDOEX campaign. A list of the abbreviations of the institutes is given in the acronyms section.

C2-C9 NMHCs (nonmethane hydrocarbons) and methyl chloride

were measured by a combination of canisters samples and gas chromatography analysis [Scheeren *et al.*, 2002]. During each flight several electropolished stainless steel canisters, provided by Utrecht University, The Netherlands, were pressurised with air samples. Within 20 to 45 days after the sampling, the canisters were analysed in Utrecht, using a Varian Star 3600 CX gas chromatograph equipped with a CP-Silica PLOT column and a flame ionisation detector for nonmethane hydrocarbons and methyl chloride or an electron capture detector for chlorocarbons [Scheeren *et al.*, 2002]. The filling time of the canisters depended on the ambient pressure, and ranged between 15 seconds at 3 km altitude and 165 seconds at 12.5 km [Lelieveld *et al.*, 1999]. During this time, the aircraft covers a distance between 2.5 km and 25 km, respectively. The accuracy of NMHC measurements is determined by the uncertainty of the PRAXAIR standard NMHC mixture that is used for calibration. The accuracy was 3 % and the precision for data values greater than 10 pptv was for ethane (C₂H₆) 4 %, acetylene (C₂H₂) 3 %, propane (C₃H₈) 10 %, propene (C₃H₆) 26 %, methyl chloride (CH₃Cl) 1 %, n-butane (n-C₄H₁₀) 9 %, i-butane (i-C₄H₁₀) 30 %, n-pentane (n-C₅H₁₂) 25 % (for values < 10 pptv), i-pentane (i-C₅H₁₂) 10 %, benzene (C₆H₆) 8 %, toluene (C₇H₈) 4 %.

Payload Configuration PH-LAB INDOEX 1999

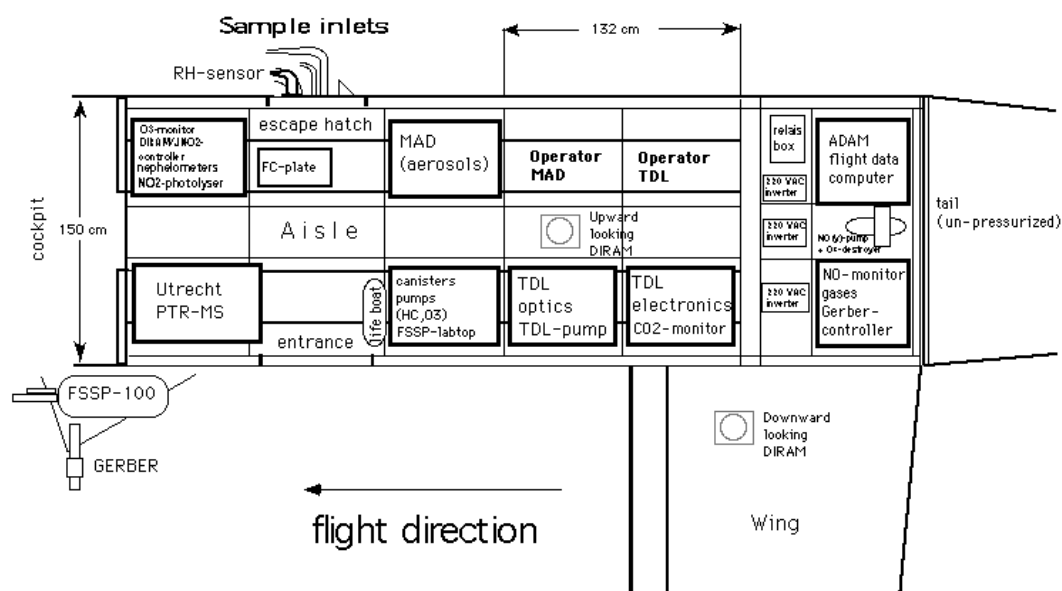


Figure 5.4: Payload configuration during the INDOEX campaign. The particle volume monitor and forward scattering spectrometer probe instruments were only part of the cloud physics payload, and therefore implemented after the March 6. Figure from <http://www.phys.uu.nl/~scheren/INDOEX/INDOEXvs1.html>.

Methane

was measured from the same canister samples as the NMHCs. It was measured at the Max-Planck-Institute for Chemistry in Mainz, Germany, using a Shimadzu GC-7 gas chromatograph with a Porapak-Q (Alltech) column and flame ionisation detector [Marik *et al.*, 2002]. Reproducibility for the measurements was between 0.4 % and 4.9 % (average 2.1 %). The accuracy of the measurements is determined by the uncertainty of the NOAA (National Oceanographic and Atmospheric Administration) standard that is used for calibration of the methane measurements.

Volatile organic compounds (VOCs)

were measured in-situ by a proton transfer mass spectrometer (PTR-MS). This technique is based on chemical ionisation of the species with H_3O^+ ions in a drift-tube reactor, and the detection of the product ions by a quadrupole mass spectrometer (Balzers 422). Calibration of the instrument relative to standard mixture of VOCs in N_2 was carried out prior to and after the campaign. Every selected mass was measured for 1 second every 12 seconds. The precision for acetone was 20 %, and for acetonitrile 30 %. The calibration uncertainty of these measurements was 20 %, so that the total accuracy of acetone was 28 %, of acetonitrile 36%. A detailed description of the instrument is given by Lindinger *et al.* [1998a] and Lindinger *et al.* [1998b].

5.3 Atmospheric layers during INDOEX

Carbon monoxide is an ideal tracer to study transport in the atmosphere, since it has a moderate lifetime of about two weeks in the tropics, and it is not influenced by clouds and wet deposition. Figure 5.5 shows an example of a CO measurements recorded on March 1, together with the altitude during the flight. Obviously, there is a connection between the measured CO mixing ratios and the altitude. This is more easily recognised, when CO measurements are plotted as function of the altitude. Figure 5.6 shows all CO measurements performed during INDOEX, together with an average altitude profile of CO mixing ratios over the entire campaign. The vertical profile is shaped like a “C”, with high concentrations in the boundary layer and upper level (between 8 and 12 km altitude) and lower concentrations in between. This shape leads to a natural division of the measured atmosphere in layers: a polluted bottom layer, an intermediate middle layer with low CO mixing ratios, and an outflow region with elevated mixing ratios on top. A study of thermodynamic profiles (Figure 5.7) reveals that the polluted layer actually consists of the marine boundary layer and a land plume layer, which is also called “residual pollution layer”. Hence, four levels are identified: the marine boundary layer with high CO concentrations from sea level up to maximum 1 km. A “residual pollution layer”, extending from the top of the marine boundary layer to about 3 km altitude, where the CO concentrations gradually decreased. An intermediate layer, between 3 and 8 km, with rather low CO concentrations, and an outflow region between 8 and 12.5 km (maximum altitude of the aircraft), where elevated CO mixing ratios were observed. In the following paragraphs, the origin and characteristics of these layers will be described.

Marine boundary layer

The highest CO mixing ratios, in the range of 77 to 355 ppbv with an average of 181 ± 48 (1σ) ppbv, were encountered in the marine boundary layer in the Northern Hemisphere. The CO concentrations measured in February 1999 in the northern Indian Ocean were up to 50 % higher than those observed in previous years [*de Laat and Lelieveld, 2002*] and comparable to levels measured in areas of Europe and North America [*Khalil and Rasmussen, 1994*]. The fact that mixing ratios of this magnitude were exceptional is illustrated by the following quote, published in the *INDOEX Research News Release*, March 1999:

“Scientists were surprised to find that a dense brownish pollution haze extended from the ocean surface to 1 to 3 km altitude... The haze layer also contains relatively high concentrations of gases including carbon monoxide, various organic compounds, and sulfur dioxide. The concentrations of these gases are conclusive evidence that the haze layer is caused by pollution... INDOEX scientists were surprised to find such a dense pollution haze layer derived from sources at least a thousand or more kilometers away.” [*principal investigators participating in INDOEX, 1999*].

The air masses in this layer originated from plumes that were transported with northeasterly and northwesterly flows from the Indian subcontinent and Southeast Asia. In the source region, the air pollution was mostly due to agricultural burning and biofuel use, which enhance carbon monoxide concentrations, as well as fossil fuel combustion and biomass burning, which cause a high aerosol loading [*Lelieveld et al., 2001*]. *de Laat and Lelieveld [2002]* state that strong continental outflow together with weak ITCZ convection, which is due to a passive phase of the Madden-Julian Oscillation¹, resulted in accumulation of high pollution levels in the northern Indian Ocean in February 1999.

¹The MJO is related to an upper tropospheric eastward propagation of atmospheric features, associated with variations in deep tropical convection. The typical period of these oscillations is 30-60 days. See chapter 2.3.

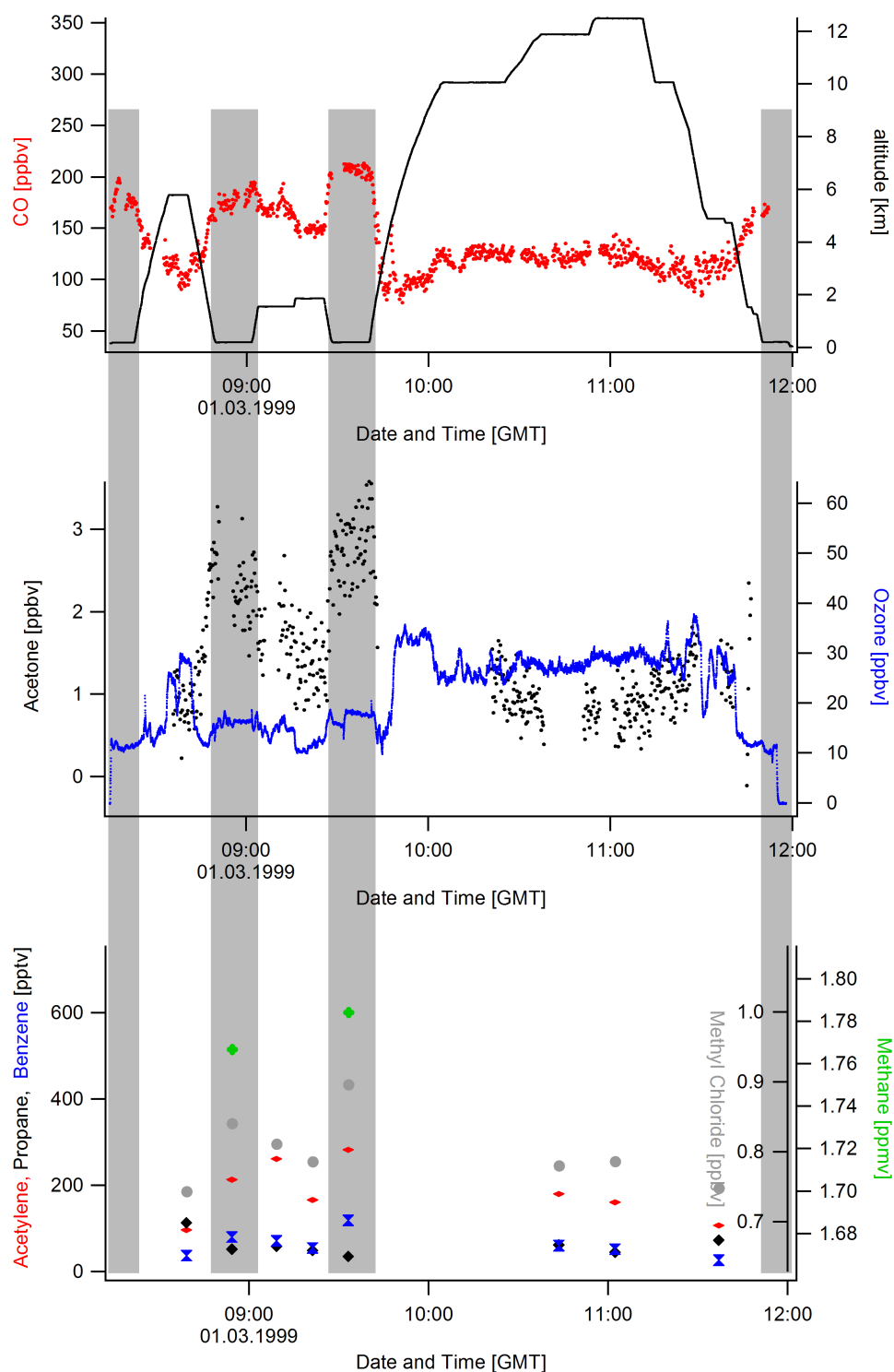


Figure 5.5: Selection of airborne measurements during the INDOEX campaign sampled on March 1. The grey shaded area denotes altitudes below 1 km, which were analysed in the variability-lifetime study. In the first half of the flight, the correlation in the general trend of CO (top graph) and acetone data (middle graph) is found. Even small scale features are found in inverse trends of CO and ozone (middle graph). The Hydrocarbon data (bottom graph) results from canister analysis, hence the smaller number of data points.

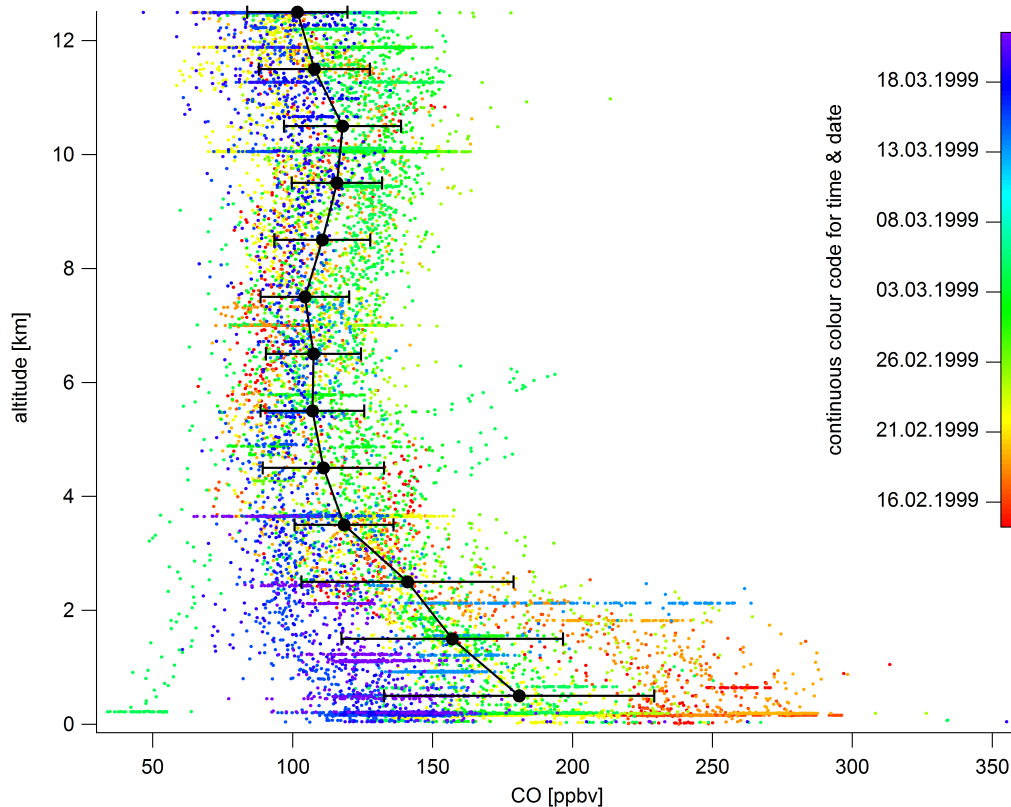


Figure 5.6: CO mixing ratios observed during INDOEX. The colour code represents the date and time of the measurements. The black markers represent the average CO concentration over the entire campaign, calculated for 1 km altitude bins between 0 and 13 km. The markers are set at the middle of the altitude bins. The bars are the standard deviation of all data points in the respective bins.

The altitude of the marine boundary layer varies between 300 m near the coast and 1 km near the equator, but did nowhere extend to more than 1 km altitude [Roswintarti *et al.*, 2001; Raman *et al.*, 2002]. Apart from two flights where we landed or flew by Sri Lanka, we did not get closer to larger landmasses than about 240 km (see Figure 5.1). Hence, the upper limit for the marine boundary layer was set to 1 km altitude. Note that most data we collected in the marine boundary layer stem from measurements taken during constant (isobaric) level flights between 150 and 200 m altitude.

During flight 11b on March 4, 1999 measurements were performed in the Southern Hemisphere. This manifested itself in very low CO mixing ratios, down to 50 ppbv, in the marine boundary layer. This is comparable to average CO mixing ratios of 54.1 ± 4.0 and 59.3 ± 3.7 ppbv observed in the marine extratropical and equatorial Southern Hemisphere, respectively, reported by Rhoads *et al.* [1997]. Obviously, there is a strong gradient in the composition of the air on both sides of the ITCZ. There is strongly polluted air in the Northern Hemispheric boundary layer and relatively pristine air in the Southern Hemisphere. Back trajectories, which were provided by the KNMI, for the Southern Hemisphere data show that the air originated from a southeasterly direction and had not been in contact with continental pollution sources for the last 10 days [Williams *et al.*, 2002]. A detailed discussion of the near equatorial CO and O₃ profiles and cross-ITCZ gradients during the INDOEX campaign can be found in Williams *et al.* [2002]. Since the Southern Hemispheric air masses have a very different origin compared to the air masses in the Northern Hemisphere, this data was excluded from the variability study.

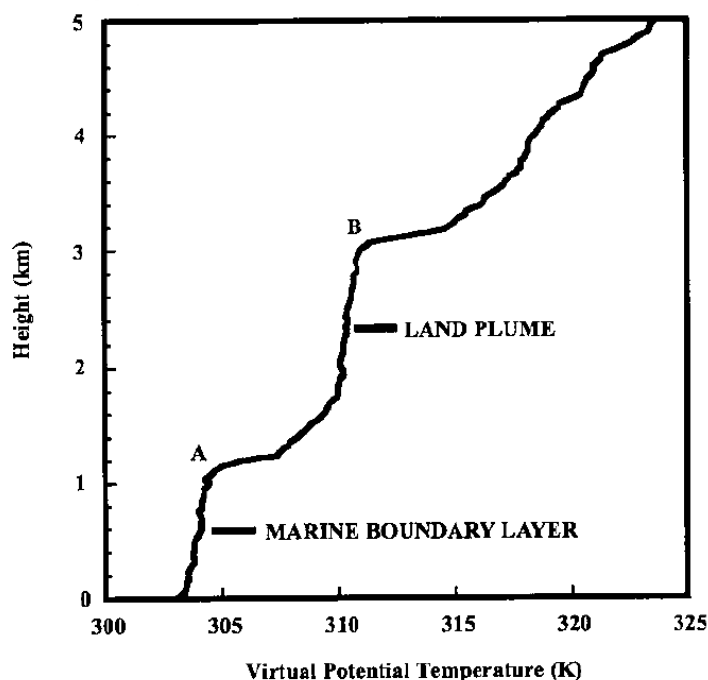


Figure 5.7: Virtual potential temperature profile taken from R/V Ron Brown on March 7, 1999 at 12 UTC. It shows the marine boundary layer in the lowest layer up to 1 km altitude, and above the land plume in the 1–3 km height layer. From *Simpson and Raman* [2004].

“Residual” pollution layer

The layer above the marine boundary layer carries polluted planetary boundary layer air from the continent to the sea. During daytime, polluted air is convected over land up to about 2 or 3 km high, and the monsoonal flow systems transport this air above the marine boundary layer, which is at this time only about 1 km high or less. Much of the air is not re-circulated in the sea-breeze circulation (Figure 5.8), which means it is not transported back towards the land at low altitudes, but stays over the sea and forms a pollution layer up to about 3 km altitude. During nighttime the planetary boundary layer stabilises with a lower vertical extent, while the daytime pollution layer persistent above is cut-off from the surface, still following the main flow system. Because of weak convection in the Indian outflow region during this season, the pollution layer coming from the continent during day and night stays intact, even 600 to 800 km away from the nearest landmass, and forms a “residual” pollution layer over the ocean [*Raman et al.*, 2002; *Lelieveld et al.*, 2001]. Vertical profiles of specific humidity show the difference between the moist boundary layer air and the dry “residual” pollution layer above. Also virtual potential temperature profiles (Figure 5.7) illustrate the difference. The CO mixing ratios in the “residual” pollution layer varied from 60 to 313 ppbv (150 ± 40 ppbv).

Intermediate layer - lower tropical free troposphere

The intermediate layer is located between 3 and 8 km altitude. This layer shows relatively low CO mixing ratios in the range of 64 - 194 ppbv (112 ± 19 ppbv), indicating photochemically processed air masses. These air masses have very different origins. *de Gouw et al.* [2001] studied back trajectories in order to identify the origins of the air masses and found that their composition was more influenced by subsidence than by convection, which is consistent with the Hadley circulation. Back trajectories

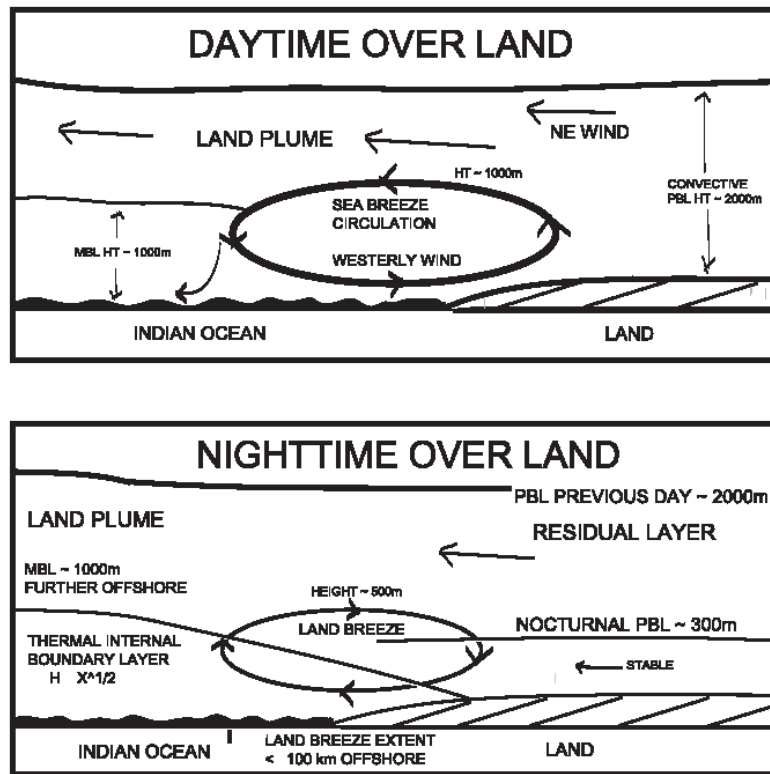


Figure 5.8: Concept of sea- and land breeze circulation for daytime (top) and nighttime (bottom). Figure from *Raman et al.* [2002].

showed that on February 16, the air originated from tropical regions over Africa near the jet stream [*de Gouw et al.*, 2001]. *Williams et al.* [2002] studied ozone, carbon monoxide and relative humidity profiles of the flights of March 4, and found evidence of upper tropospheric or even stratospheric air being mixed into this layer. In the Northern Hemisphere, the authors found subsidence and advection of stratospheric air associated with the sub-tropical jet stream to be the most probable cause. In the Southern Hemisphere they identified air that was “entrained from above a southern hemispheric tropical cyclone”. *Zachariasse et al.* [2001] analysed ozone profiles measured from the R/V Ron Brown, trajectories and ECMWF model data and concluded that ozone maxima in the free troposphere stem from air from the subtropical jet stream, which is a region where stratosphere-troposphere exchange takes place.

Top layer - upper tropical free troposphere

The top layer, 8-12.5 km, shows a broader range of CO mixing ratios between 46 and 214 ppbv (110 ± 20 ppbv). In the vertical profile, Figure 5.6, the tendency of CO mixing ratios to higher numbers in this region can be clearly identified, showing a second layer of enhanced CO mixing ratios. These elevated CO mixing ratios result from convective outflow which is connected to the ITCZ. The cloud tops of convective cells, which were present over the measurement region during the entire campaign, typically reached 10-12 km altitude. In general, the air masses originated in Southeast Asia, Indonesia, China, and even Australia [*de Gouw et al.*, 2001]. *Gettelman et al.* [2002] found the main convective outflow in the tropics to be at ~ 12 km, in contrast to the cold point of the temperature profile, which is in general located at about 17 km. The convective outflow and the temperature cold point form the lower and upper limits of the tropical tropopause layer (TTL) [*Atticks*

and Robinson, 1983; Highwood and Hoskins, 1998]. During INDOEX, the cold point was located at about 18 km altitude [Santacesaria *et al.*, 2003], so that the TTL extended from about 10 to 18 km.

Temporal development

The C-shape in the CO profile became weaker throughout the campaign. The weakening effect is illustrated by the colour code in Figure 5.6, which represents the time during the measurement campaign. The C-shape weakened in general at all altitude levels, but the decrease of boundary layer CO mixing ratios was the most obvious feature. From the start of the campaign until February 19, high CO mixing ratios of 250 ± 21 (1σ) ppbv were observed (red points). During the course of the campaign, the boundary layer concentrations became lower (180 ± 25 ppbv; green points from February 22 - March 4) and reached their lowest values towards the end of the campaign (139 ± 19 ppbv; blue points, March 13 and onwards). The few green points reaching down to 50 ppbv stem from flight 11 on March 4, when Southern Hemispheric air was sampled.

The temporal development gets clearer when plotting the average CO mixing ratio for each flight against time, which is shown in Figure 5.9 for two different altitude ranges. Figure 5.9a includes all data between 10 and 12.5 kilometres altitude, Figure 5.9b all data below 1 km altitude. In Figure 5.9b it can be clearly seen, that the “surface” CO mixing ratios decreased throughout the campaign, which was caused by the change of the wind direction associated with an anticyclone located over the Bay of Bengal. Polluted air was advected into the measurement area from the Bay of Bengal at the beginning of the campaign, while trajectories indicate an air-mass origin from the Arabian sea towards the end of the campaign (see section 5.1). As was discussed above, enhanced CO mixing ratios in the top layer were caused by convection, which occurred more often in March than in February [de Gouw *et al.*, 2001]. However, such events occur in a sporadic way, thus one does not expect to find a strong dependency of CO concentration at high altitudes on the time evolved since the start of the campaign.

Comparison with CO measurements onboard the R/V Ron Brown

Carbon monoxide was also measured onboard of the research vessel “Ronald H. Brown” during INDOEX. The measurements were performed using the tunable diode laser absorption spectrometer FLAIR (Four Laser Airborne Infra Red) [Roths, 1992], also operated by the Max-Planck-Institute for Chemistry in Mainz [Wagner, 2000]. The data is shown in Figure 5.9b (green points). The first three data points show southern hemisphere measurements, although sampled in more westerly direction compared to our measurements. The three later data points show measurements that were taken close to Male, comparable to the position of the aircraft measurements. The agreement between the measurements onboard the aircraft and the ship is good, although no direct intercomparison has been performed.

In the remainder of this chapter, INDOEX data from the northern hemisphere marine boundary layer will be studied with the help of the variability technique.

5.4 Variability during INDOEX

Figure 5.10 shows the variability of the measured trace gases in the Northern Hemispheric marine boundary layer during INDOEX (14.2. - 21.3.1999, sampled below 1 km altitude). The variability was calculated according to the procedure described in section 3.6 and illustrated in Figure 3.15 on page 33. The lifetimes of the different trace gases were calculated according to

$$\tau = \frac{1}{k_{phot} + k_{OH} \cdot [OH]} \quad (5.1)$$

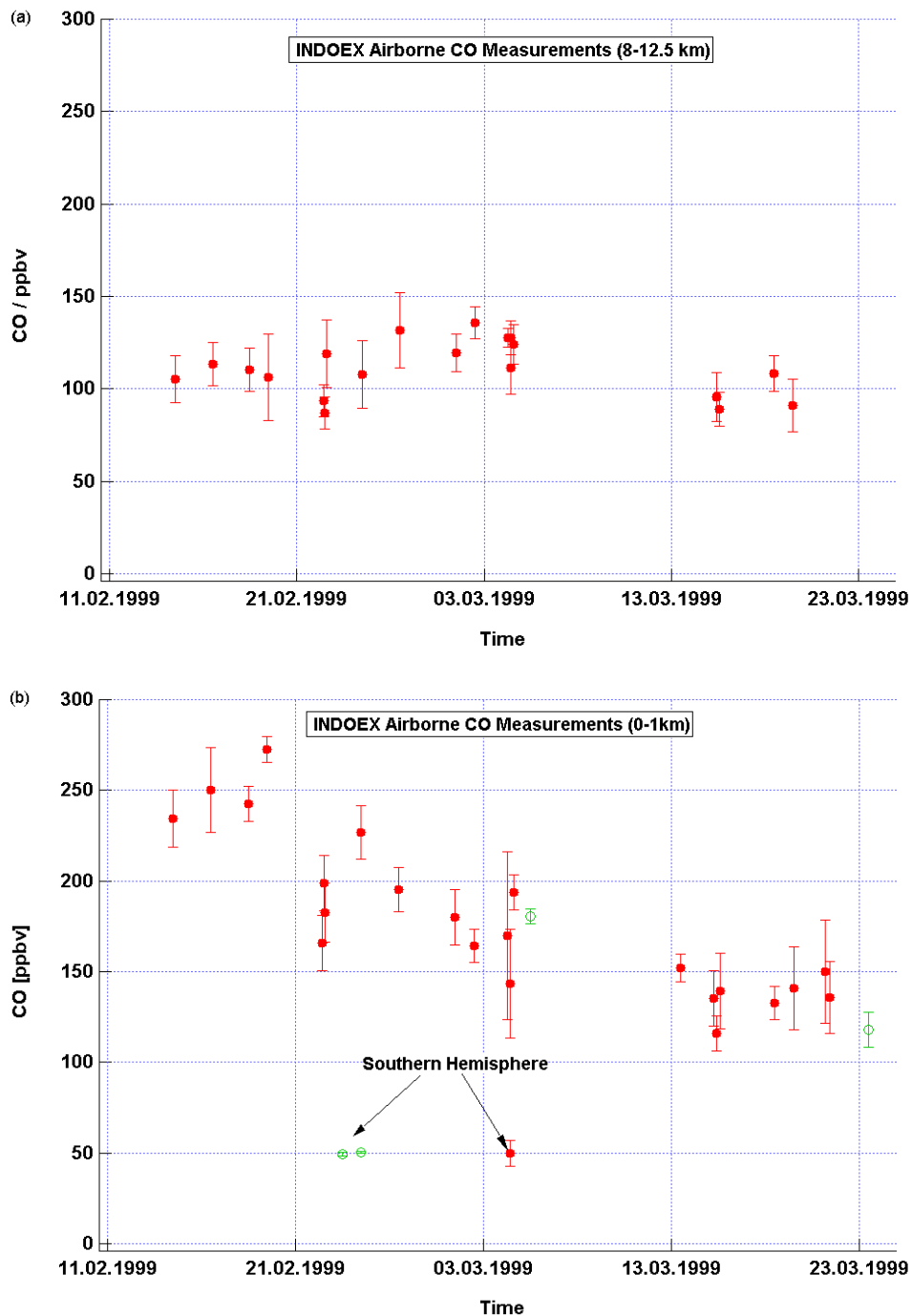


Figure 5.9: Temporal development of CO mixing ratios during INDOEX. The upper panel includes all data between 10 and 12.5 kilometres altitude, the lower one below 1 km altitude. In the lower panel CO measurements performed onboard the “R/V Ron Brown” are also included (green markers). For the ship only data in the measurement area of the aircraft and during time periods close to our aircraft measurements are shown. The southern hemisphere flight on March 4, 1999 is represented separately.

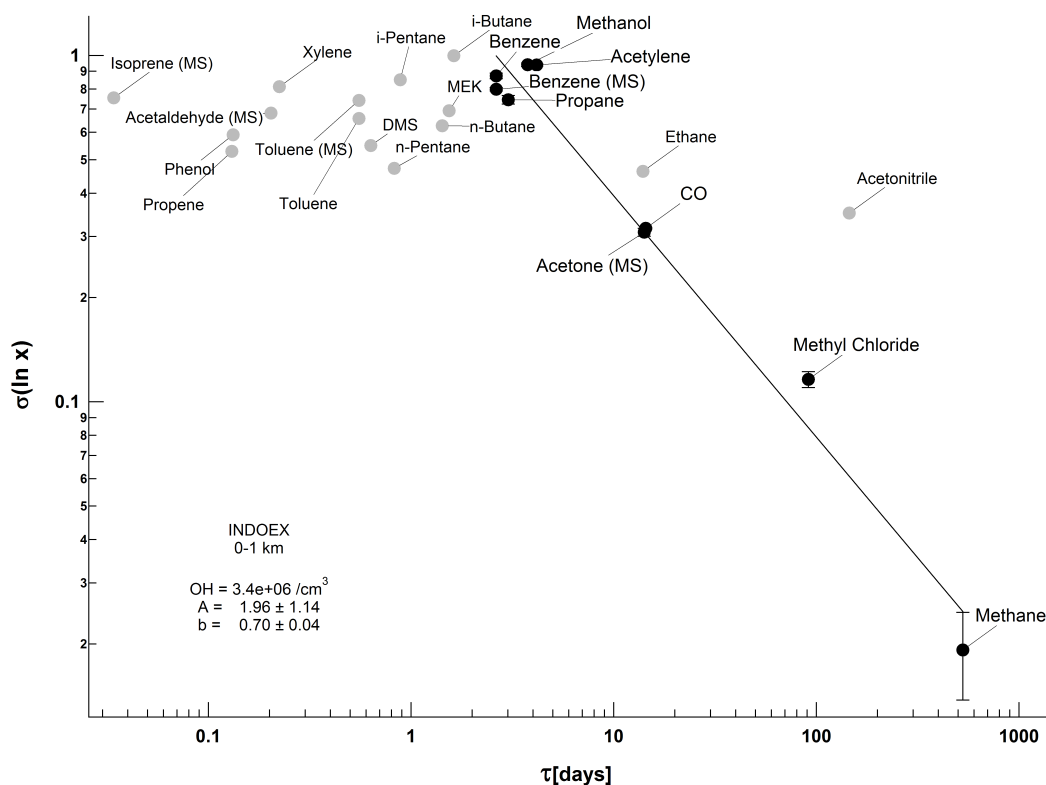


Figure 5.10: Variability plot of all data below 1 km altitude. Species following the variability-lifetime relationship are taken for the fit and represented by solid black circles. For these species, the σ -error is displayed. Note that on a logarithmic scale the error bars at smaller σ -values may appear larger than those at greater σ -values. The fit through the solid black data points is marked by the line. Species excluded from the fit (see text) are solid grey circles.

where k_{OH} is the reaction rate with respect to reaction with OH, and k_{phot} is the photolysis rate. This approach implies that the residence time for these species is determined by degradation via OH and in the case of methyl chloride, acetone, methyl ethyl ketone (MEK) and acetaldehyde also by photolysis. The reaction and photolysis rates used are given in Table 5.4. The photolysis rates in the table are average noon values over the measurement region ($5^{\circ}N - 5^{\circ}S$) from middle February until middle March at the lowest 1 km altitude, taken from the photolysis model of *Brühl and Crutzen* [1989]. Data from a standard cloud atlas was incorporated into the model to include the effect of clouds. A third of these photolysis rates is taken in this study for the average diurnal photolysis rate. Where no photolysis rate is given, this process is negligible for the calculation of the lifetime. Table 5.4 also shows the calculated lifetime in the marine boundary layer during INDOEX. Most reaction rates are temperature dependant and the CO reaction rate shows additionally a pressure dependance. For the determination of the reaction rates averaged values of temperature and pressure were calculated from onboard measurements. The average temperature below 1 km altitude was $26.5^{\circ}C$, the average pressure was 975.7 hPa. The main part of the measurements was performed between 1:00 p.m. and 4:15 p.m.. Temperature measurements performed at the Kaashidhoo Climate Observatory (KCO) based on Kaashidhoo ($4.9^{\circ}N, 73^{\circ}E$), Indian Ocean, show a minimum in temperature about 4:25 a.m. and a maximum at about 2:40 p.m., with an absolute difference of less than 1 K. Hence the measured temperatures onboard the aircraft are mostly taken during the hottest time of the day. A discussion of the effect of the temperature variation on the variability study will follow in the section 5.4.1. All reaction rate formulas, are given in table 5.4. In the following text, the issue of uncertainties for

the reaction rates will be discussed: a remark in the chemical kinetics data base of *Atkinson et al.* [2002] is quite insightful in this context. The authors state that

“For single studies of a particular reaction involving one technique, standard deviations, or even 90% confidence limits, of $\pm 10\%$ or less are frequently reported in the literature. Unfortunately, when evaluators come to compare data for the same reaction studied by more than one group of investigators and involving different techniques, the rate coefficients often differ by a factor of 2 or even more. This can only mean that one or more of the studies has involved large systematic uncertainties which are difficult to detect. This is hardly surprising since, unlike molecular reactions, it is not always possible to study atomic and free radical reactions in isolation, and consequently mechanistic and other difficulties frequently arise.”

Obviously, for reaction rates, the correct total uncertainty is often difficult to specify. In addition, the reaction rate errors found in literature are often not comparable, because they include different effects, which will be exemplified in the following. 23 different species with reaction rates from 11 different sources are presented in the INDOEX study. Nine reaction rates were taken from chemical kinetic data bases that publish evaluated chemical kinetics and photochemical data after extensive literature review [*DeMore et al.*, 1997; *Atkinson et al.*, 1997, 2001]. In these reviews the authors recommend reaction rates based on several independent techniques (if available) and the authors assign absolute uncertainties to the parameters in the reaction rates. However, they state that those errors are a subjective assessment of the evaluators, and that they are *not* determined by “rigorous, statistical analysis of the database, which is generally too limited to permit such an analysis”. Their assessment of the error is based on the knowledge of the techniques, the difficulties of the experimental measurements, the potential for systematic errors, and the number of studies conducted and their agreement or lack thereof [*DeMore et al.*, 1997]. This error is principally different from those found in other literature, for example in *DeMore and Bayes* [1999]. These authors derived relative reaction rate constants for the reaction of OH with several non-methane hydrocarbons. *DeMore and Bayes* [1999] state the errors given by them are “the standard deviations of the least-squares fit and do not reflect uncertainties in the reference rate constant”. Yet another error is given by *Wollenhaupt et al.* [2000], who used a fluorescence detection method to determine the (absolute) reaction rate of OH with acetone. The authors quote the statistical error of the parameter at room temperature. These examples point out that the errors found in literature often lack the hard to assess component of possible systematic errors, which was pointed out by *Atkinson et al.* [2002], and the errors found may result from different approaches. Thus the errors are not comparable and will not be accounted for in the presented study. Nevertheless, a sensitivity test of the OH estimation regarding the influence of “changing” reaction rates for some species is presented in section 5.4.1.

An error for the photolysis rates is hard to assess, since it includes errors in the parameters used in the models as well as possible differences between assumptions made in the model, like cloud coverage, and the actual state of the atmosphere during our measurements. In order to estimate the influence of a deviation of the photolysis rates on the estimated OH concentrations, a sensitivity test is presented in section 5.4.1, where the photolysis rates were varied by $\pm 30\%$.

The OH concentration that was used for the calculation of the lifetime was obtained by optimising the variability-lifetime relationship, according to the procedure which is explained in chapter 3.6. The OH concentration, which produces the best fit through the variability-lifetime relationship was $3.4 \cdot 10^6$ molecules/cm³ (see Figure 5.10) and will be discussed in section 5.4.1.

Species marked solid black do follow the variability-lifetime relationship and are the basis for the presented variability-lifetime analysis. These are benzene (measured by the in-situ mass spectrometer as well as the canister/gas chromatograph), propane, methanol, acetylene, acetone, CO, methyl chloride and methane. A number of other species were also measured, marked grey, but had to be excluded

from the analysis. The reasons for the exclusions will be discussed in the following paragraphs.

As the variability-lifetime study is based on statistical analysis, it is very important that only real atmospheric variability influences the standard deviation of the measured trace gases. In order to ensure this, histograms and cumulative Gaussian distribution graphs of all species were plotted. For the above named trace gases (benzene, propane, methanol, acetylene, acetone, CO, methyl chloride and methane), this analysis showed a distribution of trace gas mixing ratio due to sampling of different atmospheric air masses. The analysis proved that the measured data was above the detection limit of the instruments, and the atmospheric variability was greater than the scatter of the data due to instrumental noise. Hence, the data is appropriate for analysis in respect to atmospheric processing of the air masses.

For n-pentane, i-pentane, n-butane and toluene (measured with the GC during INDOEX), the cumulative Gaussian distribution showed a kind of binning, that means data points are not continuously distributed but accumulate at discrete values. For species whose lifetime is short compared to the transit time from the source to the measurement area, mixing ratios are very low. When the mixing ratios are close to the detection limit of the instrument and the accuracy of the data is too low, binning of the data values results. Therefore, those species are not suitable for the statistical analysis and are excluded from the variability study.

Also isoprene, phenol, acetaldehyde, xylene, DMS, propene, i-butane and MEK do not follow the variability-lifetime relationship. *Jobson et al.* [1998] and *Williams et al.* [2000] both observed, that species with a lifetime shorter than about 5 days do not follow the variability-lifetime trend. In our study, the variability of the species falls off for lifetimes shorter than 2.6 days. INDOEX measurements took place 2 to 3 days downwind from major pollution sources, which agrees very well with the fall off time of 2.6 days. The fall off could be caused by the low mixing ratios of the species, which is a result of the high reactivity. When the accuracy of the instruments is too low to measure these low mixing ratios, the resulting data variability is lower than the expected atmospheric variability.

The variability of ethane is higher than implied by the variability-lifetime relationship. In the variability-lifetime study of *Williams et al.* [2000], over the Amazonian rain forest (LBA-CLAIRE campaign²), this was also found and could be traced back to a problem in the data processing of the gas chromatograph signal. The authors found “occasional splitting of the ethane peak, possibly caused by the absence of a CO₂ trap in the system”. Apparently the analysis program integrated only one of the peaks, so only a part of the actual ethane in the sample would be appraised. Due to this “incorrect” integration the variability of ethane would then be artificially enhanced. Therefore the authors excluded ethane from the variability-lifetime study. Since then, the gas chromatographic system was altered, however, the variability of ethane is still higher than according to the variability-lifetime relationship. Therefore the argumentation of *Williams et al.* [2000] was followed and ethane excluded. However, a sensitivity study with ethane included was also performed, and will be discussed in section 5.4.1.

Finally, acetonitrile has been excluded from the variability-lifetime analysis, because acetonitrile has more sinks than are considered in the lifetime calculation. Note that for the calculation of the lifetime in Figure 5.10 only photolysis and the reaction with OH was considered. In the troposphere, acetonitrile can be removed from the atmosphere by wet deposition and by ocean uptake [*Jost et al.*, 2003]. Due to these additional sinks, the lifetime of acetonitrile can be as short as 15 days [*Hamm et al.*, 1984], compared to about 165 days when only photolysis and reaction with OH are considered. This additional sink is hard to quantify, as it requires quantitative knowledge of wet deposition on the oceans and various forms of precipitation, its dependence on temperature, pH value, size of water droplets and their number concentrations. Since we are not able to reproduce the complex source/sink

²Large Scale Biosphere-Atmosphere Experiment in Amazonia - Cooperative LBA Airborne Regional Experiment

signature of acetonitrile, this species was excluded from the analysis.

In the remainder of this work, the variability-lifetime relation will be analysed based on the species represented by solid black circles. Small instrumental artifacts, additional sinks or secondary production can cause the remaining deviation of those data points from the variability lifetime relationship. In table 5.3 the number of data points is given for those species, that were taken into account for the variability study.

species	number of points _{0-1km}	number of points _{troposphere}
Methanol	843	4818
Acetone (MS)	1165	7284
Benzene (MS)	1115	5605
Acetylene	28	95
Propane	29	96
Methyl Chloride	29	96
Benzene (GC)	29	96
CO	3250	14629
Methane	16	16

Table 5.3: Number of data points in the variability study during INDOEX, given for those species that were taken for the fit. Note that methane data is only available for the boundary layer.

species	OH reaction rate	reference	phot. rate	lifetime [days]
Methanol	$6.71 \cdot 10^{-12} \cdot e^{-\frac{600}{T}}$	<i>DeMore et al.</i> [1997]		3.8
Acetonitrile	$7.80 \cdot 10^{-13} \cdot e^{-\frac{1050}{T}}$	<i>Atkinson et al.</i> [1997]		145
Acetaldehyde	$2.49 \cdot 10^{-12} \cdot \left(\frac{T}{298}\right)^{0.73} \cdot e^{-\frac{560}{T}}$	<i>Baulch et al.</i> [1992]	$6.710 \cdot 10^{-6}$	0.20
Acetone	$8.80 \cdot 10^{-12} \cdot e^{-\frac{423}{T}}$	<i>Wollenhaupt et al.</i> [2000]	$8.637 \cdot 10^{-7}$	14
	$+1.70 \cdot 10^{-14} \cdot e^{-\frac{423}{T}}$			
DMS	$5.38 \cdot 10^{-12}$	<i>Turnipseed et al.</i> [1996]		0.63
Isoprene	$2.55 \cdot 10^{-11} \cdot e^{-\frac{409}{T}}$	<i>Atkinson</i> [1986a]		0.034
Benzene	$7.57 \cdot 10^{-12} \cdot e^{-\frac{529}{T}}$	<i>Atkinson</i> [1986a]		2.6
Toluene	$2.1 \cdot 10^{-12} \cdot e^{-\frac{322}{T}}$	<i>Atkinson</i> [1986a]		0.55
MEK	$1.3 \cdot 10^{-12} \cdot e^{-\frac{25.00}{T}}$	<i>Atkinson et al.</i> [2001]	$1.376 \cdot 10^{-5}$	1.5
Phenol	$3.7 \cdot 10^{-13} \cdot e^{-\frac{1270}{T}}$	<i>Semadeni et al.</i> [1995]		0.13
o-Xylene	$1.22 \cdot 10^{-11}$	<i>Atkinson and Aschmann</i> [1989]		0.22
p,m-Xylene	$1.66 \cdot 10^{-11} \cdot e^{-\frac{116}{T}}$	<i>Atkinson</i> [1986a]		0.22
Ethane	$8.69 \cdot 10^{-12} \cdot e^{-\frac{1070}{T}}$	<i>Atkinson et al.</i> [1997]		14
Acetylene	$k_0 = 5.5 \cdot 10^{-30}$	<i>DeMore et al.</i> [1997]		4.2
	$k_\infty = 8.3 \cdot 10^{-13} \cdot \left(\frac{T}{300}\right)^2$			
Propane	$1.00 \cdot 10^{-11} \cdot e^{-\frac{660}{T}}$	<i>DeMore et al.</i> [1997]		3.1
Propene	$4.85 \cdot 10^{-12} \cdot e^{-\frac{504}{T}}$	<i>Atkinson</i> [1986a]		0.13
Methyl Chloride	$4.00 \cdot 10^{-12} \cdot e^{-\frac{1400}{T}}$	<i>DeMore et al.</i> [1997]	$1.00 \cdot 10^{-14}$	91
i-Butane	$8.28 \cdot 10^{-13} \cdot \left(\frac{T}{298}\right)^2 \cdot e^{-\frac{275}{T}}$	<i>Talukdar et al.</i> [1994]		1.6
n-Butane	$1.68 \cdot 10^{-11} \cdot e^{-\frac{584}{T}}$	<i>DeMore and Bayes</i> [1999]		1.4
i-Pentane	$3.85 \cdot 10^{-12}$	<i>Atkinson</i> [1986a]		0.88
n-Pentane	$2.78 \cdot 10^{-12} \cdot \left(\frac{T}{298}\right)^2 \cdot e^{-\frac{115}{T}}$	<i>Talukdar et al.</i> [1994]		0.83
CO	$1.5 \cdot 10^{-13} \cdot \left(1 + 0.6 \cdot \left(\frac{p}{1013.25}\right)\right)$	<i>DeMore et al.</i> [1997]		14
Methane	$2.46 \cdot 10^{-12} \cdot e^{-\frac{1780}{T}}$	<i>DeMore et al.</i> [1997]		527

Table 5.4: Reaction rates and photolysis rates of all species presented in this study. Photolysis rates are average noon values over the measurement region (5°N - 5°S) from middle February until middle March in the lowest 1 km altitude, taken from the photolysis model of *Brühl and Crutzen* [1989]. Data from a standard cloud atlas was incorporated into the model to include the effect of clouds. The photolysis rate of MEK was scaled to HCHO with $J(\text{MEK}) = 0.42 \cdot J(\text{HCHO})$ following *Martinez et al.* [1992].

5.4.1 OH concentrations

The OH concentration can be derived from the variability-lifetime method by first assuming an OH concentration, which is then used for the calculation of the lifetime and subsequently performing a fit through the data points using the variability lifetime formula 3.28. This is performed with varying OH concentrations, so that all data points are closest to the fit line, which is with the minimum χ^2 , of the species relative to the fit found. The OH concentration associated with this χ^2 is assumed to be the average OH concentration for the data set (see also chapter 3.6). By this technique an OH concentration of $3.4 \cdot 10^6$ molecules/cm³ was found, as is shown in Figure 5.11. The error of the OH concentration resulting from the statistical errors in the fit parameters A and b can be calculated via error progression. It amounts to $0.039 \cdot 10^6$ molecules/cm³ or 1.1 %. A few sensitivity runs are performed to study the sensitiveness of the calculated OH concentrations to temperature, photolysis rates and reaction rates.

In the previous section it was shown that most reaction rates are temperature dependant. The temperature used for the calculation of the reaction rates in this study has been derived from the aircraft measurements. One has to note, that the measurement flights took place mostly during the hottest time of the day. Temperature measurements performed at the Kaashidhoo Climate Observatory showed that the temperature ranged less than 1 K over one day. Varying the temperature by 1 K in the variability study leads to OH concentrations of $(3.4^{+5.6}_{-1.3}) \cdot 10^6$ molecules/cm³. However, the true average value of the temperature for the calculation of the lifetimes is hard to assess, as the average value from the ground station is 28.7°C, about 2.2 K higher than the value from onboard measurements in the lowest 1 km altitude, which points to geographical differences as well as altitude dependance of the temperature. Further it has to be taken into account that these numbers only represent the geographical and altitude range, that was assessed by the aircraft - but since the air masses travelled some distance outside this range, which is especially important for long-lived species, the true average temperature that influenced the reaction of those species might differ.

A sensitivity test to assess the influence of photolysis rates on OH concentrations was performed by varying the photolysis rates by ± 30 %, which resulted in a variation of the OH concentration of $(3.4^{+1.1}_{-1.03}) \cdot 10^6$ molecules/cm³. The photolysis of species strongly depend on the actual cloud coverage, while in the model calculations of the photolysis rates cloud coverage as suggested by the standard cloud atlas was used. However, the difference to the actual cloudiness can be significant.

For several species the influence of reaction rates on OH concentrations was tested by using an alternative reaction rate from literature. For example, using the OH reaction rate for acetone from *Calve et al.* [1998] ($1.33 \cdot 10^{-13} + 3.82 \cdot 10^{-11} \cdot e^{-\frac{2000}{T}}$) instead of the *Wollenhaupt et al.* [2000] value

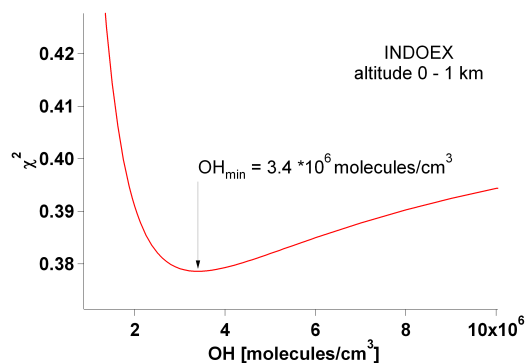


Figure 5.11: χ^2 for various OH concentrations during INDOEX for all data below 1 km altitude. The minimum in χ^2 is found for $3.4 \cdot 10^6$ molecules/cm³ OH.

(see table 5.4) leads to an OH concentration of $3.7 \cdot 10^6$ molecules/cm³. Changing the OH reaction rate of propane from the last evaluated formula [DeMore *et al.*, 1997] (see table 5.4) to the newest (not evaluated) formula of DeMore and Bayes [1999], which is $1.29 \cdot 10^{-11} \cdot e^{-\frac{730}{T}}$, does not change the derived OH concentration of $3.4 \cdot 10^6$ molecules/cm³.

In the previous section 5.4 it was discussed, why ethane was excluded from the lifetime-variability study. However, a test showed that the ethane data point would not have altered the results significantly: when ethane is included in the study, an OH concentration of $4.5 \cdot 10^6$ molecules/cm³ is derived, which is just within the photolysis error bars of the OH concentration derived without ethane.

The OH concentration of $3.4 \cdot 10^6$ molecules/cm³, derived by this study, is an average for the whole campaign along back trajectories of sampled air masses. The fact that the value is an average along the back trajectories is a result of the photochemical degradation that took place all the way from the source of the species to the sampling area.

Comparison with model results

The derived OH concentration fits well to the OH concentration calculated by several global models for this area and to the OH concentration derived from a quasi-Lagrangian experiment, which are shown in table 5.4.1. The quasi-Lagrangian experiment has been performed during INDOEX on March 1 and 2 using the measurements onboard the Citation [de Gouw *et al.*, 2001]. On March 1, two transects in the boundary layer over the Indian Ocean were made, tracks 1 and 2 (Figure 5.12). Subsequently, forward trajectories using the NOAA Hysplit model were used to predict the location of the same air masses 24 hours later. The aircraft conducted two more transects in the marine boundary layer at the predicted geographical locations on March 2, tracks 3 and 4. Afterwards, back trajectories using the KNMI trajectory model were calculated to assess the position of the air masses of day 2 on day 1. By this method, one pair of measurements could be found, tracks 1 and 3, that described the same air mass on two consecutive days. It is assumed, that the degradation of the acetone, acetonitrile, CO and NMHC is mainly due to reaction with OH, and that local sources between the tracks are negligible. The OH concentration is estimated from the ratio of the measured mixing ratios versus the OH reaction rates. By this method de Gouw *et al.* [2001] found a 24-hour mixing ratio of $3.7 \cdot 10^6$ molecules/cm³ OH, valid for March 1 and 2. The error was estimated to about 50 %. Since other sinks than reaction with OH as well as mixing with other, cleaner air masses were neglected, this method tends to overestimate the OH concentration. However, the accordance with the OH concentration that was derived from the variability-lifetime method is very good, especially since the INDOEX quasi-Lagrangian experiment covers only two days, and variations of daily average

Field Experiment	OH [molecules/cm ³]	Date	Altitude Range
INDOEX (this work)	$(3.4^{+1.1}_{-1.03}) \cdot 10^6$	February - March	0-1 km
ECHAM 4 ¹	$2.6 \cdot 10^6$	1. /2. March	0-3 km
MATCH-MPIC ²	$3 - 4 \cdot 10^6$	1. /2. March	0-3 km
INDOEX			
quasi-Lagrangian Experiment ³	$3.7 \cdot 10^6 \pm 50\%$	1. /2. March	0-3 km

Table 5.5: Results and comparison of OH concentrations for INDOEX. ¹de Laat *et al.* [2001], short name ECHAM: European Centre Hamburg Model version 4; ²Lawrence [2001]; ³de Gouw *et al.* [2001]

values of OH can be as high as a factor of 2. For example, *Berresheim et al.* [2003] directly measured daily averages of boundary layer OH concentrations between 3.6 and $6.7 \cdot 10^6$ molecules/cm³ during the MINOS³ campaign in Crete, Greece.

The daily averaged OH concentration on the first two days of March 1999 was also calculated with two atmospheric chemistry models. The ECHAM 4 model (European Centre Hamburg Model version 4) [*de Laat et al.*, 2001], using a chemistry scheme involving CH₄, CO, NO_x, and HO_x chemistry as well as higher hydrocarbons, estimated an OH concentration of $2.6 \cdot 10^6$ molecules/cm³. The tropospheric photochemistry version (MATCH-MPIC [*Lawrence et al.*, 1999, 2003a]) of the Model of Atmospheric Transport and Chemistry (MATCH [*von Kuhlmann et al.*, 2003a]) included gas-phase chemistry (with methane but neglecting NMHCs). This allowed a higher horizontal resolution (T62, about $1.9^\circ \times 1.9^\circ$) of the model. *Lawrence* [2001] (published in *de Gouw et al.* [2001]) used MATCH-MPIC to estimate an OH concentration of $3 - 4 \cdot 10^6$ molecules/cm³ for the INDOEX quasi-Lagrange experiment. As for the quasi-Lagrange experiment itself, it has to be kept in mind, that the models only estimated the average mixing ratios of March 1 and 2, whereas the variability method derived an average over the entire campaign. However, the agreement with the OH concentration of the model with the mixing ratio that was derived from the variability - lifetime methods is rather good.

Figure 5.13 shows vertical profiles of MATCH-MPIC modelled monthly averaged 24h OH concentrations for February and March. These model runs were done for the climatological year 1997. They were initialised with mean trace gas fields from *von Kuhlmann et al.* [2003a] for September 1998. The concentrations shown in the Figure are longitudinal averages between 70°E and 80°E . Different colours in the graphs denote the latitude of the respective profile. The trend goes to higher OH concentrations in the boundary layer from south to north. In March, the boundary layer concentrations are higher than in February.

The data in this Figure was computed with a newer version of the MATCH-MPIC model [*Lawrence et al.*, 2003b; *von Kuhlmann et al.*, 2003a,b] than the MATCH-MPIC model cited for the quasi-Lagrangian experiment. The new version differs from the above-mentioned one mostly due to an updated chemistry module. For the hydrocarbons, the older version included only CH₄ chemistry,

³Mediterranean Intensive Oxidant Study

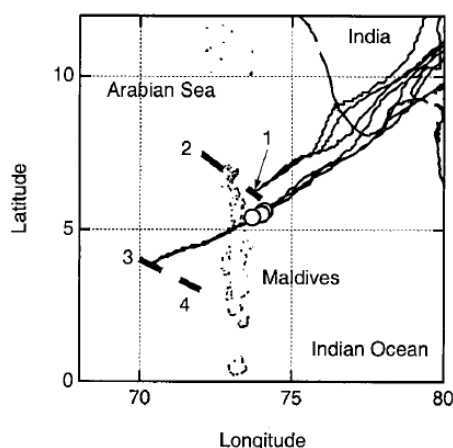


Figure 5.12: Location of the quasi-Lagrange experiment during INDOEX, performed on March 1 and 2. Tracks 1 and 2 were performed on March 1, tracks 3 and 4 were performed on March 2. The thin lines indicate the back trajectories of the air masses of track 1 and 3. The open circles indicate the position of the air mass “3” 24 hours before it was sampled. [*de Gouw et al.*, 2001]

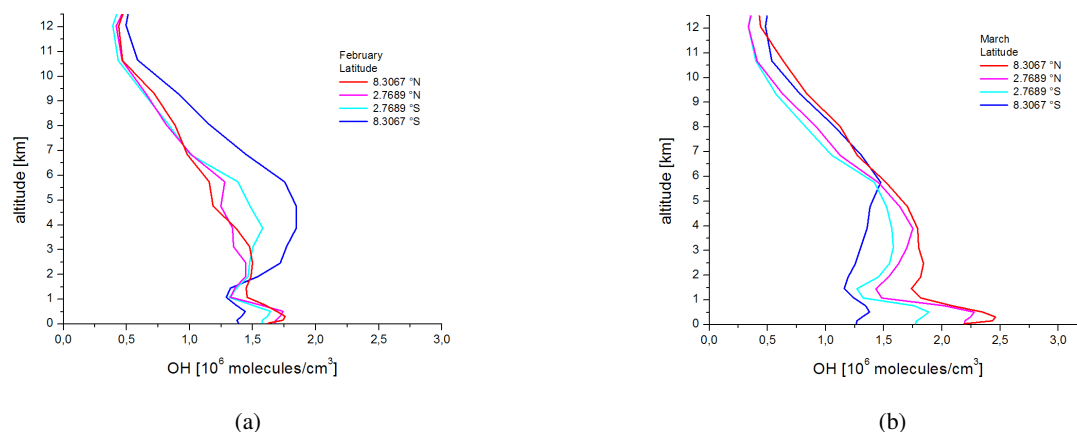


Figure 5.13: Vertical profiles of modelled monthly averaged 24h OH concentrations for February and March. Values are averages between 70°E and 80°E . Different colours in the graphs denote the latitude of the profile. The trend goes to higher OH concentrations in the boundary layer from south to north. In March, the boundary layer concentrations are higher than in February. Data from [Lawrence, 2004].

whereas the new version includes CH_4 and hydrocarbon chemistry up to isoprene. On the other hand, the horizontal grid of the data is lower in the new version run (T21, about $5.6^{\circ} \times 5.6^{\circ}$). For both models, basic meteorological parameters (pressure, temperature, horizontal winds, surface heat fluxes, and surface stresses) were obtained from the National Centers for Environmental Prediction (NCEP) global forecast/analysis system [Caplan and Pan, 2000]. The OH concentration in the boundary layer of the model is lower than the $(3.4^{+1.1}_{-1.03}) \cdot 10^6$ molecules/ cm^3 estimated by the variability-lifetime method. Note that the model computed a different climatological year than our data, and also mean trace gas fields were taken from an earlier year.

A discrepancy between actual OH concentrations in the atmosphere and the variability-lifetime OH estimation could partly be due to uncertainties in the calculated chemical reaction and photolysis rates, including the temperature and pressure values that are used as input. In addition, sampling did not occur randomly over the measurement area and in time. For example, during INDOEX, more data were recorded in the northern part of the INDOEX area, and also more in March than in February, were OH concentrations tended to be higher according to MATCH-MPIC. Moreover, the measurements were biased towards events where convection took place. The displayed geographical range of model data spans only the area in which INDOEX flights took place. Since the air masses arrived from outside this area, discrepancies between the OH concentration displayed and the concentration estimated by the variability-lifetime method are expected to some degree. The air masses originated from northerly or north westerly direction, where the trend in the MATCH data predicted higher values. However, also the model derived OH concentrations are subjected to errors or uncertainties. Evaluating the models is beyond the scope of this work, but some findings from other scientists will be reported. In order to assess uncertainties in OH fields, OH distributions from models are often evaluated with the help of methylchloroform. von Kuhlmann [2001] stated that an uncertainty of $\pm 20\%$ in the global (MCF-loss weighed) mean OH concentration is a realistic estimate. Lawrence *et al.* [2001] remarked that 30% uncertainty are commonly stated for global mean OH concentrations. von Kuhlmann [2001] compared the annual mean OH distributions of the MATCH-MPIC model with the climatological OH distribution of Spivakovsky *et al.* [2000], which was shown in chapter 3.1. He found differences up to a factor of 2 between the models, spanning the full range of uncertainties for

the local OH abundance (factor 2) given in *Spivakovsky et al.* [2000]. Discrepancies in the models are to some extent due to different meteorological input. *Spivakovsky et al.* [2000] compared their OH distribution with local measurements and found that their model underestimated OH concentrations in the northern hemispheric tropics about 15-20%. Considering all uncertainties stated above, the agreement between the OH concentration derived from the variability- lifetime method and the OH concentration calculated by the global transport models is satisfactory.

5.4.2 The parameters A and b

In the variability-lifetime relationship two parameters, A and b, are used. A brief literature review of the scientific interpretation of the parameters A and b is given in chapter 3. For the INDOEX data set an A value of 1.96 ± 1.14 and a b value of 0.70 ± 0.04 are derived. The errors are estimates of fitting errors (the estimated standard deviation of the fit coefficients). Table 5.6 shows the derived A and b values for data of the lowest 1 km altitude of the INDOEX campaign, as well as results of other campaigns, that were taken from literature.

Field experiment	A	b	Altitude Range	Geographical area	Date
LBA - Claire ¹	4.63 ± 1.21	0.64 ± 0.07	0 - 1km	Suriname	March
PEM - West B ²	4.3 ± 0.63	0.53 ± 0.02	PBL - 12km	Western Pacific	February - March
Trace A ³	2.9 ± 0.44	0.52 ± 0.02	PBL - 12km	Brazil, South Africa, South Atlantic	September - October
INDOEX (this work)	1.96 ± 1.14 5.65 ± 1.24	0.70 ± 0.04 0.63 ± 0.05	0 - 1km 0 - 12.5km	Indian Ocean	February - March
MINOS ⁴	0.85	0.23	ground-based	Crete, Greece (35°N, 25°E)	August

Table 5.6: Results and comparison of fit-parameters to $\ln(\sigma(\ln x)) = \ln(A) - b \ln(\tau)$ for INDOEX with their 1σ uncertainties. Short names of campaigns and references: ¹Large Scale Biosphere-Atmosphere Experiment in Amazonia - Cooperative LBA Airborne Regional Experiment, *Williams et al.* [2000]; ²Pacific Exploratory Mission in the Western Pacific Ocean, Phase B, *Jobson et al.* [1999]. ; ³Transport and Atmospheric Chemistry Near the Equator -Atlantic, *Jobson et al.* [1999]; ⁴Mediterranean Intensive Oxidant Study, *Gros et al.* [2003].

The parameter b can vary between 0 and 1. High b values indicate that chemical loss processes dominated the variability of the measured trace gases, whereas small b values occur where mixing of “widely different air mass ages” [*Jobson et al.*, 1999] took place. The b value in the marine boundary layer of INDOEX, 0.70 ± 0.04 , is higher than the b values for remote tropospheric sites, which *Jobson et al.* [1999] derived from model studies to be about 0.5. Obviously, chemical and photolytical loss processes have a more dominant influence on the variability of the analysed trace gases during INDOEX. This fits to the conditions of these measurements, since we sampled air masses several days downwind of sources. As stated before, the pollution found in the measurement region was surprisingly high, so the absolute values of the trace gas mixing ratios would have been misleading with regard to the remoteness of this area. The INDOEX results are compared to three other tropical data sets, namely LBA - Claire, which took place over Suriname during March, PEM - West B⁴, which covers the Western Pacific during February and March, and Trace A⁵ which covers Brazil,

⁴Pacific Exploratory Mission in the Western Pacific Ocean, Phase B

⁵Transport and Atmospheric Chemistry Near the Equator -Atlantic

South Africa and the South Atlantic during September and October, and one Mediterranean data set, MINOS⁶, which were ground based measurements carried out on Crete, Greece, in August. Our *b* value is higher than the *b* value during the LBA - Claire, PEM - West B and Trace A campaigns, which were 0.64 ± 0.07 , 0.53 ± 0.02 and 0.52 ± 0.02 respectively. Since PEM - West B and Trace A data cover the lowest 12 km of the atmosphere, they sampled more different air masses than we did during INDOEX in the marine boundary layer, where chemical loss processes played a more important role for the variability of the trace gas concentrations than mixing. For better comparison with the 1-12 km tropospheric data sets, the INDOEX measurements were also analysed over the whole altitude range, 0-12.5 km. The *b* parameter for this data set is 0.63 ± 0.05 (with an OH concentration of $0.625 \cdot 10^6$ molecules/cm³). As expected, this *b* value is lower than the *b* value of the marine boundary layer, because mixing was more important for the variability of the 0-12.5 km tropospheric data set. Compared to the PEM - West B and Trace A campaigns, our 0-12.5 km *b* value is still higher, which might be a result of the strong influence of polluted boundary layer air which was transported to the middle tropical free troposphere data by convection. The LBA-Claire study was, like the boundary layer INDOEX study, limited to the lowest 1 km altitude, and took place over the Amazonian rain forest. *Williams et al.* [2000] state that the air in this layer is advected air from the Atlantic Ocean, but also bears the signature of species that are emitted from the Amazonian rain forest, so that their *b* value is shifted towards smaller values, compared to INDOEX. During MINOS, the observed *b* value of 0.23 was significantly lower compared to the other campaigns in the table. *Gros et al.* [2003] state that this suggests conditions in Crete as intermediate between remote sites and sites in the vicinity of sources, and that a wide variety of sources was observed during their measurements - mainly from southern and eastern Europe.

From model results *Jobson et al.* [1999] derived for the case of *b* = 1, that “*A* is the standard deviation of measured transit times”. However, high *A* values can also result from the sampling of several inhomogeneous air masses. During INDOEX, an *A* value of 1.96 ± 1.14 was derived for the marine boundary layer and 5.65 ± 1.24 for the 0-12.5 km altitude range. This boundary layer value is lower than the tropical reference values of 4.63 ± 1.21 (LBA - Claire), 4.3 ± 0.63 (PEM - West B) and 2.9 ± 0.44 (Trace A). During LBA - Claire air masses were transported over the Atlantic, but were also influenced by fresh Amazonian rain forest emissions. During PEM - West B air masses were transported over the Pacific Ocean (clean or aged marine air), but showed signatures of fresh Asian plumes, and even stratospheric intrusions were sampled [*Hoell et al.*, 1997]. During those two campaigns, a wide range of sources contributed to the measured variability, and in these cases it means a wide range of different air mass ages. The same applies to the 0-12.5 km INDOEX data, where relatively fresh air masses were encountered, as well as convected air masses with possible origins in southeastern Asia, Indonesia, China and Australia, or subsidised air, which even seemed to originate from the tropopause region over Africa near the jet stream in one case (flight of February 16) [*de Gouw et al.*, 2001]. The *A* value obtained during the Trace A study is lower than the former two reference *A* values, which may be interpreted as more dominating influence of seasonal biomass burning sources in Brazil or South Africa, which were not operative during the former two reference campaigns. In the boundary layer of INDOEX, a rather uniform distribution of air mass ages was encountered, since measurements took place several days downwind of sources, and no really fresh contributions were encountered. *de Gouw et al.* [2001] estimated the age of the pollution, which they defined as the travel time of the pollutant gases from the source to the Citation aircraft, by the ratio of hydrocarbons with different lifetimes. From benzene/ethane and acetylene/ethane ratios they derived the age of the pollution to vary between 4 and 15 days. During the MINOS campaign, the *A* value was even lower than during INDOEX (boundary layer), indicating a quite narrow distribution of air mass ages, which was confirmed by age estimation via species-species ratios (15-35 h [*Salisbury et al.*,

⁶Mediterranean Intensive Oxidant Study

2003] or 15-59 h [Xu *et al.*, 2003]).

To come to the same conclusion as derived from this analysis, source distribution and source strength, atmospheric background mixing ratios as well as the backward trajectories and mixing processes would have been necessary otherwise. These require additional measurements or resort to standard data, like standard emission inventories, which are averages and thus may not describe the actual situation correctly and in its variations.

5.5 Summary and conclusions

The relationship between the variability and the lifetime of various trace gases was studied for the INDOEX experiment. The variability-lifetime concept is a powerful method for the indirect estimation of mean OH concentrations along the back trajectory of an air mass. During INDOEX a large number of trace gases has been measured, of which nine could be used for a variability-lifetime analysis. The INDOEX variability study was performed in the marine boundary layer (below 1 km). The average OH concentration has been determined by optimising the OH concentration in the lifetime calculation of the individual species. The OH concentration that was derived by this method was $3.4^{+1.1}_{-1.0} \cdot 10^6$ molecules/cm³ in the marine boundary layer, which agrees very well with model calculations for this region.

The parameters A and b, which describe the relation between the variability and lifetime, were 1.96 ± 1.14 and 0.70 ± 0.04 , respectively. The derived b value indicates that the measurement area was rather remote, with no fresh pollution sources around, so that chemical processing and photolytical degradation determined the variability of the measured trace gases rather than mixing. The A value indicates that the age distribution of the measured air masses was rather uniform, due to measurement location over the Indian Ocean far away from pollution sources and the fact that air masses sampled from the Cessna Citation mainly originated from the two source regions - the Arabian Sea and the Bay of Bengal. The presented analysis gives an impressive example on derivation of parameters from measurements on a regional scale.

Chapter 6

The STREAM campaign 1998

6.1 The measurement region

The STREAM 98 summer campaign was part of a series of Stratosphere Troposphere Experiments by Aircraft Measurements. It took place between July 1 and 15, 1998 and was based in Timmins, Canada (48.2°N, 79.3°W), which is located north of the Great Lakes area. Although remote, this region is often influenced by regional biomass burning as well as long-range transport and deep convection during summer [Wofsy *et al.*, 1994]. In addition, due to its close proximity to the polar jet stream, stratosphere-troposphere-exchange does occur frequently [Bachmeier *et al.*, 1994]. Hence, this region provides a good opportunity to study chemical and dynamical processes that influence the chemical composition of the tropopause region. Special emphasis was given to the influence of long range transport, deep convection, which rapidly transports boundary layer air into the tropopause region, and stratosphere-troposphere-exchange. Moreover, the chemistry of the lowermost stratosphere, especially the role of nitrogen oxides in the catalytic ozone cycles was studied.

Measurements were performed using the same Cessna Citation II twinjet aircraft, operated by the Technical University of Delft, The Netherlands, as during the INDOEX campaign, described in chapter 5. Due to heavy payload, the highest flight level reached during this campaign was 39000 ft or about 12 km. Air masses in the region from 44°N to 56°N and 71°W to 90°W were sampled, in general following a stacked leg flight pattern. Figure 6.1 shows the flight tracks of the 8 research flights during STREAM 98.

6.2 Meteorological background

During the STREAM campaign a meridional movement of the polar jet stream was observed, heading south, then north and then back to the south, in a wave pattern. This caused the development of a deep trough, which transported stratospheric air from high latitudes to the central region of northern Canada. Associated with this trough was a cold front. Simultaneously, tropical/subtropical Pacific air was transported to the same region by the subtropical jet stream.

The measurement flights can be classified according to their relative position to the polar front. Hoor *et al.* [2002] state that north of the polar front, usually on the cyclonic side of the polar jet, the tropopause was located at about 10.5 km - within the reach of the aircraft, so that lowermost stratospheric air was sampled. However, on the anticyclonic side of the polar jet, the tropopause was located at 13 km or higher, so that mainly tropospheric air was encountered during these flights. Measurements were performed to about 50 % in the troposphere and in the stratosphere, respectively.

Meteorological forecasts for flight planning and post flight analysis were provided by the Royal Netherlands Meteorological Institute (KNMI) using the KNMI trajectory model applied on three-

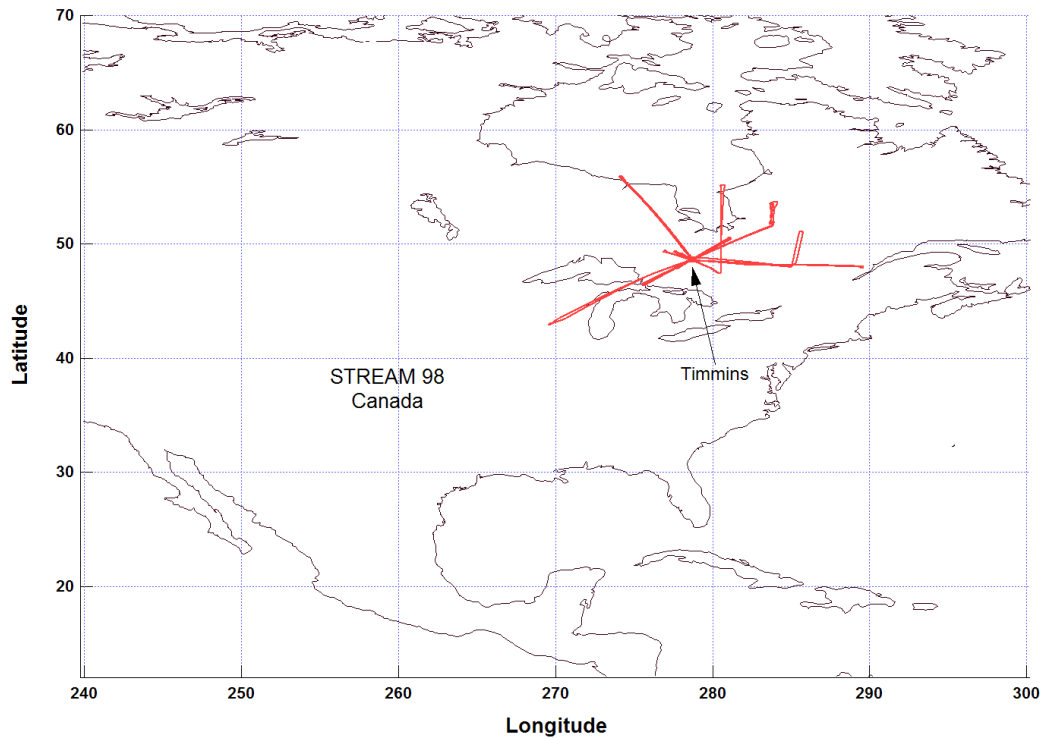


Figure 6.1: Geographical distribution of all measurement flights performed during the STREAM 98 campaign.

dimensional ECMWF (European Centre for Medium Range Weather Forecasts) wind fields [Scheele *et al.*, 1996]. The origins of air masses (polar, midlatitudinal and (sub)tropical), were deduced by calculating 10 days back trajectories along the flight track. Table 6.2 lists the respective measurement regions and dominant air mass origins. A detailed description of air mass origins and the meteorological situation can be found in Fischer *et al.* [2002] and Hoor *et al.* [2002].

Flight Label	Date	Measurement Region	Origin of Air Masses
980701	1.7.	UT, LMS	polar, midlatitudes
980703	3.7.	LMS	polar
980705	5.7.	UT (warm sector)	midlatitudes, subtropics
980708	8.7.	UT, LMS	polar, midlatitudes
980710	10.7.	UT, LMS	polar, midlatitudes
980712	12.7.	UT (warm sector)	midlatitudes
980715a	15.7.	UT (warm sector)	subtropics, tropics
980715b	15.7.	UT, tropopause fold	polar, midlatitudes (troposphere)

Table 6.1: Measurement region and origin of air masses for all measurement flights performed during STREAM 98 in July 1998. The measurement region and the air mass origin as deduced from 5-day backward trajectories are shown. LMS, lowermost stratosphere; UT, upper troposphere. Table after Hoor *et al.* [2002].

6.3 The aircraft instrumentation

Table 6.2 gives an overview of the instrumentation onboard the Citation during the STREAM 98 campaign. The payload configuration of the campaign is shown in Figure 6.2. A brief description of the instrumentation used and species measured is given below:

CO and N₂O

were measured using a tuneable diode laser absorption spectrometer (TDLAS) [Wienhold *et al.*, 1998], developed by the Max Planck Institute for Chemistry, Mainz, Germany. The time resolution of 2-3 seconds, which is limited by the gas exchange time in the White-cell, allows high temporal and spatial resolution. However, data were smoothed with a five second averaging to reduce instrumental noise. The instrument was calibrated against working gas standards in-flight, that were cross-calibrated with a gas chromatograph against NOAA (National Oceanographic and Atmospheric Administration) standards prior to and after the campaign. The total uncertainty was typically 6 %, including a noise level (3s) of 10 ppbv for N₂O and 8 ppbv for CO, respectively [Hoor *et al.*, 2002].

N₂O and CF₂Cl₂ (CFC-12)

were measured simultaneously using a gas chromatograph of the Johann Wolfgang Goethe-University, Frankfurt am Main, Germany. The gas chromatograph uses a porous layer open tubular (PLOT) capillary column in combination with a constant current, frequency modulated electron capture detector (ECD). The instrument was calibrated relative to NOAA/CMDL (Climate Monitoring & Diagnostics Laboratory) standards for both species. The precision of the N₂O and CFC-12 measurements was better than 0.5 % (equals 1.5 ppbv) and 0.6 %, respectively, and the accuracy of the calibration was better than 2.1 % and 1.8 %, respectively. The instrument is described in detail by

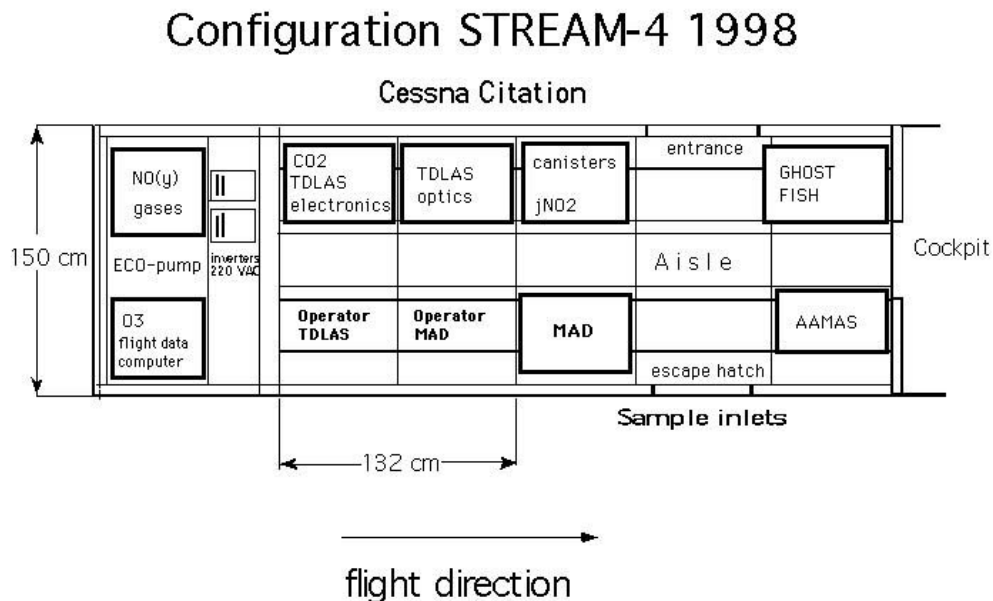


Figure 6.2: The payload configuration of the STREAM 98 campaign. A list of the abbreviations of the instruments is given in the acronyms section. Figure from <http://www.phys.uu.nl/~scheren/STREAM98/STREAM98vs1.html>.

Measured Species	Technique	Instrument by
CO, N ₂ O, CH ₄	Tunable diode laser absorption spectroscopy	MPI-A, Mainz
SO ₂ , H ₂ SO ₄ , HCl, HF, HNO ₃ , (CH ₃) ₂ CO, HCN	chemical ionisation mass spectrometer	MPI-N, Heidelberg
NMHC	Gas chromatography (from canisters)	IMAU, Utrecht
NO, NO _y	Chemiluminescence detector, heated gold converter (NO _y)	MPI-B, Mainz
CO ₂	Infrared analyser	MPI-A, Mainz
O ₃	Chemiluminescence detector	IMAU, Utrecht
CFC-11, CFC-12, N ₂ O	Gas chromatography	IMG, Frankfurt
H ₂ O	Lyman-alpha fluorescence hygrometer	ISC, Jülich
J _{NO₂}	Photo-optical detectors filter radiometer	IMAU, Utrecht
Aerosols (6 - 3500 nm) number concentration and size distribution	Optical particle counter, condensation nuclei counter, differential mobility analyser,	ITM, Stockholm
Aerosol chemical composition	filter samples	ITM, Stockholm

Table 6.2: Instrumentation onboard the Cessna Citation during the STREAM 98 campaign. A list of the abbreviations of the institutes and instruments is given in the acronyms section.

Bujok et al. [2001].

C2-C9 NMHCs (nonmethane hydrocarbons) and methyl chloride

were measured by a combination of canisters samples and gas chromatography analysis [*Lelieveld et al.*, 1999]. During each flight eight or nine electropolished stainless steel canisters, provided by Utrecht University, The Netherlands, were pressurised with air samples. Within a week after the sampling, the canisters were analysed at the Centre for Atmospheric Chemistry, York University, Canada, using a HP 5890 gas chromatograph with PLOT columns (Al₂O₃/KCl and J&GS-GasPro) and a flame ionisation detector for non-methane hydrocarbons or electron capture detector for methyl chloride (for more details see *Scheeren et al.* [2002]). The filling time of the canisters depended on the ambient pressure, and ranged between 15 seconds at 3 km altitude and 165 seconds at 12.5 km [*Lelieveld et al.*, 1999]. During this time, the aircraft covers a distance between 2.5 km and 25 km, respectively. The accuracy of canister sample measurements is determined by the uncertainty of the NIST (National Institute of Standards and Technology) standard NMHC mixture that is used for calibration. The uncertainty was smaller than 5% and the precision was between 2% and 5% for concentrations above 10 pptv, depending on the species.

Ozone

was measured by the Utrecht University, using a modified pressure-independent chemiluminescence monitor (Bendix 8002) based on reaction with ethylene [*Bregman et al.*, 1995, 1997]. The ozone monitor was calibrated absolute prior to and after the campaign. Before and after each flight it was zero checked and compared to an external ozone source. The measurements were performed with a time resolution of 1 s. The precision was 2% and the overall accuracy was about 5% [*Fischer et al.*, 2002]. During flight 980710, performed on July 10, no ozone data were taken, so that we excluded

this flight from the variability study.

HNO₃, SO₂, Acetone and Acetonitrile (CH₃CN)

were measured by the Max Planck Institute for Nuclear Physics, Heidelberg, Germany, using active chemical ionisation Mass Spectrometry (ACIMS). This technique is based on ion-molecule reactions of or with the sampled components, and a subsequent measurement of the reaction products with a quadrupole mass spectrometer. A description of the technique can be found in *Möhler and Arnold* [1991], *Möhler et al.* [1993] and references therein. The time resolution for the nitric acid, acetone and acetonitrile measurements was 3.2 s, and 128 s for SO₂. The precision was 15 % for acetonitrile and acetone, and 20 % for the other species (for SO₂ mixing ratios above 10 pptv). The accuracy for HNO₃ and SO₂ was 30 %. For acetonitrile and acetone, the accuracy depended on the water vapour mixing ratio. Water vapour measurements are only performed above a pressure level of 500 hPa, therefore an average tropospheric H₂O mixing ratio can only be given for this part of the measurements. In this upper part of the troposphere, the average H₂O mixing ratio during the STREAM 98 measurements was 283 ppmv. H₂O mixing ratios at the lower limit of the lowermost stratosphere were 65-125 ppmv [*Beuermann*, 2000], and the average H₂O mixing ratio in the lowermost stratosphere was 78 ppmv. The accuracy of acetone is $\begin{matrix} +40\% \\ -34\% \end{matrix}$ for average tropospheric conditions (above 500 hPa), and about $\pm 30\%$ for average conditions in the lowermost stratosphere. The accuracy of acetonitrile is $\begin{matrix} +52\% \\ -39\% \end{matrix}$ and about $\begin{matrix} +32\% \\ -31\% \end{matrix}$ for the troposphere and lowermost stratosphere, respectively. For further details, see *Wohlfrom* [2000].

6.4 Separation of different air masses during STREAM 98 – Definition of the tropopause

Although several exchange mechanisms exist between the troposphere and the stratosphere, these reservoirs consist of very different air masses with different age, chemical composition and history. Therefore, when studying atmospheric variability, it is crucial to differentiate between those atmospheric layers. The tropopause, separating the troposphere from the stratosphere, can be defined thermally, dynamically or chemically.

The World Meteorological Organisation (WMO) defined the thermal tropopause as the lowest altitude, at which the temperature gradient reaches -2 K km^{-1} or less and stays below this value for the next 2 km altitude. In close proximity to the jet streams, this criterion can lead to indefinite results [*Bethan et al.*, 1996]. The dynamical tropopause can be defined by potential vorticity [*Shapiro*, 1980], which has a strong gradient at the tropopause towards higher values in the stratosphere. Since the potential vorticity values available for this field study stem from simulated ECMWF wind fields, which were interpolated from a grid size of $\sim 0.7^\circ \times 0.7^\circ$ at midlatitudes [*Simmons et al.*, 1999], they can only reproduce large scale features. Therefore, we will use the chemically defined tropopause in this study, which makes use of the strong gradient of different trace gases (e.g. O₃, N₂O, CO) at the tropopause.

Beuermann [2000] used the O₃-N₂O correlation to define the chemical tropopause during the STREAM 98 measurements. He found a compact correlation between those two tracers, and with a tropospheric N₂O mixing ratio of 313 ppbv he derived that the upper tropospheric ozone concentration was 75 ppbv, which is slightly below the 80 ppbv recommended by *Bethan et al.* [1996].

Acetone is the central species for this study, since its destruction is dominated by photolysis, which is very important for the determination of the OH concentration (see section 6.5.1). Figure 6.3 shows the O₃ to acetone correlation. Stratospheric air masses (vertical branch) have high and variable O₃ mixing ratios and low acetone mixing ratios, whereas in the troposphere (horizontal branch) it

is the other way round. In the stratosphere, acetone concentrations were very close to the detection limit of the instrument. This can be seen in Figure 6.5a as a deformation of the histograms to lower values, or a curvature of the line in the cumulative Gaussian distribution. Therefore, the variability study could not be extended to this regime. The variability study was restricted to O_3 mixing ratios below 335 ppbv, because for the O_3 concentration range of 75 ppbv to 335 ppbv the deformation of the acetone Gaussian distribution did not occur. The value of 335 ppbv O_3 was found by plotting an O_3 histogram and taking away O_3 peak after peak from higher to lower values, until the acetone mixing ratios were above the detection limit. Whole O_3 peak had to be excluded, since cutting away of parts of peaks would lower the standard deviation artificially.

According to this method, tropospheric data is defined as air masses with an O_3 mixing ratio lower than 75 ppbv. Stratospheric data is defined as air masses higher than 75 ppbv O_3 . Note that because of the above given reasons, we only analyse data in the lowermost stratosphere during this study, defined for air masses with $75 \text{ ppbv} < O_3 < 335 \text{ ppbv}$. In Table 6.3 the number of mixing ratio data points is given for those species, that were taken into account for the variability study.

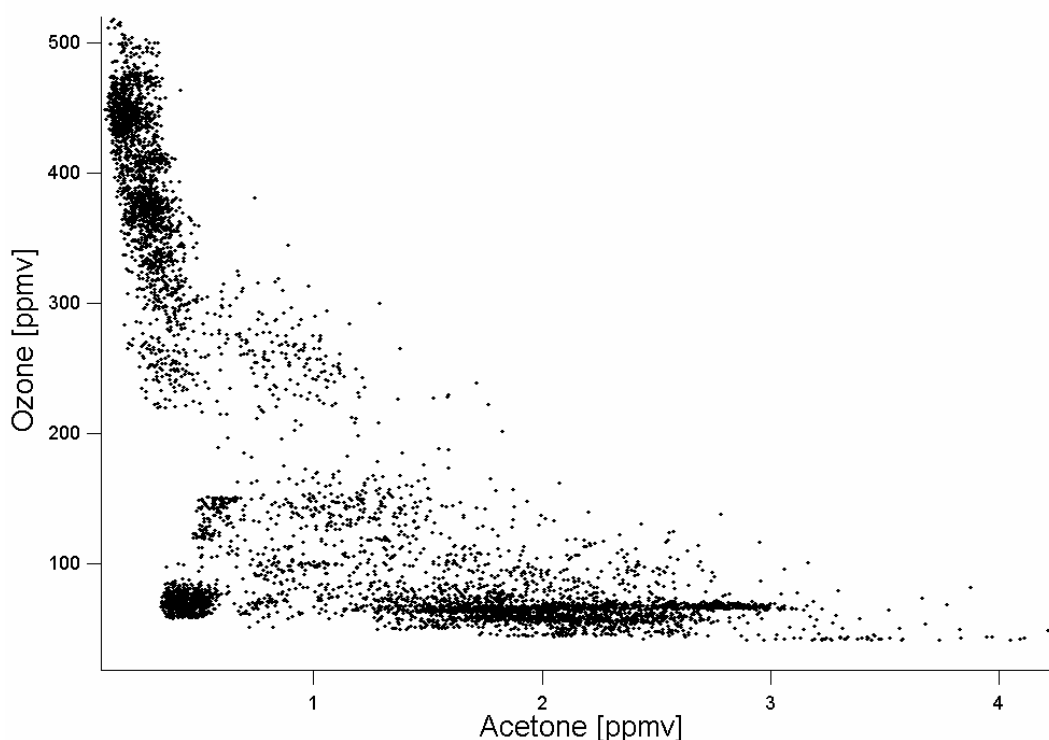
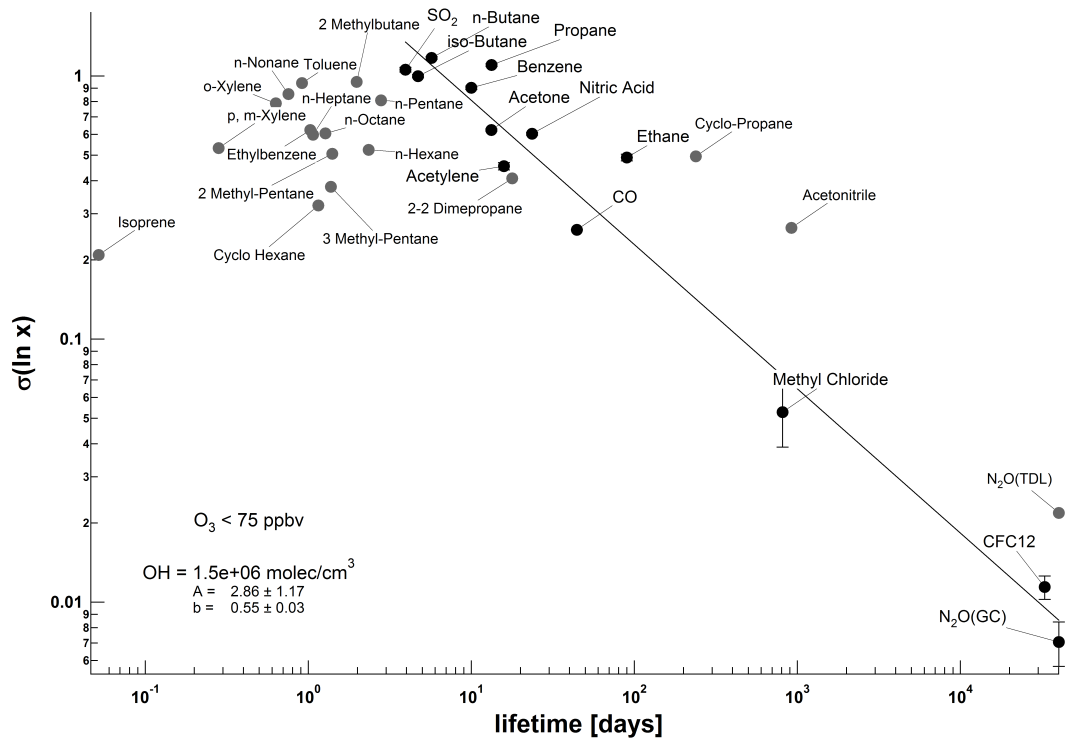


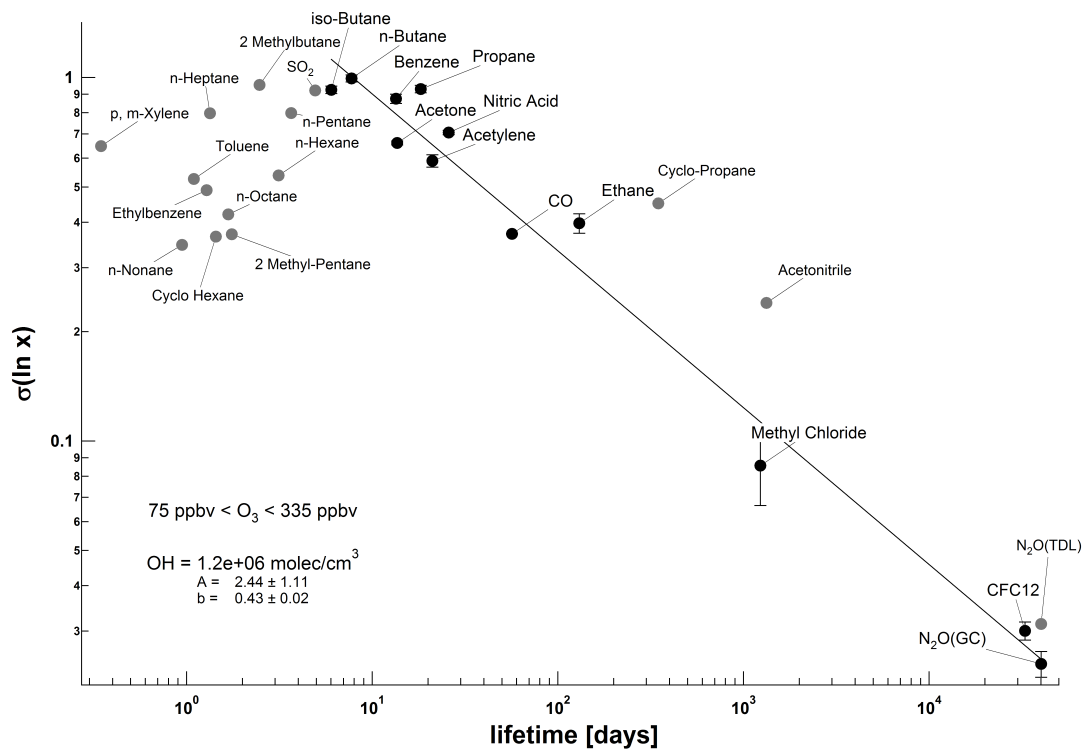
Figure 6.3: Ozone to acetone correlation. Ozone mixing ratios in the stratosphere are high and highly variable (vertical branch of the data points), and low in the troposphere (horizontal branch). Acetone mixing ratios are distributed the other way round. The bulk of data points between the two branches indicates mixing of tropospheric and stratospheric air masses.

6.5 Variability during STREAM 98

Figure 6.4 shows the variability of the measured trace gases in the troposphere and lowermost stratosphere during STREAM 98. Like for the INDOEX campaign, the lifetimes of the different trace gases were calculated according to equation 5.1. This approach implies that the residence time for each species is determined by photochemical degradation via OH and in the case of methyl chloride,



(a)



(b)

Figure 6.4: Variability plots for (a) the troposphere ($O_3 < 75$ ppbv) and (b) the lowermost stratosphere (75 ppbv $< O_3 < 335$ ppbv). Species taken for the fit are solid black circles. Errors are given for all these species, but at higher σ values they may be smaller than the solid black circles. The fit through these data points is marked by the line. Species excluded from the fit (see text) are solid grey circles.

species	number of points	
	free troposphere	lowermost stratosphere
N ₂ O(ghost)	267	123
CFC ₁₂	267	123
CO	7209	3328
Acetylene	26	12
Ethane	26	12
Methyl Chloride	27	15
Propane	26	12
Acetone	2681	1619
SO ₂	271	
iso-Butane	26	12
Benzene	26	11
Nitric Acid	2630	1316
n-Butane	26	12

Table 6.3: Number of data points in the variability study during STREAM 98, given for those species that were taken for the fit.

acetone, SO₂ and nitric acid also by photolysis. The reaction and photolysis rates used are given in Table 6.4. Where no photolysis rate is given, this process is negligible for the calculation of the lifetime. Photolysis rates are average noon values over the measurement region (45°-55° N) in the first half of July at the interpolated average pressure of the troposphere or lowermost stratosphere measurements, taken from the photolysis model of *Brühl and Crutzen* [1989]. Data from a standard cloud atlas was incorporated into the model to include the effect of clouds. A quarter of these values is taken in this study for the diurnal photolysis rate. Average values for temperature and pressure were derived from the onboard measurements (for discussion of temperature values see chapter 5.4.1). For the troposphere, the average temperature was 231.7 K, and the average pressure was 265.8 hPa. For the lowermost stratosphere, 224.4 K and 225.7 hPa were measured.

OH concentrations of $1.5 \cdot 10^6$ molecules/cm³ for the troposphere and $1.2 \cdot 10^6$ molecules/cm³ for the stratosphere were used for the calculations. These OH concentrations were obtained by optimising the variability-lifetime relationship, which was discussed in chapter 3.6. A discussion of the values will follow in section 6.5.1. The lifetime of N₂O was fixed to 110 years [*Volk et al.*, 1997] and the lifetime of CFC-12 to 90 years [*Avallone and Prather*, 1997].

Species marked solid black do follow the variability-lifetime relationship and are the basis for the presented variability-lifetime analysis. These are N₂O (measured by the in-situ gas chromatograph), CFC-12, methyl chloride, CO, ethane, acetylene, nitric acid, acetone, benzene, propane, iso-butane and n-butane for both layers, and tropospheric SO₂. Errors are given for all these species in Figure 6.4, but at higher σ values they may be smaller than the solid black circles in the graph. A number of other species were measured, marked grey, which were excluded from the analysis. The reasons will be discussed in more detail in the following paragraph.

Since this study is based on statistical analysis, it is very important that only real atmospheric variability influences the standard deviation of the measured trace gases. To verify this, histograms and cumulative Gaussian distribution graphs of all species for both stratosphere and troposphere were plotted. Figure 6.5 on page 89 shows some examples. Figure 6.5c and d show the graphs for N₂O measured by the gas chromatograph, which is a typical Gaussian distributed species, when troposphere or stratosphere are taken separately.

species	OH reaction rate	reference	Troposphere		Lowermost Stratosphere	
			phot. rate	lifetime [days]	phot. rate	lifetime [days]
CO	$1.5 \cdot 10^{-13} \cdot (1 + 0.6 \cdot (\frac{p}{1013.25}))$	1		44		57
Acetylene	$k_0 = 5.5 \cdot 10^{-30}$ $k_\infty = 8.3 \cdot 10^{-13} \cdot (\frac{T}{300})^2$	1		16		21
Ethane	$8.69 \cdot 10^{-12} \cdot e^{-\frac{1070}{T}}$	1		90		130
Methyl Chloride	$4.00 \cdot 10^{-12} \cdot e^{-\frac{1400}{T}}$	1	$1.00 \cdot 10^{-14}$	811	$5.12 \cdot 10^{-13}$	1232
Propane	$1.00 \cdot 10^{-11} \cdot e^{-\frac{660}{T}}$	1		13		19
Cyclo-Propane	$3.90 \cdot 10^{-12} \cdot e^{-\frac{1110}{T}}$			238		347
Acetone	$8.80 \cdot 10^{-12} \cdot e^{-\frac{1320}{T}}$ $+ 1.70 \cdot 10^{-14} \cdot e^{-\frac{423}{T}}$	2	$2.33 \cdot 10^{-6}$	13	$2.74 \cdot 10^{-6}$	14
SO ₂	$k_0 = 4.0 \cdot 10^{-31} \cdot (\frac{T}{300})^{-4.0}$ $k_\infty = 2.0 \cdot 10^{-12}$	3	$6.28 \cdot 10^{-12}$	3.9	$4.45 \cdot 10^{-10}$	49
Acetonitrile	$7.80 \cdot 10^{-13} \cdot e^{-\frac{1050}{T}}$	1		918		1329
iso-Butane	$8.28 \cdot 10^{-13} \cdot (\frac{T}{298})^2 \cdot e^{-\frac{275}{T}}$	4		4.7		6.0
Isoprene	$2.55 \cdot 10^{-11} \cdot e^{-\frac{300}{T}}$	5		0.052		0.061
n-Pentane	$2.78 \cdot 10^{-12} \cdot (\frac{T}{298})^2 \cdot e^{-\frac{115}{T}}$	4		2.8		3.7
2 Methylbutane	$3.90 \cdot 10^{-12}$	5		2.0		2.5
2-2 Dimethylpropane	$1.55 \cdot 10^{-12} \cdot (\frac{T}{298})^2 \cdot e^{-\frac{179}{T}}$	5		18		24
Benzene	$7.57 \cdot 10^{-12} \cdot e^{-\frac{529}{T}}$	5		10		13
Cyclo Hexane	$2.31 \cdot 10^{-12} \cdot (\frac{T}{298})^2 \cdot e^{-\frac{385}{T}}$	6 or 7		1.2		1.4
n-Hexane	$2.61 \cdot 10^{-11} \cdot e^{-\frac{480}{T}}$	8		2.3		3.2
2-3-Dimethylbutane	$6.19 \cdot 10^{-12}$	5		1.4		1.6

continued on next page

continued from previous page

species	OH reaction rate	reference	Troposphere		Lowermost Stratosphere	
			phot. rate	lifetime [days]	phot. rate	lifetime [days]
2 Methyl-Pentane	$5.5 \cdot 10^{-12}$	5		1.4		1.8
3 Methyl-Pentane	$5.6 \cdot 10^{-12}$	5		1.4		1.7
Toluene	$2.1 \cdot 10^{-12} \cdot e^{\frac{322}{T}}$	5		0.91		1.1
n-Heptane	$7.21 \cdot 10^{-12}$	5		1.1		1.3
Ethylbenzene	$7.51 \cdot 10^{-12}$	5		1.0		1.3
o-Xylene	$1.22 \cdot 10^{-11}$	10		0.63		0.79
n-Octane	$3.12 \cdot 10^{-11} \cdot e^{-\frac{380}{T}}$	5		1.3		1.68
n-Nonane	$1.02 \cdot 10^{-11}$	5		0.76		0.95
Nitric Acid	$k_0 = 2.4 \cdot 10^{-14} \cdot e^{\frac{460}{T}}$ $k_2 = 2.7 \cdot 10^{-17} \cdot e^{\frac{2199}{T}}$ $k_3 = 6.5 \cdot 10^{-34} \cdot e^{\frac{1935}{T}}$	11	$9.51 \cdot 10^{-7}$	24	$8.95 \cdot 10^{-7}$	26
p,m-Xylene	$1.66 \cdot 10^{-11} \cdot e^{\frac{146}{T}}$	5		0.28		0.35
n-Butane	$1.68 \cdot 10^{-11} \cdot e^{-\frac{584}{T}}$	8		5.7		7.7

Table 6.4: Reaction rates and photolysis rates of all species. Photolysis rates are average noon values over the measurement region (45°-55° N) in the first half of July at the interpolated average pressure of the troposphere or lowermost stratosphere measurements, taken from the photolysis model of *Brühl and Crutzen* [1989]. Data from a standard cloud atlas was incorporated into the model to include the effect of clouds. A quarter of these values is taken in this study for the diurnal photolysis rate. List of references: ¹*DeMore et al.* [1997], ²*Wollenhaupt et al.* [2000], ³*Atkinson et al.* [2002], ⁴*Talukdar et al.* [1994], ⁵*Atkinson* [1986a], ⁶*Saunders et al.* [1994], ⁷*Atkinson* [1986b], ⁸*DeMore and Bayes* [1999], ⁹*Atkinson et al.* [1984], ¹⁰*Atkinson and Aschmann* [1989], ¹¹*Brown et al.* [1999].

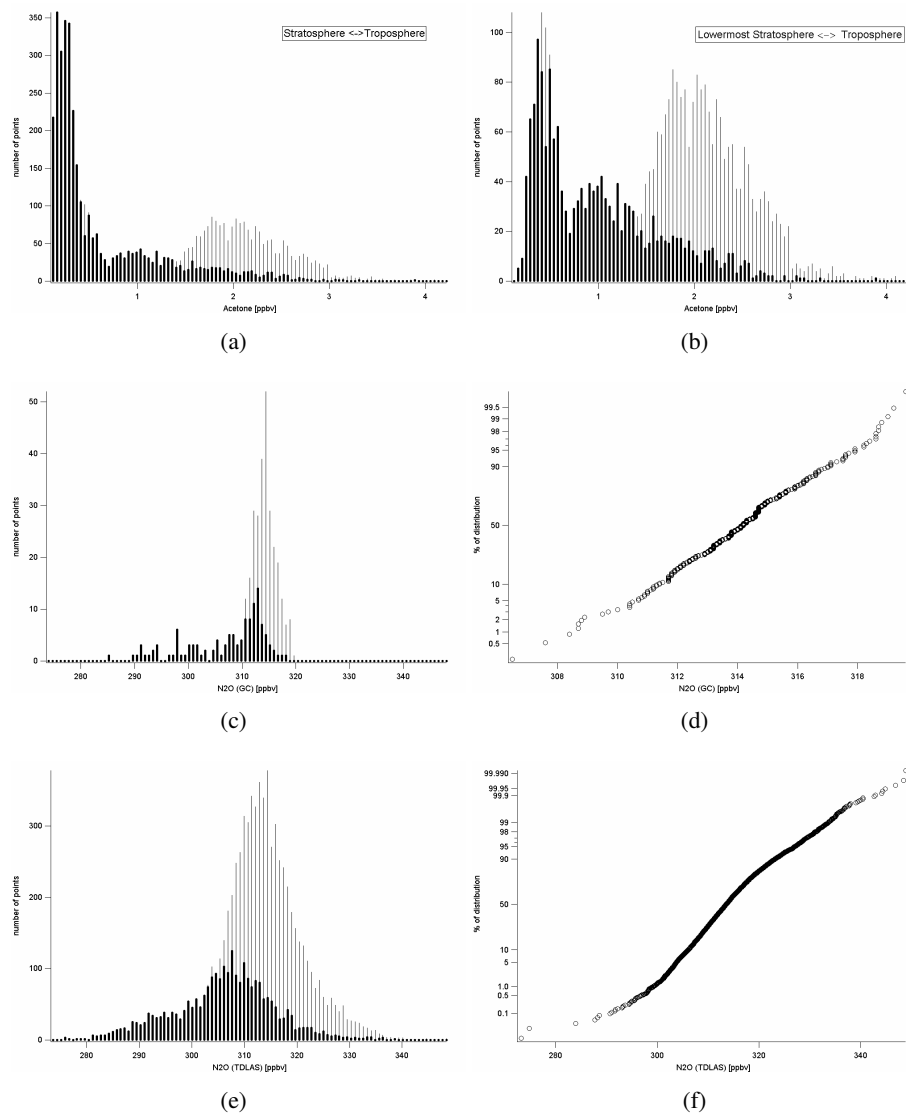


Figure 6.5: Histograms and cumulative Gaussian distribution plots for acetone (a,b), N₂O, measured by the gas chromatograph (c,d), N₂O measured by the TDLAS (e,f), SO₂ (g,h), 2,2-dimethylpropane (i,j) and cyclo propane (k,l). In the histograms (left), the thin lines represent tropospheric data (75 ppbv < O₃), the thick lines data for the lowermost stratosphere (O₃ < 335 ppbv), except for acetone. The Gaussian distributions on the right side show tropospheric data only. Acetone (a,b): the left part shows histograms of the whole stratosphere (broad lines) compared to the troposphere (thin lines), the right part shows the lowermost stratosphere (broad lines) compared to the troposphere (thin lines). N₂O (GC: c,d): the tropospheric data follows a Gaussian distribution and thus follow a straight line in the cumulative Gaussian distribution plot. N₂O (TDLAS: e,f) the TDLAS histogram is much broader, due to noise.

Some species were excluded from the variability-lifetime analysis because their concentrations were partly below the detection limit of the instrument or due to a high noise level of the instrument. This problem was observed for SO₂, which is illustrated in Figure 6.5g and h. In the troposphere, SO₂ mixing ratios were well above the detection limit, whereas in the stratosphere, the SO₂ mixing ratios were very low and close to the detection limit, which can be seen in the Gaussian distribution with one wing cut off. Therefore SO₂ is only taken into account for the tropospheric variability study.

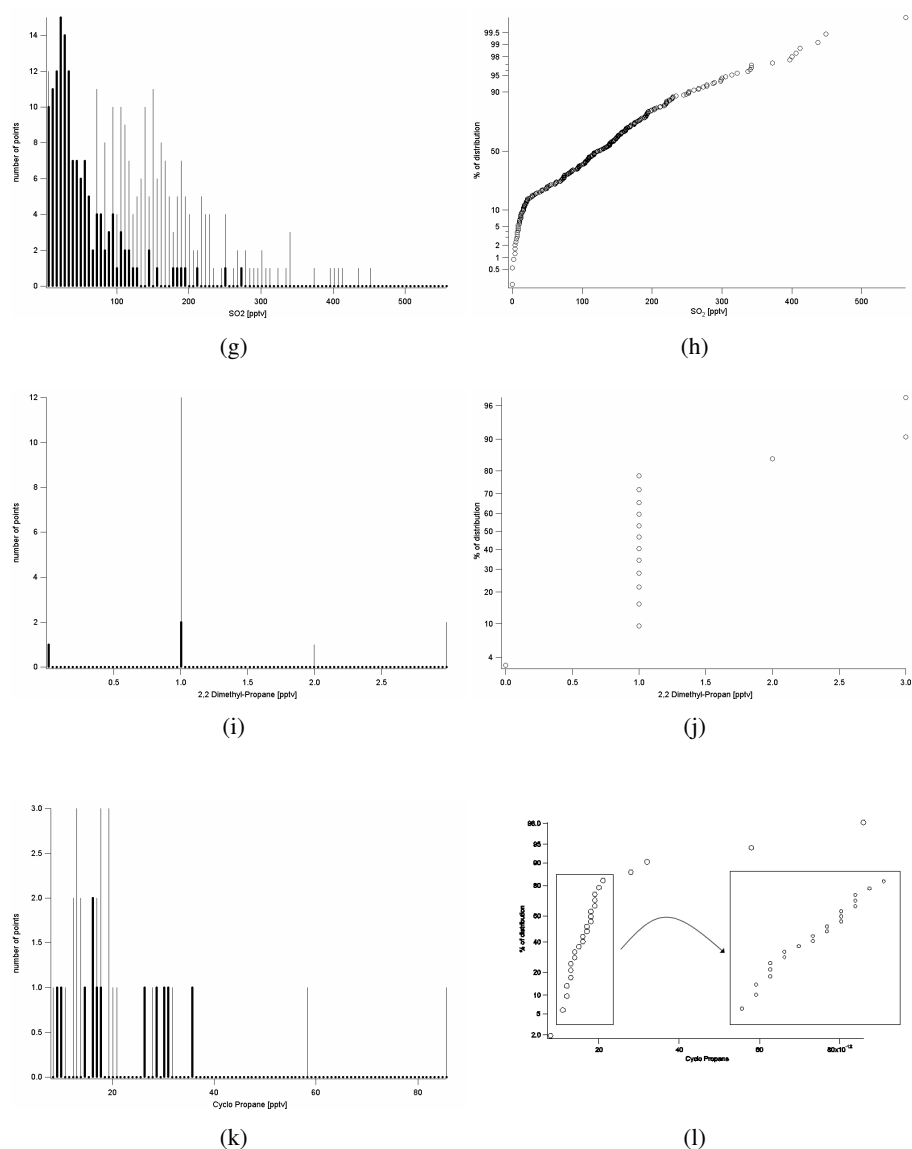


Figure 6.5: continued: SO_2 (g,h) was close to the detection limit in the lowermost stratosphere, thus it was not taken into account in this layer. 2,2-dimethylpropane (i,j), a distribution with binned data: obviously, the data points accumulate at certain values.

The following species had to be excluded from the variability study because their concentrations were too close to the instruments detection limit: isoprene, 2,3-dimethyl-butane, 2,2-dimethyl-butane, 2-methyl-pentane, 3-methyl-pentane, ethyl benzene, n-nonane, o, p and m-xylene for both layers, and SO_2 (only for the stratosphere). For N_2O , measured by the TDLAS, the instrumental noise was rather high, which resulted in an increased variability of the measurements. In both layers, the TDLAS showed higher variability than the gas chromatograph: in the troposphere, $\sigma_{\ln x}(\text{TDLAS})$ was $2.21 \cdot 10^{-2}$, $\sigma_{\ln x}(\text{GC})$ was $0.71 \cdot 10^{-2}$ and in the lowermost stratosphere $\sigma_{\ln x}(\text{TDLAS})$ was $3.13 \cdot 10^{-2}$, $\sigma_{\ln x}(\text{GC})$ was $2.43 \cdot 10^{-2}$. This becomes evident when comparing Figure 6.5e, which shows the TDLAS N_2O histograms for both layers, to Figure 6.5c, which shows N_2O data measured by the gas chromatograph. Therefore, N_2O measurements from the TDLAS were excluded and N_2O concentrations from the gas chromatograph were used for the study.

Other species are excluded from the variability lifetime analysis because of instrumental problems or measurement errors. We checked the cumulative Gaussian distribution for all measured species and found that the distribution of cyclo-propane, n-pentane, 2-methyl-butane, 2,2-dimethyl-propane, cyclo-hexane, n-hexane, toluene, n-heptane and n-octane showed accumulative bins. This means data points are not evenly distributed, but accumulate at discrete values, as shown in Figure 6.5i,j for 2,2-dimethyl-propane and 6.5k,l for cyclo-propane. For species whose lifetime is short compared to the transit time from the source to the receptor, mixing ratios are considerably low. When the instrument is close to the detection limit and the accuracy of the data is too low, binning of the data values results. Therefore, those species are not suitable for the statistical analysis and are excluded from the variability study. *Jobson et al.* [1998] and *Williams et al.* [2000] both observed, that species with a lifetime shorter than about 5 days do not follow the variability-lifetime trend. In the INDOEX MBL study, the fall off was observed at 2.6 days. In our STREAM 98 study, the variability of the species falls off for lifetimes shorter than 4 days in the troposphere and 6 days in the stratosphere, and therefore fits to the results by the other authors. The fall off could be caused by the low mixing ratios of the species, which is a result of the high reactivity. When the accuracy of the instruments is too low, atmospheric variability is suppressed.

Finally, acetonitrile has been excluded from the variability-lifetime analysis, because acetonitrile has more sinks than are considered in the lifetime calculation. Note that for the calculation of the lifetime in Figure 6.4 only photolysis and the reaction with OH was considered. In the troposphere, acetonitrile can be removed from the atmosphere by wet deposition and by ocean uptake [*Jost et al.*, 2003]. Due to these additional sinks, the lifetime of acetonitrile can be as short as 15 days [*Hamm et al.*, 1984], compared to more than 700 days when only photolysis and reaction with OH are considered. This additional sink is hard to quantify, as it requires quantitative knowledge of wet deposition on the oceans and various forms of precipitation, its dependence on temperature, pH value, size of water droplets and their number concentrations. In the lower stratosphere, as well, the lifetime of acetonitrile did not fit onto the straight line in Figure 6.4. *Schneider et al.* [1997] measured a decrease of acetonitrile in the lower stratosphere and suggested ion-catalysed destruction as additional sink. Since we are not able to reproduce the complex source/sink signature of acetonitrile, this species was excluded from the analysis.

In the section above, we have explained why we excluded some measured data from the variability analysis. In the remainder of the chapter, we will analyse the variability-lifetime relation based on the solid black points. Small instrumental artifacts, additional sinks or secondary production can cause the remaining deviation of those data points from the variability lifetime relationship. An example of this is tropospheric SO₂, which is also taken up in clouds and fog and subsequently oxidised. Wet deposition would not influence the variability of HNO₃ to the same extent like SO₂, because HNO₃ is set free when the droplet evaporates. The aerosol size distribution shows that hardly any big particles exist, so that the available surface for the uptake of SO₂ is expected to be small.

6.5.1 OH concentrations

The straight line in Figure 6.4 shows the best fit for the variability-lifetime formula. Whereas the variability was gained from the field measurements, the lifetime of each species had to be calculated with the help of their photolysis- or reaction rates. The respective rates were taken from literature or models. Lifetimes of N₂O and CFC-12 were taken from literature and fixed to 110 years [*Volk et al.*, 1997] and 90 years [*Avallone and Prather*, 1997], respectively. For chemical reactions the lifetime is not only dependant on the reaction rate but also on the concentrations of the reaction partners, like OH. By combining species for which the lifetime is dominated by its reaction with OH, with those dominated by another destruction process, e.g. photolysis, the OH concentration was found by finding the concentration which made the whole set of species fitting best to the variability-lifetime

formula. For the troposphere an OH concentration of $(1.5 \pm 0.3) \cdot 10^6$ molecules/cm³ was found. In the stratosphere $(1.2 \pm 0.25) \cdot 10^6$ molecules/cm³ was deduced. The error in the retrieved OH concentration was estimated by allowing a 30% greater or smaller photolysis rate in the lifetime calculation of the individual species. Table 6.5.1 shows our experimentally deduced OH concentrations as well as model results.

Field Experiment	OH [molecules/cm ³]	O ₃ [ppbv]	Pressure Range [hPa]
STREAM 98 (this work)	$(1.2 \pm 0.25) \cdot 10^6$	75 - 335	161 - 407
	$(1.5 \pm 0.3) \cdot 10^6$	< 75	162 - 413
TM3 97 ¹	$1.2 \cdot 10^6$		191 - 409
	$2.2 \cdot 10^6$		191 - 1009
MATCH-MPIC ² with CCM3 wind	$0.95 \cdot 10^6$		164 - 434
	$0.96 \cdot 10^6$	75 - 285	
	$0.91 \cdot 10^6$	75 - 370	
	$1.3 \cdot 10^6$		164 - 993
	$1.6 \cdot 10^6$	< 75	

Table 6.5: Results and comparison of OH concentrations for STREAM 98 (no altitude data was received with the model data sets).¹Bregman [2000], ²von Kuhlmann [2002]

Comparison with model results

We compared the retrieved OH concentrations with the OH concentrations calculated by two different chemistry transport models. The tropospheric photochemistry version (MATCH-MPIC [Lawrence *et al.*, 1999]) of the Model of Atmospheric Transport and Chemistry (MATCH [Rasch *et al.*, 1997]), was driven by wind, temperature, pressure, and surface flux fields from the NCAR-CCM3 model (National Center for Atmospheric Research - Community Climate Model [Kiehl *et al.*, 1996], middle atmosphere version (MACCM)), the latter was calculated for 1998. The horizontal resolution of the CCM3 data was $5.6^\circ \times 5.6^\circ$ (T21 resolution), in the vertical 36 levels (up to 2.6 hPa) were used as input for MATCH. The time resolution of the meteorological input data was 6 hours, so that these data were linearly interpolated to the beginning of each 30-minute MATCH time step. MATCH includes gas-phase chemistry, NMHCs up to isoprene but no stratospheric chemistry. Therefore, monthly zonal mean HALOE data were used to adjust ozone and water vapour concentrations above pressure level $(200 - 165 \cdot \cos^2 \Phi)$ hPa, where Φ is latitude. HALOE ozone was nudged to match zonal means of the model, so that longitudinal structures of the model were kept. Water vapour was fixed to the HALOE data. A detailed description of this model run can be found in von Kuhlmann *et al.* [2003a,b].

The TM3 model (a Chemistry Transport Model of the University Utrecht) [van Velthoven and Kelder, 1996; Bregman *et al.*, 2000] was run with 6 hourly mean meteorological fields from the ECMWF for the year 1997, including wind, surface pressure, temperature and humidity. The resolution of the TM3 model is $3.75^\circ \times 5^\circ$ (latitude \times longitude) with 19 vertical layers up to 10 hPa. The chemistry calculation time step was 40 minutes. TM3 includes advection, diffusion, convection, dry and wet deposition, photolysis and gas phase chemistry. Zonal averaged O₃ climatology [Fortuin and Kelder, 1998], scaled to GOME (Global Ozone Monitoring Experiment onboard the ERS-2 satellite) data, is used as ozone upper boundary for the upper three levels of the model. The influence of taking the meteorological field of the year 1997 instead of 1998 was considered negligible because of the long averaging time of a month [Bregman, pers. communication].

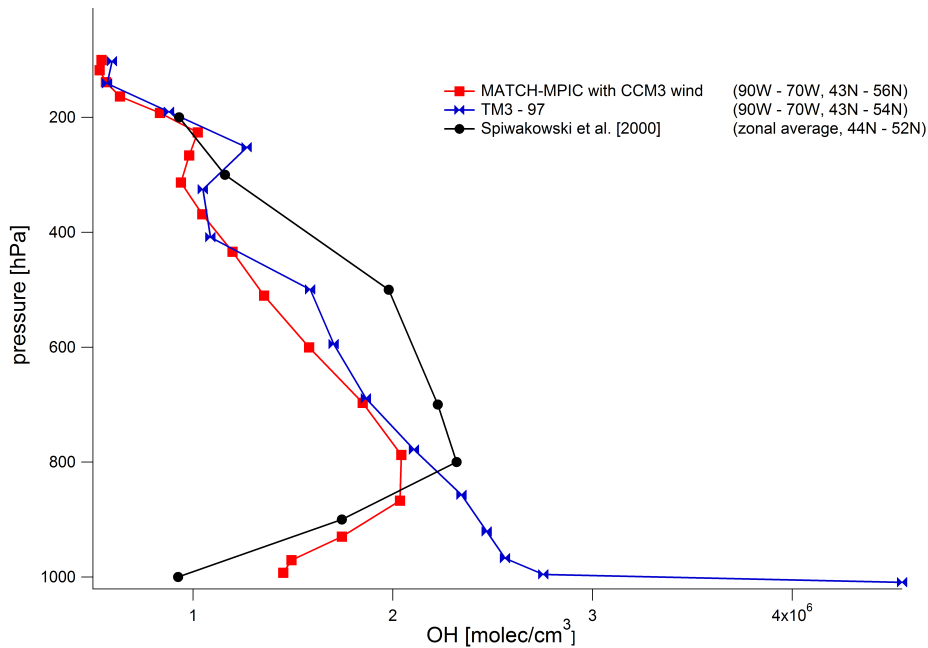


Figure 6.6: Vertical profile of OH concentrations for Northern Hemispheric midlatitudes, derived by the models MATCH-MPIC with CCM3 wind (red boxes, [von Kuhlmann, 2002]), TM3 97 (blue flies, [Bregman, 2000]) and Spivakovsky *et al.* [2000] for the month July. The zonal and meridional range of the data is given in the legend.

The OH concentrations derived from both models are monthly mean values and are shown in Table 6.5.1. The model data was averaged over the measurement region, which includes latitude, longitude and pressure levels as vertical selection criterion. Mean OH concentrations from the MATCH model were $1.3 \cdot 10^6$ molecules/cm³ in the troposphere and $9.5 \cdot 10^5$ molecules/cm³ in the stratosphere. A look on the MATCH O₃ mixing ratios showed that the tropopause in the MATCH model and during the STREAM 98 campaign were partly on different pressure levels. During STREAM, the tropopause occurred partly at pressure levels that were clearly inside the stratosphere in the Match model. Therefore, also O₃ was taken as vertical criterion for the OH comparison, with 75 ppbv for upper value of the troposphere, and 285 ppbv or 370 ppbv as upper O₃ mixing ratio of the lowermost stratosphere. Both numbers resulted from gridding in the modelled data and were below or above the O₃ mixing ratio which was actually taken during the variability analysis. With this O₃ criteria, $1.6 \cdot 10^6$ molecules/cm³ in the troposphere and $9.6(9.1) \cdot 10^5$ molecules/cm³ in the lowermost stratosphere were obtained. These data compare to a tropospheric OH concentration of $(1.5 \pm 0.3) \cdot 10^6$ molecules/cm³, and $(1.2 \pm 0.25) \cdot 10^6$ molecules/cm³ in the stratosphere, deduced by the variability method.

Average OH concentrations from the TM3 model were $2.2 \cdot 10^6$ molecules/cm³ in the troposphere and $1.2 \cdot 10^6$ molecules/cm³ in the stratosphere. The tropospheric OH concentration is higher than those derived by the variability study ($1.5 \cdot 10^6$ molecules/cm³) or by the MATCH model (1.3 or $1.6 \cdot 10^6$ molecules/cm³). A closer look into the data showed, that this is mainly due to high OH concentrations in the lower atmosphere. A difference between the models can clearly be seen in the lower atmospheric OH concentration trends (see Figure 6.6). In the TM3 model, mixing ratios increase constantly towards the Earth's surface at low altitudes, whereas in the MATCH model OH concentrations decrease at low altitudes. Spivakovsky *et al.* [2000] studied three-dimensional distributions of tropospheric OH concentrations, as well. Although the results they published are on a

more coarse altitude grid than the MATCH or TM3 model results, *Spivakovsky et al.* [2000] found the same trend as the MATCH model at lower altitudes: decreasing OH concentrations. They derived $1.6 \cdot 10^6$ molecules/cm³ in the troposphere (1000 - 200 hPa, 44°N - 52°N). The stratospheric value OH concentrations of the TM3 model and the one derived by the variability method agree very well (both $1.2 \cdot 10^6$ molecules/cm³).

The values derived from both models and by the variability method agree very well within the error bars, except for the tropospheric TM3 OH concentration which is discussed above. The stratospheric MATCH OH concentration is a bit lower than our value, though overlapping within the error. As was pointed out by *Scheeren et al.* [2003], acetone concentrations during STREAM 98 were remarkably high in the stratosphere, reaching about 1 ppbv. The MATCH model has considerable lower acetone concentrations in both troposphere and stratosphere. Since acetone is an OH precursor, this could lead to too low OH concentrations in both regions. On the other hand, *Ravishankara et al.* [2002] reported new measurements of the reaction rate of O(¹D) with N₂, a reaction competing with the reaction of O(¹D) with H₂O, which produces OH. The authors state that this could lead to 15 % less production of OH in the middle troposphere and above. Although further testing of models is necessary to assess the impact on actual OH concentrations in the middle troposphere and above, it is possible, that this compensates the effect of the too low acetone mixing ratios in the models, since the effect is reversal.

Although the uncertainties of the model calculations are generally large, the agreement between the OH concentrations deduced by the variability method and the models is good. Obviously, the dynamics and chemistry used in the models describe the processes in the real atmosphere very good on time scales that are covered by our method. Although, the TM3 model showed a lower atmospheric trend, that is not found by the other models. Nevertheless, a comparison of results by the variability method and by models for other regions and other times of the year is desirable.

6.5.2 The parameters A and b

As mentioned previously in section 3.5, the parameter b can vary between 0 and 1. High b values indicate that chemical loss processes dominated the variability of the measured trace gases, whereas small b values occur where mixing of “widely different air mass ages” [*Jobson et al.*, 1999] took place.

For STREAM 98, b is 0.55 ± 0.03 in the troposphere and 0.43 ± 0.02 in the lowermost stratosphere. Table 6.6 shows A and b values for different measurement campaigns [*Jobson et al.*, 1999], as well as our results. All referenced tropospheric b values are close to 0.5, which is, as the authors stated, characteristic for remote tropospheric data. The tropospheric b value during STREAM 98 is comparable to the remote tropospheric b value found in other campaigns. During STREAM 98, relatively freshly emitted air masses and older tropospheric air masses were sampled, such as ascended Pacific air, polluted boundary layer air, which was most probably convected from mid-latitudes and Lake Superior area (the north-westernmost of the Great Lakes) and even tropospheric air from tropical regions.

The ASHOE¹ and AASE II² data approach the b = 1 limit, indicating that the air masses had been more isolated and thus variability was dominated by chemical loss processes. b is only 0.68 for the extra tropical SPADE³ data. The authors interpreted mixing of midlatitude air and vortex air as the cause for the lower b value during SPADE. The b value of 0.43 ± 0.02 obtained in this study is even lower, indicating that mixing, in this case between stratospheric and tropospheric air, even more dominated the variability in the region of the stratosphere analysed in this paper. All referenced

¹Airborne Southern Hemisphere Ozone Experiment

²Airborne Arctic Stratospheric Expedition II

³Stratospheric Aerosols and Dynamics Expedition

Field experiment	A	b	Altitude Range	Geographical area	Date
ABLE 3B ¹	1.6 ± 0.15	0.46 ± 0.02	PBL - 6km	Hudson Bay Lowlands, northern Quebec	July-August
TRACE A ²	2.9 ± 0.44	0.52 ± 0.02	PBL - 12km	South Atlantic, Brazil, southern Africa	September - October
PEM - West B ³	4.3 ± 0.63	0.53 ± 0.02	PBL - 12km	Western Pacific	February - March
STREAM 98 (this work)	2.86 ± 1.17	0.55 ± 0.03	7 - 13km (free trop.)	Canada (43°N-56°N)	July
ASHOE ⁴ (extratropical)	1.6 ± 0.18	0.97 ± 0.06	17 - 20km	Southern Hemisphere (20°N - 69°S)	March- Novembre
AASE II ⁵	3.3 ± 0.32	0.90 ± 0.05	17 - 20km	Northern Hemisphere (15°N - 90°N)	February - March
SPADE ⁶ (extratropical)	1.0 ± 0.03	0.68 ± 0.01	17 - 20km	Northern Hemisphere (15°N - 60°N)	May
STREAM 98 (this work)	2.44 ± 1.11	0.43 ± 0.02	7 - 13km (1m strat.)	Canada (43°N-56°N)	July

Table 6.6: Results and comparison of Fit-parameters A and b for STREAM 98. Other data from *Jobson et al.* [1999]. Short names of campaigns: ¹Arctic Boundary Layer Expedition 3B; ²Transport and Atmospheric Chemistry Near the Equator -Atlantic; ³Pacific Exploratory Mission in the Western Pacific Ocean, Phase B; ⁴Airborne Southern Hemisphere Ozone Experiment; ⁵Airborne Arctic Stratospheric Expedition II; ⁶Stratospheric Aerosols and Dynamics Expedition.

stratospheric data, presented in Table 6.6, have been obtained above 400 K potential temperature. Since the stratospheric measurements analysed in this study reaches to lower theta levels, the influence of tropospheric air masses onto the air masses in the lowermost stratosphere must be studied. Tracer-tracer correlations can be used for this, when the two species in question have an opposite source/sink distribution regarding the tropospheric and stratospheric reservoirs [*Fischer et al.*, 2000, 2001]. When no mixing occurred, the tracer-tracer correlation of O₃ versus CO would have an “L”-shape, with one stratospheric branch and one tropospheric branch. When transport processes across the tropopause occur, a third branch will be added, with intermediate trace gas concentrations, showing influence of both reservoirs [*Hoor et al.*, 2002]. *Hoor et al.* [2002] used the correlation between O₃ and CO to differentiate between tropospheric and stratospheric air masses and to identify a mixing layer above the local tropopause influenced by troposphere stratosphere transport. They identified the upper limit of this mixing layer to be at approximately 400 ppbv O₃, which corresponds to a potential temperature level of 360 K. Hence, the referenced stratospheric data in Table 6.6 were mostly taken above the mixing layer, whereas our measurements were performed in the mixing layer. This is also illustrated by the altitude ranges covered: the reference data extend from 17 to 20 km altitude; our data cover 7 to 13 km altitude. This interpretation is consistent with the b values measured.

Obviously, in both the troposphere and the lowermost stratosphere during STREAM 98, mixing of air masses with clearly different ages took place. In both layers aged air masses are mixed with younger air masses - in the troposphere, the planetary boundary layer is a source of young air masses; in the lowermost stratosphere, the troposphere is the source of “young” air. This resulted in b values of about 0.5 in both studied layers.

From model results *Jobson et al.* [1999] derived for the case of $b = 1$, that “ A is the standard deviation of measured transit times”. High A values can also result of the sampling of several inhomogeneous air masses. For STREAM 98, the A value is similar in the troposphere and the lowermost stratosphere: A is 2.86 ± 1.17 in the troposphere and 2.44 ± 1.11 in the lowermost stratosphere. The tropospheric A values given in Table 6.6 cover a wide range, as geographical locations and seasons and thus sampled air masses differ.

AASE II took place in winter, when the vortex blocks the dynamic cycle, so that the air inside the vortex is rather isolated and thus ages without mixing with the air outside the vortex. As the measurements covered a latitude range from 15°N to 90°N , the air inside and outside the vortex was sampled. Sampling of these different air masses most probably resulted in a higher A value than for SPADE and ASHOE, where only outside-vortex air was sampled. The STREAM 98 measurements covered a smaller latitude range, between 44°N and 56°N , but as these measurements were conducted in the lowermost stratosphere, influences of two reservoirs, the troposphere and the stratosphere, lead to broader concentration distributions and thus larger standard deviations of the measured trace gases.

The same applies to the tropospheric data. The A value of 2.86 ± 1.17 obtained in this study lies within the range of A values obtained in other measurement campaigns. Reference values vary between 1.6 during ABLE 3B⁴ and 4.3 during PEM West-B⁵. The air masses sampled during ABLE-3B were of arctic origin and thus not as variable as the air masses sampled during STREAM 98, as stated in the discussion of the b parameter. During PEM-West B strong influence of fresh Asian plumes was found, clean or aged marine air and even stratospheric intrusions were sampled [*Hoell et al.*, 1997]. All these data were included in the tropospheric variability-lifetime analysis; hence, a higher A value was obtained from the PEM-West B analysis.

6.6 Summary and conclusions

The variability study was performed for two atmospheric layers during the STREAM campaign, the free troposphere ($\text{O}_3 < 75$ ppb) and the lowermost stratosphere ($75 \text{ ppb} < \text{O}_3 < 335$ ppb). Of the large number of trace gases sampled during the campaign, 13 (12) species could be used for the variability-lifetime analysis. The average OH concentration along the back trajectory of the sampled air mass has been determined by optimising the OH concentration in the lifetime calculation of the individual species. The OH concentrations that we derived by this method were $(1.5 \pm 0.3) \cdot 10^6$ molecules/cm³ in the troposphere and $(1.2 \pm 0.25) \cdot 10^6$ molecules/cm³ in the lowermost stratosphere, which agree very well with model calculations for the respective regions.

In the free troposphere the parameters A and b , which describe the relation between the variability and lifetime, were 2.86 ± 1.17 and 0.55 ± 0.03 , respectively. To our knowledge, the variability study was performed for the first time in the lowermost stratosphere. Here the values for A and b were very similar as for the free tropospheric layer, 2.44 ± 1.11 and 0.43 ± 0.02 , respectively. These A and b values indicate that both layers were influenced by air masses with very different air mass ages; the free troposphere by boundary layer, free tropospheric and stratospheric air masses, the lowermost stratosphere by stratospheric and free tropospheric air masses. The reported measurements were performed close to the polar jet stream, where mixing between stratospheric and tropospheric air

⁴Arctic Boundary Layer Expedition 3B

⁵Pacific Exploratory Mission in the Western Pacific Ocean, Phase B

masses occurs very frequently. The strong convective activity in the measurement region causes the mixing of boundary layer air into the free troposphere.

Information about the data quality, the consistency of data sets and atmospheric processes controlling the lifetime of individual species can be obtained by studying compounds that do not follow the linear variability-lifetime relation. Several NMHCs, for example isoprene and ethyl benzene, showed a much smaller variability as expected based on their lifetime, which was caused by the very low concentrations, close to the detection limit of the instrument. N_2O (TDLAS) showed a much higher variability as expected, which was caused by the high noise level of the instrument. Moreover, the relatively high variability of acetonitrile was most probably caused by additional sinks, which were not considered in the lifetime calculation.

The estimation of OH concentrations from measurements and the derivation of the A and b parameters using the variability method offers the opportunity to compare chemistry and dynamics of in-situ measurements and helps understanding the processes controlling the chemical composition of the tropopause region.

Chapter 7

Summary and outlook

7.1 Summary

In this thesis, the variability-lifetime relation of atmospheric tracers was investigated using the variability of the concentrations of a whole range of trace gases that were measured during two airborne measurement campaigns, INDOEX 99 and STREAM 98. The airborne TDLAS (Tunable Diode Laser Absorption Spectroscopy) measurements performed by our institute are presented in more detail, all other data were by courtesy of other participants of the INDOEX and STREAM 98 campaigns. The hydroxyl radical concentrations along the back trajectory of the air masses were estimated for both campaigns. Furthermore, the state of mixing of the atmosphere was investigated using the variability-lifetime relationship.

The *Indian Ocean Experiment* (INDOEX) was designed to study the impact of anthropogenic trace gases and aerosols on the chemistry and radiative forcing over the Indian Ocean. To achieve this, combined measurements of several platforms took place in 1998 and 1999. In the course of the intensive field phase, which took place in spring 1999, various trace gas measurements, aerosol- and radiation measurements were performed from onboard the research aircraft Cessna Citation. A total of 23 individual flights were performed between February 14 until March 21 from the island Hulhule (4.2° N, 73.5° E), Republic of Maldives, and refuelling stops at Gan (0.7° S, 73.2° E), the southernmost island of the Maldives, or at Colombo (6.9° N, 79.9° E), Sri Lanka.

The STREAM 98 summer campaign was part of a series of *Stratosphere Troposphere Experiments by Aircraft Measurements*. During STREAM 98 chemical and dynamical processes that influence the chemical composition of the tropopause region were studied, with special emphasis on the influence of long range transport, deep convection and stratosphere-troposphere-exchange as well as the chemistry of the lowermost stratosphere. Between July 1 and 15, 1998 a total of 8 measurement flights were performed from onboard the Cessna Citation, which was based in Timmins, Canada (48.2° N, 79.3° W).

During INDOEX a large number of trace gases have been measured, of which nine were used for a variability-lifetime analysis. The variability-lifetime relation proved to be a good method to indirectly method to determine the OH concentration. The average OH concentration along the back trajectory of the sampled air mass has been determined by optimising the OH concentration in the lifetime calculation of the individual species. The INDOEX variability study was performed in the marine boundary layer (below 1 km). The OH concentration that we derived by this method was $3.4_{-1.0}^{+1.1} \cdot 10^6$ molecules/cm³.

The STREAM 98 variability study was performed for two layers in the atmosphere, the upper free troposphere (altitude > 7 km and O₃ < 75 ppbv) and the lowermost stratosphere (75 ppbv < O₃ < 335 ppbv), for which 13 respectively 12 species were used. During STREAM 98, the OH

concentrations that were derived by this method are $1.5 \pm 0.3 \cdot 10^6$ molecules/cm³ in the troposphere and $(1.2 \pm 0.25) \cdot 10^6$ molecules/cm³ in the lowermost stratosphere. For both campaigns, the results agree very well with model calculations for the respective regions.

During INDOEX, the parameters A and b, which describe the relation between the variability and lifetime, were 1.96 ± 1.14 and 0.70 ± 0.04 , respectively. The derived b value indicates that the measurement area was rather remote, with no fresh pollution sources around, so that chemical processing and photolytical degradation determined the variability of the measured trace gases rather than mixing. The A value indicates that the age distribution of the measured air masses was rather uniform, due to the measurement location over the Indian ocean far away from pollution sources and the fact that air masses sampled from the Cessna Citation mainly originated from two source regions - the Arabian Sea and the Bay of Bengal.

During STREAM 98 the parameters A and b were 2.86 ± 1.17 and 0.55 ± 0.03 , respectively, in the free troposphere. These A and b values indicate this atmospheric layer (the free troposphere) was influenced by air masses with very different air mass ages: by boundary layer and free tropospheric air masses. To our knowledge, the variability study was performed for the first time in the lowermost stratosphere, where the A and b were very similar to those of the free tropospheric layer, 2.44 ± 1.11 and 0.43 ± 0.02 , respectively. In the lowermost stratosphere, as well, the A and b values indicate the influence of air masses with very different air mass ages: stratospheric and free tropospheric air masses. The reported measurements were performed close to the polar jet stream, where mixing between stratospheric and tropospheric air masses occurs very frequently. The strong convective activity in the measurement region causes the mixing of boundary layer air into the free troposphere.

7.2 Outlook

The variability method is a powerful tool for assessing data quality, for understanding atmospheric processes controlling the lifetime of species, determining the state of mixing of the atmosphere and for deriving mean OH concentrations.

The assessment of the data quality of the measurements with help of the variability method, among others, showed that the detection limits of some instruments were too close to the measured mixing ratios, which made the measurements unsuitable for statistical analysis with the variability study. Furthermore, it has to be taken into account that a statistical analysis like this requires a minimum number of data points. This may not always be given for canister measurements during short campaigns, when different layers of the atmosphere shall be studied. Moreover, a sufficient number of species and a choice of species in the short, middle and long lifetime range are necessary for performing a reliable variability lifetime study. The definition of short and long depends on the time scale on which the scientist wishes to conclude. In addition, it would be of advantage for the reliability of the results to have not only one species, in our case acetone, whose atmospheric removal is influenced significantly by other sinks than reaction with OH, but several. For example methylethylketone (MEK) is removed by photolysis and reaction with OH, analog to acetone. Another possibility are alkenes, which react with OH and with O₃. A difficulty would then be the estimation of O₃ concentrations along the back trajectory of the air mass. The use of solely radioactive decaying species, like radon, has the advantage that it does not react with OH at all, but instead the decay is well known, constant and independent of any other parameter, which has to be estimated. That makes it very well suited for the variability - lifetime study. On the other hand, it does not have the same sources as typical trace gases, therefore travel times could be different. However, the sources of radon are, as for other typical trace gases, located on the continents, so that the variability study can well be applied when the sampling takes place far away, e.g. on a remote site like an island [Ehhalt *et al.*, 1998; Williams *et al.*, 2001]. It is desirable, that the above mentioned requirements are taken into account

in the planning of future campaigns.

In the variability study, the two parameters A and b are derived. Parameter b is a measure for the remoteness of the site and the derived values fit well to the results from other campaigns. However, the parameter A, which was proposed to mirror the width of air mass ages that influences the trace gas composition in the measurement region, should be studied more closely. Although the presented results can be explained with this assumption, a wider range of measurements and also comparison with model studies could provide more insight into this aspect and help interpret the results of future campaigns.

The INDOEX 99 and STREAM 98 analysis showed that OH concentrations can be obtained from trace gas concentrations by means of the variability study. This opens an opportunity to retrieve OH concentrations in a measurement region, even when direct measurements, which are still costly and complex, were not performed. However, comparisons between in-situ OH measurements and results obtained from the variability study are desirable, particularly with regard to the long term trends of OH concentrations, which is a hot topic in atmospheric sciences at present. For example, *Lelieveld et al.* [2002] used a global chemistry transport model to study the stability of OH chemistry. The authors found remarkable stability in global OH concentrations during the last century, but state that OH concentrations decreased substantially in the marine troposphere, which was compensated on a global scale by an increase over the continents associated with strong pollution emissions of nitrogen oxides. Repeated measurements in the same regions could serve to assess this trend. A tight grid of measurements would help to resolve regional differences and to clarify the role of anthropogenic emissions with regard to the complex hydroxyl radical chemistry, which could lead to increase or destruction of the atmospheric cleaning agent, as well. Since correlations between anthropogenic pollution and severe diseases of the respiratory and cardiovascular system, or even mortality, were found, changes in the mixing ratios of trace gases and especially the hydroxyl radical as cleaning agent of the atmosphere, remain a major point of concern, both in public and academic interest.

References

- Atkinson, R. (1986a), Kinetics and mechanisms of the gas-phase reactions of the hydroxyl radical with organic compounds under atmospheric conditions, *Chem. Rev.*, *86*, 69.
- Atkinson, R. (1986b), Estimations of OH radical rate constants from H-atom abstraction from C-H and O-H bonds over the temperature range 250 – 1000 K, *Int. J. Chem. Kinetics*, *18*, 555.
- Atkinson, R., and S. M. Aschmann (1989), Rate constants for the gas-phase reactions of the OH radical with a series of aromatic hydrocarbons at 296 ± 2 K, *Int. J. Chem. Kinetics*, *21*, 355.
- Atkinson, R., W. P. L. Carter, S. M. Aschmann, A. M. Winer, and J. N. Pitts, Jr. (1984), Kinetics of the reaction of OH radicals with a series of branched alkanes at 297 ± 2 K, *Int. J. Chem. Kinetics*, *16*, 469.
- Atkinson, R., D. L. Baulch, R. A. Cox, R. F. Hampson, Jr., J. A. Kerr, M. J. Rossi, and J. Troe (1997), Evaluated kinetic and photochemical data for atmospheric chemistry: Supplement vi, *J. Phys. Chem. Ref. Data*, *26*, 1329–1499.
- Atkinson, R., D. L. Baulch, R. A. Cox, J. N. Crowley, R. F. Hampson, Jr., J. A. Kerr, M. J. Rossi, and J. Troe (2001), Summary of Evaluated Kinetic and Photochemical Data for Atmospheric Chemistry: Web version December 2001, IUPAC Subcommittee on Gas Kinetic Data Evaluation for Atmospheric Chemistry.
- Atkinson, R., D. L. Baulch, R. A. Cox, J. N. Crowley, R. F. Hampson, Jr., J. A. Kerr, M. J. Rossi, and J. Troe (2002), Summary of evaluated kinetic and photochemical data for atmospheric chemistry: Web version December 2002, IUPAC Subcommittee on Gas Kinetic Data Evaluation for Atmospheric Chemistry.
- Atticks, M. J., and G. D. Robinson (1983), Some features of the structure of the tropical tropopause, *Q. J. R. Meteorol. Soc.*, *109*, 295–308.
- Avallone, L. M., and M. J. Prather (1997), Tracer-tracer correlations: Three-dimensional model simulations and comparisons to observations, *J. Geophys. Res.*, *102*, 19,233–19,246.
- Bachmeier, A. S., M. C. Shipham, E. V. Browell, W. B. Grant, and J. M. Klossa (1994), Stratospheric/tropospheric exchange affecting the northern wetlands regions of Canada during summer 1990, *J. Geophys. Res.*, *99*, 1793–1804.
- Baulch, D. L., C. J. Cobos, R. A. Cox, C. Esser, P. Frank, T. Just, J. A. Kerr, M. J. Pilling, J. Troe, R. W. Walker, and J. Warnatz (1992), Evaluated kinetic data for combustion modelling, *J. Phys. Chem. Ref. Data*, *21*, 411–429.
- Bell, M. L., and D. L. Davis (2001), Reassessment of the Lethal London Fog of 1952: Novel Indicators of Acute and Chronic Consequences of Acute Exposure to Air Pollution, *Environ. Health Perspect.*, *109*(Supplement 3), 389–394.

- Berresheim, H., C. Plass-Dülmer, T. Elste, N. Mihalopoulos, and F. Rohrer (2003), OH in the coastal boundary layer of Crete during MINOS: Measurements and relationship with ozone photolysis, *Atmos. Chem. Phys.*, *3*, 639–649.
- Bethan, S., G. Vaughan, and S. J. Reid (1996), A comparison of ozone and thermal tropopause heights and the impact of tropopause definition on quantifying the ozone content of the troposphere, *Quart. J. R. Meteorol. Soc.*, *122*, 929–944.
- Beuermann, J. (2000), Einfluss von Transportprozessen auf die Wasserdampfverteilung in der Tropopausenregion, Ph.D. thesis, Rheinische Friedrich-Wilhelms-Universität, Bonn.
- Bjerknes, J. (1969), Atmospheric teleconnections from the equatorial Pacific, *Mon. Weather Rev.*, *97*, 163–172.
- Blake, N. J., S. A. Penkett, K. C. Clemittshaw, P. Anwyl, P. Lightman, A. R. W. Marsh, and G. Butcher (1993), Estimates of atmospheric Hydroxyl Radical Concentrations from the Observed Decay of Many Reactive Hydrocarbons in Well-Defined Urban Plumes, *J. Geophys. Res.*, *98*, 2851–2864.
- Bolin, B., and H. Rodhe (1973), A note on concepts of age distribution and transit time in natural reservoirs, *Tellus*, *25*, 58–62.
- Brasseur, G., and S. Solomon (1986), *Aeronomy of the middle atmosphere*, Kluwer Acad., Norwell, Mass.
- Brauers, T., U. Ashmutat, U. Brandenburger, H.-P. Dorn, M. Hausmann, M. Heßling, A. Hofzumahaus, F. Holland, C. Plass-Dülmer, and D. H. Ehhalt (1996), Intercomparison of tropospheric OH radical measurements by multiple folded long-path laser absorption and laser induced fluorescence, *Geophys. Res. Lett.*, *18*, 2545–2548.
- Bregman, A. (2000), private communication.
- Bregman, A., P. F. J. van Velthoven, F. Wienhold, H. Fischer, T. Zenker, A. Waibel, A. Frenzel, F. Arnold, G. W. Harris, M. J. A. Bolder, and J. Lelieveld (1995), Aircraft measurements of O₃, HNO₃ and N₂O in the winter arctic lower stratosphere during the stratosphere-troposphere experiment by aircraft measurements (STREAM), *J. Geophys. Res.*, *100*(D6), 11,245–11,260.
- Bregman, A., M. van den Broek, K. S. Carslaw, R. Müller, T. Peter, M. Scheele, and J. Lelieveld (1997), Ozone depletion in the late winter lower Arctic stratosphere: Observations and model results, *J. Geophys. Res.*, *102*(D9), 10,815–10,828.
- Bregman, A., J. Lelieveld, M. van den Broek, P. Siegmund, H. Fischer, and O. Bujok (2000), The N₂O and O₃ relationship in the lowermost stratosphere: a diagnostic for mixing processes as represented by a three dimensional chemistry-transport model, *J. Geophys. Res.*, *105*, 17,279–17,290.
- Brenninkmeijer, C. A. M., M. R. Manning, D. C. Lowe, G. Wallace, R. J. Sparks, and A. Volz-Thomas (1992), Interhemispheric Asymmetry in OH Abundance Inferred from Measurements of Atmospheric ¹⁴CO, *Nature*, *356*, 50–52.
- Brewer, A. W. (1949), Evidence for a world circulation provided by measurements of the helium and water vapor distribution in the stratosphere, *Q. J. R. Meteorol. Soc.*, *75*, 351–363.
- Brown, S. S., R. K. Talukdar, and A. R. Ravishankara (1999), Reconsideration of the Rate Constant for the Reaction of Hydroxyl Radicals with Nitric Acid, *J. Phys. Chem. A*, *103*, 3031–3037.

- Brühl, C., and P. J. Crutzen (1989), On the disproportionate role of tropospheric ozone as a filter against solar UV-B radiation, *Geophys. Res. Lett.*, *16*, 703–706.
- Bujok, O., V. Tan, E. Klein, R. Nopper, R. Bauer, M.-T. Gerhards, A. Afchine, D. McKenna, A. Engel, U. Schmidt, F. Wienhold, and H. Fischer (2001), GHOST - a novel airborne gas chromatograph for in situ measurements of long-lived tracers in the lower stratosphere, *J. Atmos. Chem.*, *39*, 37–64.
- Calve, S. L., D. Hitier, G. L. Bras, and A. Mellouki (1998), Kinetic studies of OH reactions with a series of ketones, *J. Phys. Chem. A*, *102*, 4579 – 4584.
- Caplan, P., and H.-L. Pan (2000), Changes to the 1999 NCEP Operational MRF Model Analysis/Forecast System, *NCEP Pub. No. 452*, National Centers for Environmental Prediction, Silver Spring.
- Chan, C. Y., T. M. Hard, A. A. Mehrabzadeh, L. A. George, and R. J. O'Brien (1990), Third generation FAGE Instrument for Tropospheric Hydroxyl Radical Measurement, *J. Geophys. Res.*, *95*, 18,569–18,576.
- Chapman, S. (1930), On ozone and atomic oxygen in the upper atmosphere, *Phil. Mag.*, *10*, 369.
- Chapman, S., and R. S. Lindzen (1970), *Atmospheric Tides, Thermal and Gravitational*, Gordon and Breach, New York.
- Chu, P. S. (1984), Time and space variability of rainfall and surface circulation in the northeast brazil-tropical atlantic sector, *J. Met. Soc. Japan*, *62*, 363–70.
- Colman, J., D. R. Blake, and F. S. Rowland (1998), Atmospheric residence time of CH₃Br estimated from the junge spatial variability relation, *Science*, *281*, 392–396.
- Crutzen, P. J., J.-U. Groöf, C. Brühl, R. Müller, and J. M. Russell, III (1995), A reevaluation of the ozone budget with halocarbon data: No evidence for the ozone deficit, *Science*, *268*, 705–708.
- de Gouw, J. A., C. Warneke, H. A. Scheeren, C. van der Veen, M. Bolder, M. Scheele, J. Williams, S. Wong, L. Lange, H. Fischer, and J. Lelieveld (2001), Overview of the Trace Gas Measurements Onboard the Citation Aircraft during the Intensive Field Phase of INDOEX, *J. Geophys. Res.*, *106*(D22), 28,453–28,467, INDOEX Special Issue.
- de Laat, A. T. J., and J. Lelieveld (2002), Interannual variability of the Indian winter monsoon circulation and consequences for pollution levels, *J. Geophys. Res.*, *107*(D24), doi:10.1029/2001JD001483.
- de Laat, A. T. J., J. A. de Gouw, J. Lelieveld, and A. Hansel (2001), Model analysis of trace gas measurements and pollution impact during INDOEX, *J. Geophys. Res.*, *106*(D22), 28,469–28,480, INDOEX Special Issue.
- de Reus, M., R. Krejci, J. Williams, H. Fischer, R. Scheele, and J. Ström (2001), Vertical and horizontal distributions of the aerosol number concentration and size distribution over the northern Indian Ocean, *J. Geophys. Res.*, *106*(D22), 28,629–28,641.
- DeMore, W. B., and K. D. Bayes (1999), Rate Constants for the Reactions of Hydroxyl Radical with Several Alkanes, Cycloalkanes, and Dimethyl Ether, *J. Phys. Chem. A*, *103*, 2649–2654.

- DeMore, W. B., S. P. Sander, D. M. Golden, R. F. Hampson, M. J. Kurylo, C. J. Howard, A. R. Ravishankara, C. E. Kolb, and M. J. Molina (1997), Chemical kinetics and photochemical data for use in stratospheric modeling. evaluation number 12, *JPL Publication 97-4*, Jet Propulsion Laboratory, Pasadena, CA.
- Dobson, G. M. B. (1956), Origin and distribution of polyatomic molecules in the atmosphere, *Proc. R. Soc. London, Ser. A*(236), 187–193.
- Ehhalt, D. H., F. Rohrer, A. Wahner, M. J. Prather, and D. R. Blake (1998), On the use of hydrocarbons for the determination of tropospheric OH concentrations, *J. Geophys. Res.*, *103*, 18,981–18,997.
- Eisele, F. L., and D. J. Tanner (1991), Ion-assisted tropospheric OH measurement, *J. Geophys. Res.*, *96*, 9295–9308.
- Eriksson, E. (1971), Compartment models and reservoir theory, *Ann. Rev. Ecol. Syst.*, *2*, 67–84.
- Finlayson-Pitts, B. J., and J. N. Pitts, Jr. (2000), *Chemistry of the Upper and Lower Atmosphere*, Academic Press, San Diego.
- Fischer, H., F. G. Wienhold, P. Hoor, O. Bujok, C. Schiller, P. Siegmund, M. Ambaum, H. A. Scheeren, and J. Lelieveld (2000), Tracer correlations in the northern high latitude lowermost stratosphere: Influence of cross-tropopause mass exchange, *Geophys. Res. Lett.*, *27*, 97–100.
- Fischer, H., P. Hoor, and J. Lelieveld (2001), Seasonal variation of cross-tropopause transport inferred from chemical tracer measurements, *SPARC Newsletter*, *17*, 18–22.
- Fischer, H., D. Brunner, G. W. Harris, P. Hoor, J. Lelieveld, D. S. McKenna, J. Rudolph, H. A. Scheeren, P. Siegmund, H. Wernli, J. Williams, and S. Wong (2002), Synoptic tracer gradients in the upper troposphere over central Canada during the STREAM 1998 summer campaign, *J. Geophys. Res.*, *107*, doi:10.1029/2000JD000312.
- Fortuin, J. P. F., and H. Kelder (1998), An ozone climatology based on ozonesonde and satellite measurements, *J. Geophys. Res.*, *103*(D24), 31,709–31,734.
- Frost, R. (1960), Pressure variation over Malaya and the resonance theory, *Scientific Paper No. 4*, Air Ministry Meteorological Office, London.
- Gottelman, A., M. L. Salby, and F. Sassi (2002), Distribution and influence of convection in the tropical tropopause region, *J. Geophys. Res.*, *107*(D10), doi:10.1029/2001JD001048.
- Gibbs, A. G., and W. G. N. Slinn (1973), Fluctuations in Trace Gas Concentrations in the Troposphere, *J. Geophys. Res.*, *78*, 574–576.
- Graedel, T. E., and P. J. Crutzen (1994), *Chemie der Atmosphäre, Bedeutung für Klima und Umwelt*, Spektrum akademischer Verlag, Heidelberg.
- Gray, W. M., and J. Schaeffer (1991), *Teleconnections Linking World Wide Climate Anomalies*, chap. El Nino and QBO influences on tropical cyclone activity, pp. 257–84, John Wiley, Chichester.
- Gray, W. M., J. Schaeffer, and J. A. Knaff (1992), Influence of the stratospheric QBO on ENSO variability, *J. Met. Soc. Japan*, *70*, 975–95.
- Gros, V., J. Williams, J. A. van Aardenne, G. Salisbury, R. Hofmann, M. G. Lawrence, R. von Kuhlmann, J. Lelieveld, M. Krol, H. Berresheim, J. M. Lobert, and E. Atlas (2003), Origin of anthropogenic hydrocarbons and halocarbons measured in the summertime european outflow (on Crete in 2001), *Atmos. Chem. Phys.*, *3*, 1223–1235.

- Hamm, S., J. Hahn, G. Helas, and P. Warneck (1984), Acetonitrile in the troposphere: Residence time due to rainout and uptake by ocean, *Geophys. Res. Lett.*, *11*, 1207–1210.
- Hamrud, M. (1983), Residence time and spatial variability for gases in the atmosphere, *Tellus*, *35B*, 295–303.
- Hastenrath, S., and A. Rosen (1983), Patterns of Indian monsoon rainfall oscillations, *Tellus*, *35A*, 324–331.
- Hauglustaine, D. A., G. P. Brasseur, S. Walters, P. J. Rasch, J.-F. Müller, L. K. Emmons, and M. A. Carroll (1998), MOZART, a global chemical transport model for ozone and related chemical tracers; 2. Model results and evaluation, *J. Geophys. Res.*, *103(D21)*, 28,291–28,335.
- Heicklen, J., K. Westberg, and N. Cohen (1971), Discussion remark, in *Chemical Reactions in Urban Atmospheres: proceedings of the symposium held at general Motors research Laboratories, Warren, Michigan, 1969*, edited by C. S. Tuesday, pp. 55–59, General Motors Research Laboratories; Symposium on Chemical Reactions in Urban Atmospheres (1969 : Warren, Mi), American Elsevier, New York.
- Highwood, E. J., and B. J. Hoskins (1998), The tropical tropopause, *Q. J. R. Meteorol. Soc.*, *124*, 1579–1604.
- Hoell, J. M., D. D. Davis, S. C. Liu, R. E. Newell, H. Akimoto, R. J. McNeal, and R. J. Bendura (1997), The Pacific Exploratory Mission-West Phase B: February-March, 1994, *J. Geophys. Res.*, *102(D23)*, 28,223–28,239.
- Hofzumahaus, A., U. Aschmutat, U. Brandenburger, T. Brauers, H.-P. Dorn, M. Hausmann, M. Helling, F. Holland, C. Plass-Dülmer, and D. H. Ehhalt (1998), Intercomparison of tropospheric OH measurements by different laser techniques during the POPCORN campaign 1994, *J. Atmos. Chem.*, *31*, 227–246.
- Holgate, S. T., J. M. Samet, H. S. Koren, and R. L. Maynard (Eds.) (1999), *Air Pollution and Health*, Academic Press, San Diego.
- Holton, J. R., P. H. Haynes, M. E. McIntyre, A. R. Douglass, R. B. Rood, and L. Pfister (1995), Stratosphere-troposphere exchange, *Rev. Geophys.*, *33*, 403–439.
- Hoor, P. (2001), Flugzeuggetragene Spurengasmessungen in der Tropopausenregion, Ph.D. thesis, Johannes-Gutenberg Universität, Mainz.
- Hoor, P., H. Fischer, J. Lelieveld, and D. Brunner (2002), Seasonal variations of a mixing layer in the lowermost stratosphere as identified by the CO-O₃ correlation from in situ measurements, *J. Geophys. Res.*, *107(D5)*, doi:10.1029/2000JD000289.
- Houghton, J. T., Y. Ding, D. J. Griggs, M. Noguer, P. van der Linden, X. Dai, K. Maskell, and C. Johnson (2001), IPCC, 2001: Climate Change 2001: The Scientific Basis. Contribution of Working Group I to the Third Assessment Report of the Intergovernmental Panel on Climate Change, *Ipc wgi assessment report*, Intergovernmental Panel on Climate Change, Cambridge University Press, Cambridge, United Kingdom and New York, NY, USA.
- Jaenicke, R. (1982), *Physical aspects of the atmospheric aerosol, in Chemistry of the unpolluted and polluted troposphere*, D. Reidel Publ. Co., Boston.

- Jöckel, P., C. A. M. Brenninkmeijer, and P. J. Crutzen (2002), A discussion on the determination of atmospheric OH and its trends, *Atmos. Chem. Phys. Discuss.*, 2, 1261–1286.
- Jobson, B. T., D. D. Parrish, P. Goldan, W. Kuster, F. C. Fehsenfeld, D. R. Blake, N. J. Blake, and H. Niki (1998), Spatial and temporal variability of nonmethane hydrocarbon mixing ratios and their relation to photochemical lifetime, *J. Geophys. Res.*, 103D, 13,557–13,567.
- Jobson, B. T., S. A. McKeen, D. D. Parrish, F. C. Fehsenfeld, D. R. Blake, A. H. Goldstein, S. M. Schauffler, and J. C. Elkins (1999), Trace gas mixing ratio variability versus lifetime in the troposphere and stratosphere: Observations, *J. Geophys. Res.*, 104, 16,091–16,113.
- Johnston, N. A. C., J. J. Colman, D. R. Blake, M. J. Prather, and F. S. Rowland (2002), On the variability of tropospheric gases: Sampling, loss patterns, and lifetime, *J. Geophys. Res.*, 107(D11), doi:10.1029/2001JD000669.
- Jost, C., J. Trentmann, D. Sprung, M. O. Andreae, and K. Dewey (2003), Deposition of acetonitrile to the Atlantic Ocean off Namibia and Angola and its implications for the atmospheric budget of acetonitrile, *Geophys. Res. Lett.*, 30(16), doi:10.1029/2003GL017347.
- Junge, C. E. (1963), *Air Chemistry and Radioactivity*, Academic Press, New York, London.
- Junge, C. E. (1974), Residence time and variability of tropospheric trace gases, *Tellus*, 26, 477–488.
- Junge, C. E., W. Seiler, and P. Warneck (1971), The atmospheric ^{12}CO and ^{14}CO budget, *J. Geophys. Res.*, 76, 2866–2879.
- Khalil, M. A. K., and R. A. Rasmussen (1994), Global decrease in atmospheric carbon monoxide concentration, *Nature*, 370, 639–641.
- Kiehl, J. T., J. J. Hack, G. B. Bonan, B. A. Boville, B. P. Briegleb, D. L. Williamson, and P. J. Rasch (1996), Description of the NCAR Community Climate Model (CCM3), *NCAR Technical Note NCAR/TN-420+STR*, National Center for Atmospheric Research, Boulder, Colorado.
- Knaff, J. A., and W. M. Gray (1994), Extended range prediction of Asian monsoon rainfall, in *Proceedings of International Conference on Monsoon Variability and Prediction*, vol. WMO/TD No. 619, edited by WCRP-84, pp. 436–43, Trieste, Italy.
- Kormann, R., H. Fischer, C. Gurk, F. Helleis, T. Klüpfel, K. Kowalski, R. Königstedt, U. Parchatka, and V. Wagner (2002), Application of a multi-laser tunable diode laser absorption spectrometer for atmospheric trace gas measurements at sub-ppbv levels, *Spectrochemical Acta Part A*, 58(11), 2489–2498.
- Krol, M., P. J. van Leeuwen, and J. Lelieveld (1998), Global OH trend inferred from methylchloroform measurements, *J. Geophys. Res.*, 103, 10,697–10,711.
- Lawrence, M. G. (1996), Photochemistry in the Tropical Pacific Troposphere: Studies with a Global 3D Chemistry-Meteorology Model, Ph.d. thesis, Georgia Institute of Technology.
- Lawrence, M. G. (2001), unpublished manuscript.
- Lawrence, M. G. (2004), personal communication.
- Lawrence, M. G., P. J. Crutzen, P. J. Rasch, B. E. Eaton, and N. M. Mahowald (1999), A model for studies of tropospheric photochemistry: Description, global distributions, and evaluation, *J. Geophys. Res.*, 104(D21), 26,245–26,777.

- Lawrence, M. G., P. Joeckel, and R. von Kuhlmann (2001), What does the global mean OH concentration tell us?, *Atmos. Chem. Phys.*, *1*, 37–49.
- Lawrence, M. G., P. J. Rasch, R. von Kuhlmann, J. Williams, H. Fischer, M. de Reus, J. Lelieveld, P. J. Crutzen, M. Schultz, P. Stier, H. Huntrieser, J. Heland, A. Stohl, C. Forster, H. Elbern, H. Jakobs, and R. R. Dickerson (2003a), Global chemical weather forecasts for field campaign planning: predictions and observations of large-scale features during MINOS, CONTRACE, and INDOEX, *Atmos. Chem. Phys.*, *3*, 267–289.
- Lawrence, M. G., R. von Kuhlmann, M. Salzmann, and P. J. Rasch (2003b), The balance of effects of deep convective mixing on tropospheric ozone, *Geophys. Res. Lett.*, *30*, doi:10.1029/2003GL017644.
- Lelieveld, J., A. Bregman, H. A. Scheeren, J. Ström, K. S. Carslaw, H. Fischer, P. C. Siegmund, and F. Arnold (1999), Chlorine activation and ozone destruction in the northern lowermost stratosphere, *J. Geophys. Res.*, *104*, 8201–8214.
- Lelieveld, J., P. J. Crutzen, V. Ramanathan, M. O. Andreae, C. A. M. Brenninkmeijer, T. Campos, G. R. Cass, R. R. Dickerson, H. Fischer, J. A. de Gouw, A. Hansel, A. Jefferson, D. Kley, A. T. J. de Laat, S. Lal, M. G. Lawrence, J. M. Lobert, O. L. Mayol-Bracero, A. P. Mitra, T. Novakov, S. J. Oltmans, K. A. Prather, T. Reiner, H. Rodhe, H. A. Scheeren, D. Sikka, and J. Williams (2001), The Indian Ocean Experiment: Widespread Air Pollution from South and Southeast Asia, *Science*, *291*, 1031–1036.
- Lelieveld, J., W. Peters, F. J. Dentener, and M. C. Krol (2002), Stability of tropospheric hydroxyl chemistry, *J. Geophys. Res.*, *107*(D23), doi:10.1029/2002JD002272.
- Lenschow, D. H., and D. Gurarie (2002), A simple model for relating concentrations and fluctuations of trace reactive species to their lifetimes in the atmosphere, *J. Geophys. Res.*, *107*(D24), doi:10.1029/2002JD002526.
- Levy, H. (1971), Normal atmosphere: large radical and formaldehyde concentrations predicted, *Science*, *173*, 141–143.
- Lindinger, W., A. Hansel, and A. Jordan (1998a), On-line monitoring of volatile organic compounds at pptv levels by means of Proton-Transfer- Reaction Mass Spectrometry (PTR-MS) medical applications, food control and environmental research, *Int. J. of Mass Spectrometry and Ion Processes*, *173*, 191–241.
- Lindinger, W., A. Hansel, and A. Jordan (1998b), Proton-transfer-reaction mass spectrometry (PTR-MS): on-line monitoring of volatile organic compounds at pptv levels, *Chem. Soc. Rev.*, *27*, 347.
- Madden, R. A., and P. R. Julian (1971), Description of a 40-50 day oscillation in the zonal wind in the tropical Pacific, *J. Aerosol Sci.*, *28*, 701–8.
- Madden, R. A., and P. R. Julian (1972), Description of global scale circulation cells in the tropics with a 40-50 day period., *J. Aerosol Sci.*, *29*, 1109–23.
- Marik, T., H. Fischer, P. Bergamaschi, F. Conen, and K. Smith (2002), Seasonal variation in stable isotope ratios in methane from rice fields, *Global Biogeochem. Cycles*, *1094*(16/4), doi:10.1029/2001GBC001428.

- Martinez, R. D., A. A. Buitrago, N. W. Howell, C. H. Hearn, and J. A. Joens (1992), The near U.V. absorption spectra of several aliphatic aldehydes and ketones at 300 K, *Atmos. Environ.*, *26, Part A*, 785–792.
- McAvaney, B., C. Covey, S. Joussaume, V. Kattsov, A. Kitoh, W. Ogana, A. Pitman, A. Weaver, R. Wood, Z.-C. Z. K. AchutaRao, A. Arking, A. Barnston, R. Betts, C. Bitz, G. Boer, P. Brannon, A. Broccoli, F. Bryan, M. Claussen, R. Colman, P. Delecluse, A. D. Genio, K. Dixon, P. Duffy, L. Dümenil, M. England, T. Fichet, G. Flato, J. Fyfe, N. Gedney, P. Gent, C. Genthon, J. Gregory, E. Guilyardi, S. Harrison, N. Hasegawa, G. Holland, M. Holland, Y. Jia, P. Jones, M. Kageyama, D. Keith, K. Kodera, J. Kutzbach, S. Lambert, S. Legutke, G. Madec, S. Maeda, M. Mann, G. Meehl, I. Mokhov, T. Motoi, T. Phillips, J. Polcher, G. Potter, V. Pope, C. Prentice, G. Roff, F. Semazzi, P. Sellers, D. Stensrud, T. Stockdale, R. Stouffer, K. Taylor, K. Trenberth, R. Tol, J. Walsh, M. Wild, D. Williamson, S.-P. Xie, X.-H. Zhang, and F. Zwiers (2001), Model evaluation, in *Climate Change 2001: The Scientific Basis*, edited by J. S. Y. Qian, chap. 8, Cambridge University Press, Cambridge, United Kingdom and New York, NY, USA.
- McGregor, G. R., and S. Nieuwolt (1998), *Tropical Climatology*, second ed., John Wiley & Sons, Chichester, England.
- McKeen, S. A., M. Trainer, E. Y. Hsie, R. K. Tallamraju, and S. C. Liu (1990), On the indirect determination of atmospheric OH radical concentrations from reactive hydrocarbon measurements, *J. Geophys. Res.*, *95*, 7493–7500.
- McKenna, D. S., C. J. Hord, and J. M. Kent (1995), Hydroxyl radical concentrations and Kuwait oil fire emission rates for March 1991, *J. Geophys. Res.*, *100(D12)*, 26,005–26,026.
- Möhler, O., and F. Arnold (1991), Flow reactor and triple quadrupole mass spectrometer investigations of negative ion reactions involving HNO₃: Implications for atmospheric HNO₃ detection by chemical ionization mass spectrometry, *J. Atmos. Chem.*, *13*, 33–61.
- Möhler, O., T. Reiner, and F. Arnold (1993), A novel aircraft-based tandem mass-spectrometer for atmospheric ion and trace gas measurements, *Rev. Sci. Instrum.*, *64*, 1199–1207.
- Ministry of Health (1954), Mortality and morbidity during the London fog of December 1952, *Non-parliamentary papers*, Ministry of Health.
- Mitra, A. P. (1999), INDOEX (India): Introductory note, *Curr. Sci.*, *76*, 886–889.
- Ogallo, L. (1979), Rainfall variability in Africa, *Mon. Wea. Rev.*, *107*, 1133–1139.
- Perner, D., D. H. Ehhalt, H. W. Pätz, U. Platt, E. P. Röth, and A. Volz (1976), OH-Radicals in the Lower Troposphere, *Geophys. Res. Lett.*, *3*, 466–468.
- Perner, D., U. Platt, M. Trainer, G. Hübler, J. Drummond, W. Junkermann, J. Rudolph, B. Schubert, A. Volz, D. H. Ehhalt, K. J. Rumpel, and G. Helas (1987), Measurement of Tropospheric OH Concentrations: A Comparison of Field Data with Model Predictions, *J. Atmos. Chem.*, *5*, 185–216.
- Potter, T. D., and B. R. Colman (Eds.) (2003), *Handbook of Weather, Climate, and Water : Atmospheric Chemistry, Hydrology, and Societal Impacts*, *Handbook of Weather, Climate, and Water*, vol. 1, John Wiley and Sons, New Jersey.

- principal investigators participating in INDOEX (1999), INDOEX researchers document the impact of pollutants on climate processes over the tropical Indian Ocean, INDOEX Research News Release, INDOEX International Project Office, Male International Airport, Maldives.
- Prinn, R. G., R. F. Weiss, B. R. Miller, J. Huang, F. N. Alyea, D. M. Cunnold, P. J. Fraser, D. E. Hartley, and P. G. Simmonds (1995), Atmospheric Lifetime and Trends of CH_3CCl_3 and Global OH Concentrations, *Science*, 269, 187–192.
- Raman, S., D. d. S. Niyogi, M. Simpson, and J. Pelon (2002), Dynamics of the elevated land plume over the Arabian Sea and the Northern Indian Ocean during northeasterly monsoons and during the Indian Ocean experiment (INDOEX), *Geophys. Res. Lett.*, 29(16), doi:10.1029/2001GL014193.
- Ramanathan, V., P. J. Crutzen, J. Lelieveld, A. P. Mitra, D. Althausen, J. Anderson, M. O. Andreae, W. Cantrell, G. R. Cass, C. E. Chung, A. D. Clarke, J. A. Coakley, W. D. Collins, W. C. Conant, F. Dulac, J. Heintzenberg, A. J. Heymsfield, B. Holben, S. Howell, J. Hudson, A. Jayaraman, J. T. Kiehl, T. N. Krishnamurti, D. Lubin, G. McFarquhar, T. Novakov, J. A. Ogren, I. A. Podgorny, K. Prather, K. Priestley, J. M. Prospero, P. K. Quinn, K. Rajeev, P. Rasch, S. Rupert, R. Sadourny, S. K. Satheesh, G. E. Shaw, P. Sheridan, and F. P. J. Valero (2001), Indian Ocean Experiment: An integrated analysis of the climate forcing and effects of the great Indo-Asian haze, *J. Geophys. Res.*, 106(D22), 28,371–28,398, INDOEX Special Issue.
- Rasch, P. J., N. M. Mahowald, and B. E. Eaton (1997), Representations of transport, convection, and the hydrologic cycle in chemical transport models: Implications for the modeling of short lived and soluble species, *J. Geophys. Res.*, 102, 127–28,138.
- Ravishankara, A. R., E. J. Dunlea, M. A. Blitz, T. J. Dillon, D. E. Heard, M. J. Pilling, R. S. Strekowski, J. M. Nicovich, and P. H. Wine (2002), Redetermination of the rate coefficient for the reaction of $\text{O}(^1\text{D})$ with N_2 , *Geophys. Res. Lett.*, 29(15), doi:10.1029/2002GL014850.
- Rhoads, K. P., P. Kelly, R. R. Dickerson, T. P. Carsey, M. Farmer, D. L. Savoie, and J. M. Prospero (1997), Composition of the troposphere over the Indian Ocean during the monsoonal transition, *J. Geophys. Res.*, 102, 18,981–18,995.
- Rodhe, H. (2000), *Earth System Science*, chap. Modeling Biogeochemical Cycles, p. 62 ff., Academic Press, Amsterdam.
- Roedel, W. (1994), *Physik unserer Umwelt: Die Atmosphäre*, 2. ed., Springer Verlag, Heidelberg.
- Roswintarti, O., S. Raman, U. C. Mohanty, and D. S. Niyogi (2001), Application of three-dimensional triple nested mesoscale model for assessing the transport and boundary layer variability over the Indian Ocean during INDOEX, *Curr. Sci. India*, 80(Suppl.), 69–76.
- Roths, J. (1992), Entwicklung eines flugtauglichen laserspektroskopischen Spurengassensors und dessen Einsatz bei der TROPOZ-II-Flugmeßkampagne, Ph.D. thesis, Mainz.
- Salisbury, G., J. Williams, R. Holzinger, V. Gros, N. Mihalopoulos, M. Vrekoussis, R. Sarda-Estève, H. Berresheim, R. von Kuhlmann, M. Lawrence, and J. Lelieveld (2003), Ground-based PTR-MS measurements of reactive organic compounds during the MINOS campaign in Crete, July–August 2001, *Atmos. Chem. Phys.*, 3, 925–940.
- Santacesaria, V., R. Carla, R. MacKenzie, A. Adriani, F. Cairo, G. D. C. Kiemle, G. Redaelli, J. Beuermann, C. Schiller, T. Peter, B. Luo, H. Wernli, F. Ravegnani, A. Ulanovsky, V. Yushkov, N. Sitnikov, S. Balestri, and L. Stefanutti (2003), Clouds at the tropical tropopause: A case study

- during the APE-THESEO campaign over the western Indian Ocean, *J. Geophys. Res.*, *108*(D2), doi:10.1029/2002JD002166.
- Saunders, S. M., D. L. Baulch, K. M. Cooke, M. J. Pilling, and P. I. Smurthwaite (1994), Kinetics and mechanisms of the reactions of OH with some oxygenated compounds of importance in tropospheric chemistry, *Int. J. Chem. Kinetics*, *26*, 113–130.
- Scheele, M. P., P. C. Siegmund, and P. F. J. van Velthoven (1996), Sensitivity of trajectories to data resolution and its independence on the starting point: In or outside a tropopause fold, *Meteorol. Appl.*, *3*, 267–273.
- Scheeren, H. A., J. Lelieveld, J. A. de Gouw, C. van der Veen, and H. Fischer (2002), Methyl chloride and other chlorocarbons in polluted air during INDOEX, *J. Geophys. Res.*, *107*(D19), doi:10.1029/2001JD001121.
- Scheeren, H. A., H. Fischer, J. Lelieveld, P. Hoor, J. Rudolph, F. Arnold, B. Bregman, C. Brühl, A. Engel, C. van der Veen, and D. Brunner (2003), Reactive organic species in the northern extratropical lowermost stratosphere: Seasonal variability and implications for OH, *J. Geophys. Res.*, *108*(D24), doi:10.1029/2003JD003650.
- Schneider, J., V. Bürger, and F. Anrold (1997), Methyl cyanide and hydrogen cyanide measurements in the lower stratosphere: Implications for methyl cyanide sources and sinks, *J. Geophys. Res.*, *102*, 501–506.
- Semadeni, M., D. W. Stocker, and J. A. Kerr (1995), The temperature dependence of the OH radical reactions with some aromatic compounds under simulated tropospheric conditions, *Int. J. Chem. Kinetics*, *27*, 287–304.
- Shapiro, L. J. (1982), Hurricane climatic variations, part 1: patterns and cycles, *Mon. Wea. Rev.*, *110*, 1007–1013.
- Shapiro, M. A. (1980), Turbulent mixing within tropopause folds as a mechanism for the exchange of chemical constituents between the stratosphere and troposphere, *J. Aerosol Sci.*, *37*, 994–1002.
- Simmons, A. J., A. Untch, C. Jacob, P. Kallenberg, and P. Unden (1999), Stratospheric water vapour and tropical tropopause temperatures in ECMWF analyses and multi-year simulations, *Q. J. R. Meteorol. Soc.*, *125*, 353–386.
- Simpson, M. D., and S. Raman (2004), Role of the land plume in the transport of ozone over the ocean during INDOEX (1999), *Boundary-Layer Meteorol.*, *111*, 133–152.
- Singh, H. B. (1977), Atmospheric halocarbons: evidence in favour of reduced average hydroxyl radical concentrations in the troposphere, *Geophys. Res. Lett.*, *3*, 101–104.
- Slinn, W. G. N. (1988), A simple model for Junge's relationship between concentration fluctuations and residence times for tropospheric trace gases, *Tellus*, *40B*, 229–232.
- Smith, R. K. (2003), Lectures on tropical meteorology.
- Spivakovsky, C. M., J. A. Logan, S. A. Montzka, Y. J. Balkanski, M. Foreman-Fowler, D. B. A. Jones, L. W. Horowitz, A. C. Fusco, C. A. M. Brenninkmeijer, M. J. Prather, S. C. Wofsy, and M. B. McElroy (2000), Three-dimensional climatological distribution of tropospheric OH: Update and evaluation, *J. Geophys. Res.*, *105*(D7), 8931–8980.

- Talukdar, R. K., A. Melouki, T. Gierczak, S. Barone, S.-Y. Chiang, and A. R. Ravishankara (1994), Kinetics of the reactions of OH with alkanes, *Int. J. Chem. Kinetics*, *26*, 973–990.
- Turnipseed, A. A., S. B. Barone, and A. R. Ravishankara (1996), Reaction of OH with dimethyl sulfide. 2. Products and mechanisms, *J. Phys. Chem.*, *100*, 14,703 – 14,713.
- van Velthoven, P. F. J., and H. Kelder (1996), Estimates of stratosphere-troposphere exchange: Sensitivity to model formulation and horizontal resolution, *J. Geophys. Res.*, *101*, 1429.
- Verver, G. H. L., D. R. Sikka, J. M. Lobert, G. Stossmeister, and M. Zachariasse (2001), Overview of the meteorological conditions and atmospheric transport processes during INDOEX 1999, *J. Geophys. Res.*, *106*(D22), doi:10.1029/2001JD900203, INDOEX Special Issue.
- Volk, C. M., J. W. Elkins, D. W. Fahey, G. S. Dutton, J. M. Gillan, M. Loewenstein, J. R. Podolske, K. R. Cham, and M. R. Gunson (1997), Evaluation of source gas lifetimes from stratospheric observations, *J. Geophys. Res.*, *102*, 25,543–25,564.
- von Kuhlmann, R. (2001), Tropospheric Photochemistry of Ozone, its Precursors and the Hydroxyl Radical: A 3D-Modeling Study Considering Non-Methane Hydrocarbons, Ph.D. thesis, Johannes Gutenberg-Universität, Mainz.
- von Kuhlmann, R. (2002), private communication.
- von Kuhlmann, R., M. G. Lawrence, P. J. Crutzen, and P. J. Rasch (2003a), A model for studies of tropospheric ozone and nonmethane hydrocarbons: Model description and ozone results, *J. Geophys. Res.*, *108*(D9), doi:10.1029/2002JD002893.
- von Kuhlmann, R., M. G. Lawrence, P. J. Crutzen, and P. J. Rasch (2003b), A model for studies of tropospheric ozone and non-methane hydrocarbons: Model evaluation of ozone related species, *J. Geophys. Res.*, *108*, doi:10.1029/2002JD003348.
- Wagner, V. (2000), Formaldehyd in der maritimen Grenzschicht über dem Indischen Ozean, Ph.D. thesis, Universität Bielefeld, Bielefeld.
- Wang, C. C., and L. I. Davis (1974), Ground-state population distribution of OH determined with a tunable diode laser, *Appl. Phys. Lett.*, *25*, 34–35.
- Wang, Y. (2000), Global Tropospheric OH: Observational Constraints and Model Simulations, in *IG-Activities Newsletter*, vol. 21, edited by A. Pszenny, pp. 18–21, International Global Atmospheric Chemistry, IGAC Core Project Office, Cambridge, USA.
- Warneck, P. (2000), *Chemistry of the natural atmosphere, International Geophysics Series*, vol. 71, p. 124, 2 ed., Academic Press, San Diego.
- Weinstock, B. (1971), Discussion remark, in *Chemical Reactions in Urban Atmospheres: proceedings of the symposium held at general Motors research Laboratories, Warren, Michigan, 1969*, edited by C. S. Tuesday, pp. 54–55, General Motors Research Laboratories; Symposium on Chemical Reactions in Urban Atmospheres (1969 : Warren, Mi), American Elsevier, New York.
- White, J. U. (1976), Very Long Optical Paths in Air, *J. Opt. Soc. Am.*, *66*, 411–416.
- Wienhold, F. G. (1992), Entwicklung eines TTFM-Diodenlaserspektrometers (Two Tone Frequency Modulation) zum Spurengasnachweis mit hoher zeitlicher Auflösung, Master's thesis, Universität Mainz.

- Wienhold, F. G., H. Fischer, P. Hoor, V. Wagner, R. Königstedt, G. W. Harris, J. Anders, R. Grisar, M. Knothe, W. J. Riedel, F. J. Lübken, and T. Schilling (1998), TRISTAR - a tracer in-situ TDLAS for atmospheric research, *Appl. Phys. B*, 67, 411–417.
- Williams, J., H. Fischer, G. W. Harris, P. J. Crutzen, P. Hoor, A. Hansel, R. Holzinger, C. Warnecke, W. Lindinger, B. Scheeren, and J. Lelieveld (2000), Variability-lifetime relationship for organic trace gases: A novel aid to compound identification and estimation of OH concentrations, *J. Geophys. Res.*, 105(D16), 20,473–20,486.
- Williams, J., V. Gros, B. Bonsang, and V. Kazan (2001), HO cycle in 1997 and 1998 over the southern Indian Ocean derived from CO, radon, and hydrocarbon measurements made at Amsterdam Island, *J. Geophys. Res.*, 106(D12), 12,719–12,725.
- Williams, J., H. Fischer, S. Wong, P. J. Crutzen, R. Scheele, M. Zachariasse, and J. Lelieveld (2002), Near equatorial CO and O₃ profiles over the Indian Ocean during the winter monsoon: high O₃ levels in the middle troposphere and interhemispheric exchange, *J. Geophys. Res.*, 107(D19), doi:10.1029/2001JD001126.
- Wofsy, S. C., S.-M. Fan, D. R. Blake, J. D. Bradshaw, S. T. Sandholm, H. B. Singh, G. W. Sachse, and R. C. Harriss (1994), Factors influencing atmospheric composition over subarctic North America, *J. Geophys. Res.*, 99(D1), 1887–1897.
- Wohlfrom, K.-H. (2000), Messung atmosphärischer Spurengase und Ionen mit flugzeuggetragenen Massenspektrometern: Neue Erkenntnisse für Ozon, Aerosole und den Einfluss des Luftverkehrs auf die Atmosphäre, Ph.D. thesis, University Heidelberg, Heidelberg.
- Wollenhaupt, M., S. A. Carl, A. Horowitz, and J. N. Crowley (2000), Rate Coefficients for Reaction of OH with Acetone between 202 and 395 K, *J. Phys. Chem. A*, 104(14), 2695–2705.
- Xu, X., J. Williams, C. Plass-Dülmer, H. Berresheim, G. Salisbury, L. Lange, and J. Lelieveld (2003), GC×GC measurements of C7-C11 aromatic and n-alkane hydrocarbons on Crete, in air from Eastern Europe during the MINOS campaign, *Atmos. Chem. Phys.*, 3, 1461–1475.
- Zachariasse, M., H. G. J. Smit, P. F. J. van Velthoven, and H. Kelder (2001), Cross-tropopause and interhemispheric transports into the tropical free tropopause over the Indian Ocean, *J. Geophys. Res.*, 106(D22), 28,441–28,452.

Acknowledgements

I would like to thank my promoter Prof. Dr. Franz-Josef Lübken for his interest in the forthcoming of this thesis, comments and discussions and the assessment of the thesis.

Special thanks to my second promoter and director of the Airchemistry Department of the Max-Planck-Institute of Chemistry in Mainz, Prof. Dr. Jos Lelieveld, for enabling my work at his institute and for his appraisal of my thesis and his interest in my work.

Thanks to Prof. Dr. Paul Josef Crutzen, my third promoter and former director of the Airchemistry Department of the Max-Planck-Institute of Chemistry in Mainz, for enabling my work at his institute and my participation in the campaigns, STREAM 98 and INDOEX.

I am very grateful to Dr. Horst Fischer, my supervisor, for employing me in his working group, enabling me to take part in those very interesting scientific campaigns and introducing me to the interesting field of laser spectroscopy, for many valuable discussions, ideas as regards contents, his endless patience, making it possible for me to visit conferences and summer schools, and for the promotion of this thesis.

I am indebted to Dr. Marian de Reus for tireless proofreading of my thesis, for her support, encouragement and friendship and also for getting me out into fresh air by babysitting her (and Dr. Lutz Lange's) daughter Annika.

I would like to thank all members of the former TDLAS and recently OptSpec working group for the nice atmosphere and for their interest in my work. I am grateful to Rainer Königstedt, whose improvisational skills and his support both in laboratory and in the field have been invaluable. I owe special thanks to Dr. Peter Hoor for introducing me to the TRISTAR and Licor instruments and the enlightenment that the "scientific kick" is not just a myth when it comes to the preparation of an airborne campaign. Thanks to Christian Gurk for exploring the *Demods* with me.

Thanks to Dr. Jonathan Williams, who introduced me to variability as well as IGOR, and later raised my self-confidence by asking me IGOR questions, and for sharing an office with me - although we sometimes had different ideas on how to furnish it.

Thanks also to all members of the STREAM Team and INDOEX participants (for the great teamwork), who made the campaigns to what they were. I learned a lot and really had fun during them, in spite of all the stress and long working days. Special thanks to the Team of the TU Delft and the pilots, especially Hessel Benedictus, Alwin Kraeger, Jaap Quartel and Jurrie van Osnabrugge. They introduced me to aeronautics, and I shared so many exciting moments with them - strike in India, overcoming bureaucracy and lots of forms, missing emigration forms, being (falsely!) suspected of spying, being diverted and running low on gas, false fire alarm onboard and a leak in the hull (for which none of us was responsible). And Cor Dam and Kees van Woerkom for improvising and making things possible that would not have been, otherwise.

Acknowledgements to all the people and their co-workers who provided access to their data: Dr.

B. Scheeren, C. van der Veen, M. Boulder and Prof. Dr. J. Lelieveld for the nonmethane hydrocarbon and methyl chloride data; Dr. T. Marik for the methane data during INDOEX; Dr. C. Warneke and Dr. J. de Gouw for volatile organic compounds data during INDOEX; Dr. T. Wetter for N₂O and CF₂Cl₂ (CFC-12) data during STREAM 98; K.-H. Wohlfrom, Dr. A. Wollny and Prof. Dr. F. Arnold for the HNO₃, SO₂, acetone and acetonitrile (CH₃CN) data during STREAM 98; M. Boulder, Prof. Dr. J. Lelieveld, Dr. B. Scheeren for ozone data during STREAM 98; H. Cremer (STREAM 98) respectively A. Kreager and C. Dam (both INDOEX) for providing aircraft data; Dr. Ch. Brühl for photolysis rate data; Dr. R. von Kuhlmann (STREAM 98) and Dr. M. Lawrence (INDOEX) for the MATCH-MPIC model data; and Dr. B. Bregman for the TM3 model data.

Thanks to all people involved in solving problems, when I managed to travel to the Maldives (INDOEX) without a passport: Dr. Horst Fischer for pulling out all stops in order to get that %&S* piece of paper to me... Thanks to Hessel Benedictus, Alwin Kraeger and KLM operators for convincing the immigrations officers during transfer flights to let me in (people involved in the campaigns will know the advantage of being allowed to leave the aircraft at refuelling or overnight stops...). Lots of thanks to Dr. Bert Scheeren, for convincing the Maldivian officials to let me and my passport immigrate separately. Thanks to Prof. Dr. Paul Josef Crutzen for personally bringing my passport to me during the INDOEX campaign. Moreover, I am very grateful that he did not make me come up to the stage on the official opening of the campaign on Hulhule, to come and get it.

Thanks to all the “girls” of the Ada-Lovelace-Project, I enjoyed working for the project very much - although I let it divert me much too easily. A special thanks to Birte Peter for her continuous support.

I am grateful to family Dr. Orth, who welcomed me so heartily in their family and gave me a second home in Mainz. I like to recall the many trips between Mainz and Bonn spend in the pleasant company of Mrs. Strähle, and the refreshing walks with Dr. Orth and her dogs Balu or later Pelle.

Thanks to my friends, who had an open ear for me and kept me grounded, especially Sandra.

Very special thanks to my parents, who never stopped believing in me, for their support, both morally and financially, and their patience.

My most affectionate thanks to Michael - for being there and loving me.